MEDICAL RADIOLOGY

Radiation Oncology

L. W. Brady
H.-P. Heilmann
M. Molls

New Technologies in Radiation Oncology

W. Schlegel
T. Bortfeld
A.-L. Grosu
Editors

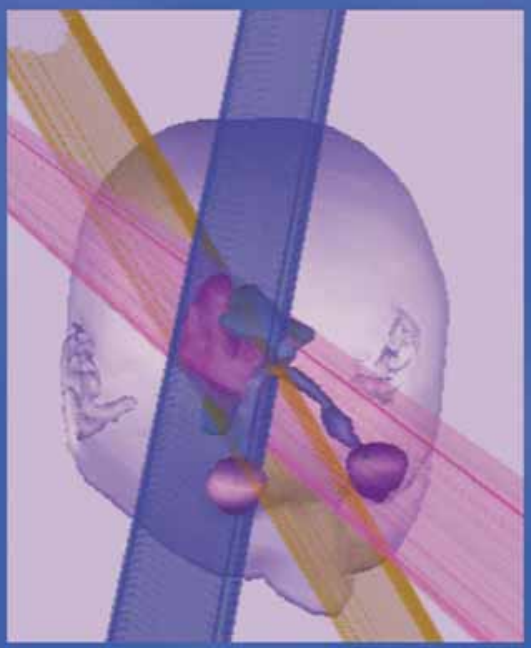

Springer

MEDICAL RADIOLOGY
Radiation Oncology

Editors:
L. W. Brady, Philadelphia
H.-P. Heilmann, Hamburg
M. Molls, Munich

ЗНАНИЕ

W. Schlegel · T. Bortfeld · A.-L. Grosu (Eds.)

New Technologies in Radiation Oncology

With Contributions by

J. R. Adler · N. Agazaryan · D. Baltas · Y. Belkacémi · R. Bendl · T. Bortfeld · L. G. Bouchet
G. T. Y. Chen · K. Eilertsen · M. Fippel · K. H. Grosser · A.-L. Grosu · P. Häring
J.-M. Hannoun-Lévi · G. H. Hartmann · K. K. Herfarth · J. Hesser · R. Hinderer
G. D. Hugo · O. Jäkel · M. Kachelriess · C. P. Karger · M. L. Kessler · C. Kirisits
P. Kneschaurek · S. Kriminski · E. Lartigau · S.-L. Meeks · E. Minar · M. Molls · S. Mutic
S. Nill · U. Oelfke · D. R. Olsen · N. P. Orton · H. Paganetti · A. Pirzkall · R. Pötter
B. Pokrajac · A. Pommert · B. Rhein · E. Rietzel · M. A. Ritter · M. Roberson · G. Sakas
L. R. Schad · W. Schlegel · C. Sholz · A. Schweikard · T. D. Solberg · L. Sprague
D. Stsepankou · S.E. Tenn · C. Thieke · W. A. Tomé · N. M. Wink · D. Yan · M. Zaider
N. Zamboglou

Foreword by

L. W. Brady, H.-P. Heilmann and M. Molls

With 299 Figures in 416 Separate Illustrations, 246 in Color and 39 Tables

Springer

Wolfgang Schlegel, PhD
Professor, Abteilung Medizinische Physik
in der Strahlentherapie
Deutsches Krebsforschungszentrum
Im Neuenheimer Feld 280
69120 Heidelberg
Germany

Thomas Bortfeld, PhD
Professor, Department of Radiation Oncology
Massachusetts General Hospital
30, Fruit Street
Boston, MA 02114
USA

Anca-Ligia Grosu, MD
Privatdozent, Department of Radiation Oncology
Klinikum rechts der Isar
Technical University Munich
Ismaningerstrasse 22
81675 München
Germany

Medical Radiology · Diagnostic Imaging and Radiation Oncology
Series Editors: A. L. Baert · L. W. Brady · H.-P. Heilmann · M. Molls · K. Sartor

Continuation of Handbuch der medizinischen Radiologie
Encyclopedia of Medical Radiology

Library of Congress Control Number: 2004116561

ISBN 3-540-00321-5 Springer Berlin Heidelberg New York
ISBN 978-3-540-00321-2 Springer Berlin Heidelberg New York

Springer is part of Springer Science+Business Media

http//www.springeronline.com

Printed in Germany

Medical Editor: Dr. Ute Heilmann, Heidelberg
Desk Editor: Ursula N. Davis, Heidelberg
Production Editor: Kurt Teichmann, Mauer
Cover-Design and Typesetting: Verlagsservice Teichmann, Mauer

Printed on acid-free paper – 21/3151xq – 5 4 3 2 1 0

Foreword

Radiation oncology is one of the most important treatment facilities in the management of malignant tumors. Although this specialty is in the first line a physician's task, a variety of technical equipment and technical know-how is necessary to treat patients in the most effective way possible today.

The book by Schlegel et al., "New Technologies in Radiation Oncology," provides an overview of recent advances in radiation oncology, many of which have originated from physics and engineering sciences. 3D treatment planning, conformal radiotherapy, with consideration of both external radiotherapy and brachytherapy, stereotactic radiotherapy, intensity-modulated radiation therapy, image-guided and adaptive radiotherapy, and radiotherapy with charged particles are described meticulously . Because radiotherapy is a doctor's task, clinically orientated chapters explore the use of therapeutic radiology in different oncologic situations. A chapter on quality assurance concludes this timely publication.

The book will be very helpful for doctors in treating patients as well as for physicists and other individuals interested in oncology.

Philadelphia — Luther W. Brady
Hamburg — Hans-Peter Heilmann
Munich — Michael Molls

Preface

In the 1960s radiation therapy was considered an empirical, clinical discipline with a relatively low probability of success. This situation has changed considerably during the past 40 years.

Radiation therapy is based heavily on fields such as physics, mathematics, computer science and radiation biology as well as electrical and mechanical engineering, making it a truly interdisciplinary field, unparalleled by any other clinical discipline. Now radiation therapy can be applied so safely, precisely and efficiently that the previously feared side effects no longer play a role. At the same time, tumour control, and the probability of cure, has significantly increased for many tumour patients. This change from an empirical and qualitative discipline to a scientifically based, precise clinical science has been accompanied by groundbreaking innovations in physics and technology (Fig. 1).

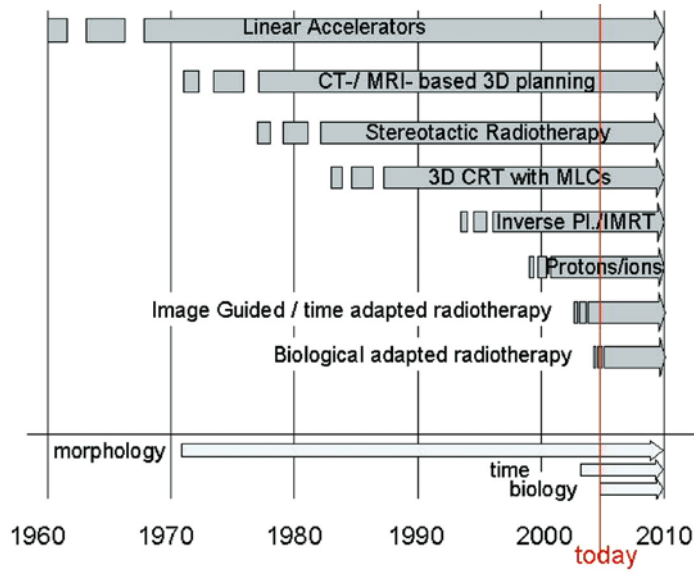

- The first important step was the replacement of cobalt-60 and betatrons as irradiation sources by electron-linear accelerators (also known as "linacs") between 1960 and 1980. Modern computer-controlled linacs are comparatively compact and reliable, have a high mechanical accuracy and deliver sufficiently high dose rates. Having become the "workhorses" of radiation oncology, they have been introduced in nearly every radiotherapy department in the world, providing the basis of modern precision radiotherapy.
- The next important milestone, which sparked a revolution not only in radiological diagnostics but also in radiotherapy, was the invention of X-ray computed tomography (CT). Computed tomography was introduced to the radiotherapy process at the end of the 1970s, and this resulted in 3D computerized treatment planning, now a standard tool in all radiotherapy departments.

- The CT-based treatment planning was later supplemented with medical resonance imaging (MRI). By combining CT and MRI, and using registered images for radiotherapy planning, it is now possible to assess tumour morphology more precisely, and thus achieve improved definition of planning target volumes (PTV), improving both percutaneous radiotherapy and brachytherapy.
- The computer revolution, characterized by the development of small, powerful and inexpensive desktop computers, had tremendous impact on radiation therapy. With new tools from 3D computer graphics, implemented in parallel with 3D treatment planning, it was possible to establish "virtual radiotherapy planning", a method to plan and simulate 3D irradiation techniques. New 3D dose calculation algorithms (e.g. "pencil-beam algorithms") made it possible to precalculate the 3D dose distributions with sufficient accuracy and with acceptable computing times.
- With the aforementioned advent of 3D imaging, 3D virtual therapy simulation and 3D dose calculation, the preconditions for introducing an individualized, effective local radiation treatment of tumours were fulfilled. What was still missing was the possibility to transfer the computer plans to the patient with high accuracy. This gap was filled by the introduction of stereotaxy into radiotherapy in the early 1980s. Prior to this development, stereotaxy was used in neurosurgery as a tool to precalculate target points in the brain and to precisely guide probes to these target points within the tumour in order to take biopsies or implant radioactive seeds. The transfer of this technique to radiotherapy resulted in significantly enhanced accuracy in patient positioning and adjustment of radiation beams. Stereotactic treatment techniques were first developed for single-dose irradiations (called "radiosurgery"), then for fractionated treatments in the brain and the head and neck region ("stereotactic radiotherapy"). Later, it became possible to transfer stereotactic positioning to extracranial tumour locations ("extracranial stereotactic radiotherapy") as well. This opened up the possibility for high-precision treatments of tumours in nearly all organs and locations.
- The next important step which revolutionized radiotherapy came again from the field of engineering. The development of computerized multi-leaf collimators (MLCs) in the middle of the 1980s ensured the clinical breakthrough of 3D conformal radiotherapy. With the advent of MLCs, the time-consuming fabrication of irregularly shaped beams with cerrobend blocks could be abandoned. Conformal treatments became less expensive and considerably faster, and were applied with increasing frequency. The combination of 3D treatment planning and 3D conformal beam delivery resulted in safe and efficient treatment techniques, which allowed therapists to escalate tumour doses while at the same time lowering the dose in organs at risk and normal tissues.
- By the mid 1990s, 3D conformal radiotherapy was supplemented by a new treatment technique, which is currently becoming a standard tool in modern clinics: intensity-modulated radiotherapy (IMRT) using MLC-beam delivery or tomotherapy, in combination with inverse treatment planning. In IMRT the combination of hardware and software techniques solves the problem of irradiating complex target volumes with concave parts in the close vicinity of critical structures, a problem with which radio-oncologists have had to struggle from the very beginning of radiotherapy. In many modern clinics around the world, IMRT is successfully applied, e.g. in the head and neck and in prostate cancer. It has the potential to improve results in many other cancer treatments as well.
- The IMRT with photon beams can achieve a level of conformity of the dose distribution within the target volume which can, from a physical point of view, not be improved further; however, the absolute dose which can be delivered to the target volume is still limited by the unavoidable irradiation exposure of the surrounding normal tissue. A further improvement of this situation is possible by using particle radiation. Compared with photon beams, the interaction of particle beams (like protons or heavier charged particles) with tissue is completely different. For a single beam, the dose delivered to

the patient has a maximum shortly before the end of the range of the particles. This is much more favourable compared with photons, where the dose maximum is located just 2–3 cm below the surface of the patient's body. By selecting an appropriate energy for the particle beams and by scanning particle pencil beams over the whole target volume, highly conformal dose distributions can be reached, with a very steep dose fall-off to surrounding tissue, and a much lower "dose bath" to the whole irradiated normal tissue volume. Furthermore, from the use of heavier charged particles, such as carbon-12 or oxygen-16, an increase in RBE can be observed shortly before the end of the range of the particles. It is expected that this radiobiological advantage over photons and protons will result in a further improvement in local control, especially for radioresistant tumours. However, particle therapy, both with protons and heavier charged particles, is still in the early stages of clinical application and evaluation on a broad scale. Ongoing and future clinical trials must demonstrate the benefit of these promising, but costly, particle-beam treatments.

At the beginning of the new millennium, the field of adaptive radiotherapy evolved from radio-oncology:

- After 3D CT and MRI enabled a much better understanding of tumour morphology, and thus spatial delineation of target volumes, the time has arrived where the temporal alterations of the target volume can also be assessed and taken into account. Image-guided and time-adapted radiotherapy (IGRT and ART) are characterized by the integration of 2D and 3D imaging modalities into the radiotherapy work flow. The vision is to detect deformations and motion between fractions (inter-fractional IGRT) and during irradiation (intra-fractional IGRT), and to correct for these changes either by gating or tracking of the irradiation beam. Several companies in medical engineering are currently addressing this technical challenge, with the goal of implementing IGRT and ART in radiotherapy as a fast, safe and efficient treatment technique.
- Another innovation which is currently on the horizon is biological adaptive radiotherapy. The old hypothesis that the tumour consists of homogeneous tissue, and therefore a homogeneous dose distribution is sufficient, can no longer be sustained. We now know that a tumour may consist of different subvolumes with varying radiobiological properties. We are trying to characterize these properties more appropriately by functional and molecular imaging using new tracers in PET and SPECT imaging and by functional MRI (fMRI) and MR spectroscopy, for example. We now have to develop concepts to include and integrate this information into radiotherapy planning and beam delivery, firstly by complementing the morphological gross tumour volume (GTV) by a biological target volume (BTV) consisting of subvolumes of varying radioresistance, and secondly by delivering appropriate inhomogeneous dose distributions with the new tools of photon- and particle-IMRT techniques ("dose painting"). Furthermore, biological imaging can give additional information concerning tumour extension and tumour response to radiotherapy or radiochemotherapy.

Currently, we have reached a point where, besides the 3D tumour morphology, time variations and biological variability within the tumour can also be taken into account. The repertoire of radiation oncology has thus been expanded tremendously. Tools and methods applied to radiotherapy are increasing in number and complexity. The speed of these developments is sometimes breathtaking, as radiation oncologists are faced more and more with the problem of following and understanding these modern innovations in their profession, and putting the new developments into practice. This book gives an introduction into the aforementioned areas. The authors of the various chapters are specialists from the involved disciplines, either working in research and development or in integrating and using the new methods in clinical application. The authors endeavoured to explain the very often complicated and complex subject matter in an understandable manner. Naturally, such a

collection of contributions from a heterogeneous board of authors cannot completely cover the whole field of innovations. Some overlap, and variations in the depth of descriptions and explanations were unavoidable. We hope that the book will be particularly helpful for physicians and medical physicists who are working in radiation oncology or just entering the field, and who are trying to achieve an overview and a better understanding of the new technologies in radiation oncology.

The motivation to compile this book can be traced back to the editors of the book series Medical Radiology/Radiation Oncology, by Michael Molls, Munich, Luther Brady, Philadelphia, and Hans-Peter Heilmann, Hamburg. We thank them for continuous encouragement and for not losing the belief that the work will eventually be finished. We extend thanks to Alan Bellinger, Ursula Davis, Karin Teichmann and Kurt Teichmann, who did such an excellent job in preparing the book. Most of all, thanks to all the authors, who wrote their chapters according to our suggestions, and a very special thanks to those who did this work within the short period of time before the deadline.

Heidelberg — Wolfgang Schlegel
Boston — Thomas Bortfeld
Munich — Anca-Ligia Grosu

Contents

1 New Technologies in 3D Conformal Radiation Therapy: Introduction and Overview

Wolfgang Schlegel

CONTENTS

1.1 Clinical Demand for New Technologies in Radiotherapy

Radiotherapy is, after surgery, the most successfully and most frequently used treatment modality for cancer. It is applied in more than 50% of all cancer patients.

Radiotherapy aims to deliver a radiation dose to the tumor which is high enough to kill all tumor cells. That is from the physical and technical point of view a difficult task, because malignant tumors often are located close to radiosensitive organs such as the eyes, optic nerves and brain stem, spinal cord, bowels, or lung tissue. These so-called organs at risk must not be damaged during radiotherapy. The situation is even more complicated when the tumor itself is radioresistant and very high doses are needed to reach a therapeutic effect.

W. Schlegel, PhD
Professor, Abteilung Medizinische Physik in der Strahlentherapie, Deutsches Krebsforschungszentrum, Im Neuenheimer Feld 280, 69120 Heidelberg, Germany

At the time of being diagnosed, about 60% of all tumor patients are suffering from a malignant localized tumor which has not yet disseminated, i.e., no metastatic disease has yet occurred; thus, these patients can be considered to be potentially curable. Nevertheless, about one-third of these patients (18% of all cancer patients) cannot be cured, because therapy fails to stop tumor growth.

This is the point where new technologies in radiation oncology, especially in 3D conformal radiotherapy, come into play: it is expected that they will enhance local tumor control. In conformal radiotherapy, the dose distribution in tissue is shaped in such a way that the high-dose region is located in the target volume, with a maximal therapeutic effect throughout the whole volume. In the neighboring healthy tissue, the radiation dose has to be kept under the limit for radiation damage. This means a steep dose falloff has to be reached between the target volume and the surroundings; thus, in radiotherapy there is a rule stating that with a decrease of dose to healthy tissue, the dose delivered to the target volume can be increased; moreover, an increase in dose will also result in better tumor control (tumor control probability, TCP), whereas a decrease in dose to healthy tissue will be connected with a decrease in side effects (normal tissue complication probability, NTCP). Increase in tumor control and a simultaneous decrease in side effects means a higher probability of patient cure.

In the past two decades, new technologies in radiation oncology have initiated a significant increase in the quality of conformal treatment techniques. The development of new technologies for conformal radiation therapy is the answer to the wishes and guidelines of the radiation oncologists. The question of whether clinical improvements are driven by new technical developments, or vice versa, should be answered in the following way: the development of new technologies should be motivated by clinical constraints.

In this regard the physicists, engineers, computer scientists, and technicians are service providers to the radiologists and radiotherapists, and in this con-

text new technologies in conformal radiation therapy are technical answers to a clinical challenge.

An improvement in one field automatically entails the necessity of an improvement in other fields. Conformal radiation therapy combines, in the best case, the advantages of all new developments.

1.2 Basic Principles of Conformal Radiotherapy

The basic idea of conformal radiation therapy is easy to understand and it is close to being trivial (Fig. 1.1). The problem is that depth dose of a homogeneous photon field is described by an exponentially decreasing function of depth. Dose deposition is normally higher close to the surface than at the depth of the tumor.

To improve this situation normally more than one beam is used. Within the overlapping region of the beams a higher dose is deposited. If the apertures of the beams are tailored (three dimensionally) to the shape of the planning target volume (PTV) masking the organs at risk (OAR), then the overlapping region should fit the PTV. In the case of an OAR close to the PTV, this is not true for such a simple beam configuration such as the one shown in Fig. 1.1. In such cases one needs a more complex beam configuration to achieve an acceptable dose distribution; however, the general thesis is that, using enough beams, it should be possible to a certain extent to fit a homogeneous dose distribution to the PTV while sparing the OARs. One hopes that the conformity of dose distributions can be increased using individually tailored beams compared with, for example, a beam arrangement using simple rectangular-shaped beams, and for the majority of cases this is true. Nevertheless, there are cases, especially with concave-shaped target volumes and moving targets, where conventional conformal treatment planning and delivery techniques fail. It is hoped that these problems will be solved using intensity-modulated radiotherapy (IMRT; see Chap. 23) and adaptive radiotherapy (ART; see Chaps. 24–26), respectively.

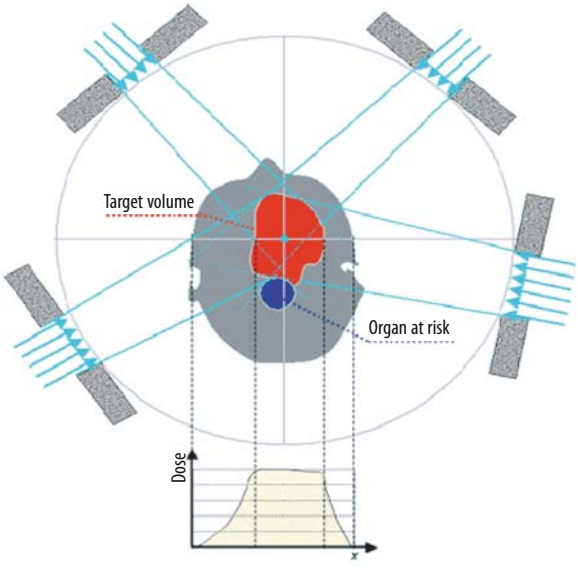

Fig. 1.1. Basic idea of conformal radiotherapy

1.3 Clinical Workflow in Conformal Radiotherapy

The physical and technical basis of the radiation therapy covers different aspects of all links in the "chain of radiotherapy" (Fig. 1.2) procedure. All parts of the "chain of radiation therapy" are discussed in other chapters separately and in great detail, and an overview on the structure of this book within this context is given in Table 1.1.

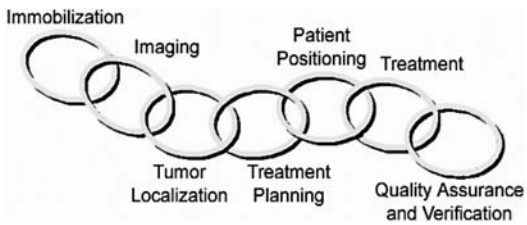

Fig. 1.2. Chain of radiotherapy. (From Schlegel and Mahr 2001)

Table 1.1 Structure of the book with respect to the chain of radiotherapy

Part of the radiotherapy chain	Described in chapter
Patient immobilization	21, 22
Imaging and information processing	2–6
Tumor localization	7–11
Treatment planning	13, 14
Patient positioning	12, 21, 22, 26
Treatment	20–28
Quality assurance and verification	32, 33

1.3.1 Patient Immobilization

It is obvious that a reliable and exact fixation of the irradiated body area or organ is a substantial prerequisite for conformal radiation therapy. Modifications of the position of the patient relative to the treatment machine can lead to dangerous dose errors.

Numerous immobilization devices and techniques have been developed for radiotherapy, most of them using casts and moulds.

The highest immobilization accuracy is required when patients have to be treated with single-dose irradiation under stereotactical boundary conditions (see Chaps. 21, 22).

1.3.2 Imaging and Tumor Localization

Presently tumors and organs at risk are localized with 3D imaging techniques. One of the most important implicit constraints facing a technician developing new radiation therapy treatment techniques is that the segmented OAR and PTV are identical with the true organs and the true tumor. This is not a trivial statement, and it is still the subject of controversy. It is well known that different observers, and even the same observer, may create slightly different outlines at sequential attempts to define OARs and the PTV.

Without doubt, advances in the field of medical imaging, especially in the use of computed tomography (CT), magnetic resonance imaging (MRI), ultrasound (US), and positron emission tomography (PET), have led to improved precision in tumor localization. In particular, the gross tumor volume can be reconstructed in three dimensions from tomographic slices, and taken in the tumor region, thus forming the basis for 3D treatment planning (see Chaps. 2–5, 7, 8). Computed tomography is an ideal basis for 3D treatment planning, as it has the potential to quantitatively characterize the physical properties of heterogeneous tissue in terms of electron densities which is essential for dose calculation (see Chaps. 15, 16). On the other hand, MRI is very often superior to CT, especially for the task of differentiating between healthy tissue and tumor tissue (see Chap. 9). In addition, MRS and PET imaging have the potential to include information on tumor metabolism and heteronegeity (see Chaps. 10, 11, 13).

1.3.3 Treatment Planning

Computer-assisted 3D treatment planning can be considered as state of the art in most modern hospitals. The planning process can be divided into the following steps:

1. Determination of the target volume and organs at risk
2. Virtual therapy simulation
3. Dose calculation
4. Visualization and evaluation of dose distributions

The goal of treatment planning is the determination of a suitable and practicable irradiation technique which results in a conformal dose distribution; thus, treatment planning is a typical optimization problem. Whereas in conventional "forward planning" a trial-and-error method is applied for interactive plan optimization (see Chap. 14), the new method of "inverse planning" is able to automatically calculate a treatment technique which leads to the best coverage of the target volume and sufficient sparing of healthy tissue (see Chap. 17).

1.3.3.1 Defining Target Volumes and Organs at Risk

The best way of determining the PTV and OAR is on the basis of multiple-modality 3D image data sets such as X-ray computed tomography (CT), magnetic resonance (MRI and MRS), and PET. Routinely, X-ray CT is the most common tomographic imaging method (see Chaps. 7–8, 13).

The registration of all these imaging modalities for the purpose of defining target volumes and organs at risk is highly desirable. Three-dimensional image registration is a computer tool which is able to match the 3D spatial information of the different imaging modalities by use of either external or internal anatomic landmarks. The involved methods are described in Chap. 5. The problem of target-volume definition using multi-modal imaging techniques from the radio-oncologist's point of view are described in Chaps. 10 and 13.

Another problem that is more important, if highly conformal dose distributions are delivered, is organ movement. It is clear that in conformal therapy organ movements cannot be ignored.

Time-adapted radiotherapy is a field which is trying to solve this problem, and some chapters of this

book report the approaches which are currently being investigated (see Chaps. 8, 24–26).

1.3.3.2 Definition of the Treatment Technique

Conformal radiation therapy basically requires 3D-treatment planning. After delineating the therapy-relevant structures, various therapy concepts are simulated as part of an iterative process. The search for "optimal" geometrical irradiation parameters – the "irradiation configuration" – is very complex. The beam directions and the respective field shapes must be selected. The various possibilities of volume visualization, such as Beams Eye View, Observers View, or Spherical View, are tools which support the radiotherapist with this process (Chap. 14).

1.3.3.3 Dose Calculation

The quality of treatment planning depends naturally on the accuracy of the dose calculation. An error in the dose calculation corresponds to an incorrect adjustment of the dose distribution to the target volume and the organs at risk. The calculation of dose distributions has therefore always been a special challenge for the developers of treatment-planning systems.

The problem which has to be solved in this context is the implementation of an algorithm which is fast enough to fulfill the requirements of daily clinical use, and which has sufficient accuracy. Most treatment-planning systems work with so-called pencil-beam algorithms, which are semi-empiric and meet the requirements in speed and accuracy (see Chap. 15). If too many heterogeneities, such as air cavities, lung tissue, or bony structures, are close to the target volume, the use of Monte Carlo calculations is preferred. Monte Carlo calculations simulate the physical rules of interaction of radiation with matter in a realistic way (see Chap. 16). In the case of heterogeneous tissue they are much more precise, but also much slower, than pencil-beam algorithms.

1.3.3.4 Evaluation of the 3D Dose Distribution

The 3D-treatment planning leads to 3D-dose distributions, which must be evaluated in an appropriate way. In particular this concerns the occurrence of hot and cold spots, as well as the homogeneity and conformity of the dose distribution. Numerous computer graphics and mathematical tools have been developed to support the evaluation of dose distribution.

The weak point in treatment planning still is that the evaluation of dose distributions occurs usually on the basis of the physical dose distribution and not on the basis of quantified radiobiological or clinical effects. Physical dose is only a surrogate for the effects that radiation induces in healthy tissue as well as in the target volume. In the context of radiotherapy planning, it has always been emphasized that radiobiological models to predict normal tissue complication probabilities (NTCP) and tumor control probabilities (TCP) would be much better suited to treatment planning than the sole consideration of physical dose distributions. Unfortunately, lack of clinical data still hinders the development of adequate biological planning algorithms.

Some planning programs permit the calculation of values for the TCP and for the NTCP as yardsticks for the biological effect of the dose distribution; however, radiobiological models are still the topic of much controversial discussion (see Chap. 18).

1.4 Patient Positioning

The fifth link in the chain of radiotherapy is the link between treatment planning and the irradiation, the so-called problem of patient positioning. The problem here is to accurately transfer the planned irradiation technique to the patient. In practice, this means that the patient first of all has to be placed in exactly the same position as during 3D imaging. This is performed with a suitable immobilization device which can be used during imaging and treatment. Secondly, the treatment couch with the patient has to be adjusted until the isocenter position matches the pre-calculated coordinates. A variety of different techniques are currently used to reach this goal: conventionally, X-ray simulators are used to control the patient's position with the use of radiographic imaging. In connection with 3D-treatment planning, the use of digital reconstructed radiographs (DRRs) has been established (see Chaps. 4, 14). More recently, stereotactic patient positioning techniques have been introduced, techniques which initially could only be applied to target volumes in the brain but presently can also be applied to extracranial targets (see Chaps. 21, 22). The most modern approach to patient positioning is the use of navigational techniques, which offer not only tools to position the patient at

the beginning of each fraction but also can monitor movement during irradiation (see Chap. 26). A promising approach to the problem of patient positioning is image-guided therapy (IGRT), where a 2D or even 3D X-ray imaging procedure is integrated in the irradiation unit, thus offering the possibility of controlling and monitoring the position of the target volume under treatment (Chaps. 24–26). This approach, which has the advantage that the treatment conditions could be dynamically matched to a moving and changing target volume, is also called adaptive radiotherapy (ART).

1.5 Treatment

The next and most essential link in the chain of radiotherapy, of course, is treatment, itself characterized by radiation delivery. Modern radiotherapy, especially when there is a curative intention, is practiced as 3D conformal radiotherapy. Most conformal radiotherapy treatments are performed by external radiation with photons, but the obvious physical and probably also biological advantages of charged particle therapy with proton or carbon beams are currently leading to a worldwide increasing number of particle-therapy installations. On the other hand, 3D conformal therapy with internal sources (brachytherapy) has also been established and proven to be very efficient for special indications.

1.5.1 Photons

The most common treatment modality presently is the use of a high-energy X-ray machine (Linac) in conjunction with a conformal irradiation technique realized by multiple irregular-shaped fixed beams. Beam shaping is often still performed with blocks, but computer-controlled multi-leaf collimators (MLCs) are increasingly replacing them. The MLCs also have the potential for intensity-modulated radiotherapy (IMRT), which can be considered as the most advanced treatment technique of 3D conformal radiotherapy with photons. Whereas the general aspects of conventional conformal radiation therapy are described briefly in Chap. 20, IMRT techniques are described in Chap. 23 and ART in Chaps. 24–26.

1.5.2 Charged-Particle Therapy

The use of heavier charged particles, such as protons and ^{12}C, is still restricted to a very limited number of centers worldwide. The physical advantages of heavier charged particles are obvious: due to the Bragg peak, they result in a favorable dose distribution in healthy tissue. ^{12}C beams, which is high linear energy transfer radiation, also seem to have radiobiological advantages (see Chaps. 27, 28). The high costs of charged-particle irradiation units are the major hindrance to broader introduction.

1.5.3 Brachytherapy

The implantation of radioactive sources into tumors has the potential to produce conformal dose distributions with a very steep dose gradient to neighboring structures and shows an excellent sparing effect for normal tissue. Depending on the tumor type, it can be applied either in short-term irradiations (with high dose rates) or in a long-term irradiation with radio-emitters at low dose rates. In Chaps. 19, the 2D- and 3D-planning techniques which are presently applied in modern brachytherapy are described, and Chaps. 29–31 describe clinical applications in vascular and prostate brachytherapy.

1.6 Quality Management in Radiotherapy

All steps and links of the chain of radiotherapy are subject to errors and inaccuracies, which may lead to treatment failure or injury of the patient. A careful network of quality assurance and verification has to be established in a radiotherapy unit in order to minimize these risks. A quality management system has to cover all the components involved and all aspects of the chain, e.g., dosimetry, software and hardware testing, standardization, documentation, archiving, etc. Three-dimensional conformal radiotherapy includes medical, biological, mechanical and electronic engineering, and computer science, as well as mathematical and physical aspects and components, and can be considered to be among

the most complex and critical medical treatment techniques currently available. For this reason, efficient quality management is an indispensable requirement for modern 3D conformal radiotherapy (see Chaps. 32, 33).

References

Schlegel W, Mahr A (2001) 3D conformal radiotherapy: introduction to methods and techniques. Springer, Berlin Heidelberg NewYork

Basics of 3D Imaging

2 3D Reconstruction

Jürgen Hesser and Dzmitry Stsepankou

CONTENTS

Röntgen's contribution to X-ray imaging is a little over 100 years old. Although there was early interest in the extension of the technique to three dimensions, it took more than 70 years for a first prototype. Since then, both the scanner technology, reconstruction algorithm, and computer performance have been developed so significantly that in the near future we can expect new techniques with suppressed artefacts in the images. Current developments of such methods are discussed in this chapter.

2.1 Problem Setting

We begin with a presentation of the inverse problem: Given a set of X-ray projections p of an object, try to compute the distribution of attenuation coefficients μ in this object. We can define the projection function P: $p=P(\mu)$. Formally, reconstruction is therefore the calculation of an inverse of P, i.e. $\mu=P^{-1}(p)$. This inverse need not necessarily exist or, even if it does exist, it may be unstable in the sense that small errors in the projection data can lead to large deviations in the reconstruction.

In order to determine the projection function P we have to look at the physical imaging process more closely. X-ray projection follows the Lambert-Beer law. It describes the attenuation of X-rays penetrating an object with absorption coefficient μ and thickness d. A ray with initial intensity I_0 is attenuated to $I=I_0e^{-\mu d}$. If the object's attenuation varies along the ray, one can write $I=I_0e^{-\int\mu(x)dx}$, where the integral is along the path the ray passes through the object. We divide by I_0 and take the negative logarithm: $p=-\ln(I/I_0)=\int\mu(x)dx$. Let $u(x)$ describe the contribution of each volume element (infinitely small cube) to the absorption of the considered ray, the integral can be written as $p=\int_{\text{volume}}\mu(x)u(x)dx$, where the integration is now over the full volume. Discretizing the volume, we consider homogenous small cubes with a non-vanishing size, each having an absorption coefficient μ_i; thus, the integral is replaced by a sum reading: $p=\sum_i\mu_i u_i$, where u_i is a weighting factor. Solving for μ_i requires a set of such equations being independent of each other; therefore, n projections of size m^2 result in $n\cdot m^2$ different rays. For each of them $p_j=\sum_i\mu_i u_{ij}$ which can be rewritten in vector format $\vec{p}=U\vec{\mu}\cdot$ $\vec{p}$ describes all $n\cdot m^2$ different rays, $\vec{\mu}$ represents the absorption coefficients for all discrete volume elements and matrix element $(U)_{ij}=u_{ij}$ says how much a volume element i contributes to the projection result of ray j, i.e. all what we have to do is to invert this set of equations, namely $\vec{\mu}=U^{-1}\vec{p}$.

Under certain restrictions imposed on the projection directions this set of equations is solvable, i.e. U^{-1} exists. A direct calculation of the inverse of the matrix U, however, is impossible for present-day computers due to the extraordinary large number of more than 10^7 variables for typical problems. The following methods are, therefore,

J. Hesser, PhD, Professor
D. Stsepankou
Department of ICM, Universitäten Mannheim und Heidelberg, B6, 23–29, C, 68131 Mannheim, Germany

techniques that allow solving such systems more efficiently.

2.2 Parallel-Beam Reconstruction Using the Fourier-Slice Theorem

We start with the simplest case, parallel-beam reconstruction in two dimensions. To understand how the reconstruction is realized, let us assume a circle-like object in a rectangular 2D region (Fig. 2.1). The negative logarithm of the projection data is backprojected (or distributed) along the ray direction. This results, as seen in Fig. 2.2, in a rough approximation of the object. The projection data are smoothed and processed by a special filter (Fig. 2.3). It has the property that all contributions accumulate where the object is located and around the object negative and positive contributions cancel out.

Parallel-beam reconstruction belongs to the first approaches used for CT (Cormack 1963; Hounsfield 1973). A significant increase in scanning time was subsequently achieved by fan-beam configurations.

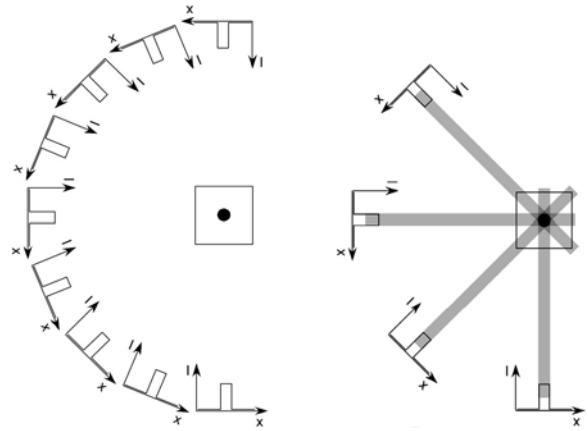

Fig. 2.1. *Left:* projection data from point like object. *Right:* backprojection of $-\log(I/I_0)$

2.3 Fan-Beam Reconstruction

Fan-beam CT reduces scanning times since it captures a full scanline in parallel. Nevertheless, the parallel-beam reconstruction technique can be used as well, since individual parallel rays can be selected from each fan and considered as a parallel projection (as shown in Fig. 2.5). In order to find enough paral-

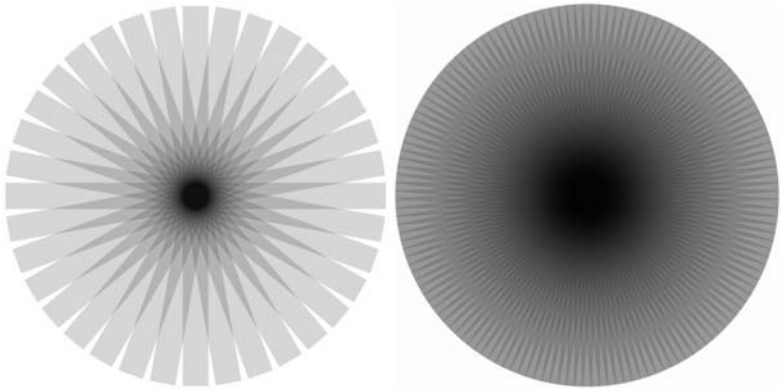

Fig. 2.2. Simulated backprojection for 18 projections (*left*) and 72 projections (*right*)

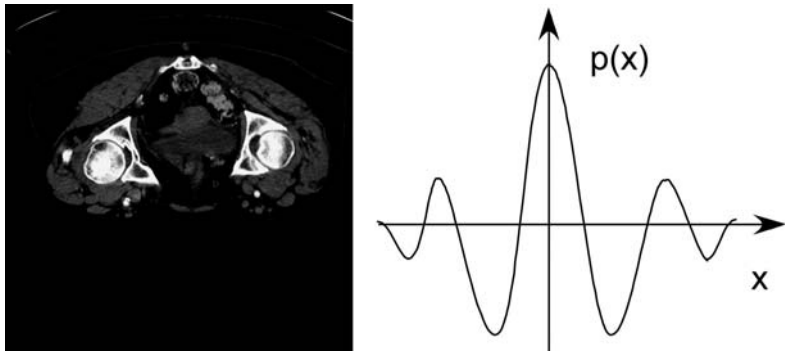

Fig. 2.3. Result for backprojection with filtering (360 projections); *right:* the filter. (From Chang and Herman 1980)

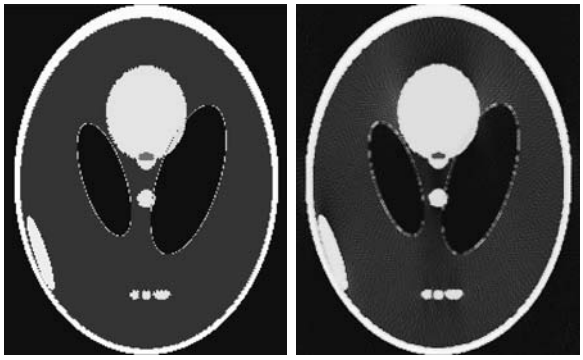

Fig. 2.4. Results on simulated data. Shepp-Logan phantom (Shepp and Logan 1974; *left*), filtered backprojection result for 360 projections (*right*)

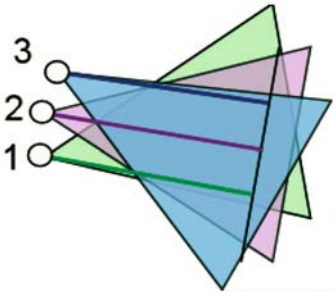

Fig. 2.5. Three different fan-beam projections are shown [shown as *triangles* with different colours; *circles* denote the X-ray sources (*1–3*)]. We identify three approximately parallel rays in the three projections shown as *green*, *violet*, and *blue*. These could be interpreted as a selection of three rays of a parallel projection arrangement.

lel rays, a sufficient number of projections covering 180°+ fan-beam angle is required.

Fan-beam CT was used for a long time until in the 1990s Kalender invented the spiral CT, i.e. a fan-beam CT where the table is shifted with constant speed through the gantry so that the X-ray source follows a screw line around the patient (Kalender et al. 1990).

2.4 Reconstruction Methods of Spiral CT

For spiral CT the projection lines do not lie in parallel planes as for fan-beam CT. Linear interpolation of the captured data on parallel planes allows use of the fan-beam reconstruction method. Data required for interpolation may come from either projections being 360 or 180° apart where the latter yields a better resolution.

In recent years, CT exams with several detector lines have been introduced reducing the overall scanning time for whole-body scans. Despite the divergence of the rays in different detector rows, standard reconstruction techniques are used. Recently, further developments have reconstructed optimally adapted oblique reconstruction planes that are later interpolated into a set of parallel slices (Kachelriess et al. 2000).

2.5 Cone-Beam Reconstruction

For cone-beam reconstruction we differentiate between exact methods, direct approximations, and iterative approximations.

2.5.1 Exact Methods

Exact reconstruction algorithms have been developed (Grangeat 1991; Defrise and Clack 1994; Kudo and Saito 1994), but they currently do not play a role in practice due to the long reconstruction time and high memory consumption. Cone-beam reconstruction imposes constraints on the motion of the source-detector combination around the patient. As shown in Fig. 2.6, a pure rotation around the patient does not deliver information about all regions and therefore a correct reconstruction is not possible; however, trajectories, as shown in Fig. 2.7, for example, solve this problem (Tam et al. 1998).

2.5.2 Filtered Backprojection for Cone Beams

In filtered backprojection (FBP) the projection data is filtered with an appropriate filter mask, backprojected and finally accumulated (Feldkamp et al. 1984; Yan and Leahy 1992; Schaller et al. 1997). For small cone-beam angles fairly good results are obtained, but for larger angles the conditions for parallel beams are violated leading to typical artefacts. Nevertheless, filtered backprojection is currently the standard for commercial cone-beam systems (Euler et al. 2000). From the computational point of view, FBP is more time-consuming compared with the parallel beam, fan beam, or spiral reconstruction since the latter use the Fourier transform to solve backprojection

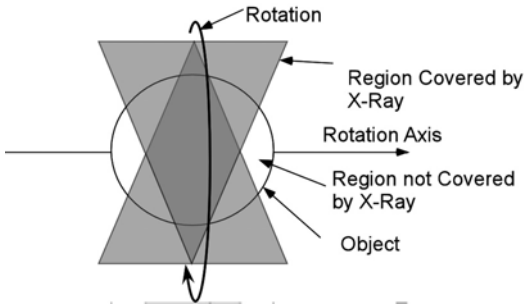

Fig. 2.6. Using only a circular path about the object, one is not able to reconstruct parts of the volume.

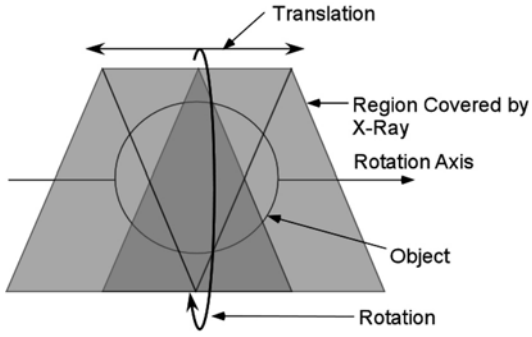

Fig. 2.7. Source detector motion that allows reconstructing the volume for cone beam configurations

fast. Although fast FBP implementations exist (Toft 1996), they do not reach a similar reconstruction quality.

2.6 Iterative Approaches

Filtered backprojection can be characterized as an example of direct inversion techniques. For particularly good reconstruction quality FBP is not the method of choice since it can produce severe artefacts especially in the case of the presence of high-contrast objects or a small number of projection data. Iterative techniques promise better reconstructions.

2.6.1 Algebraic Reconstruction Techniques

The algebraic reconstruction technique (ART; Gordon et al. 1970) is one of the first approaches to solve the reconstruction problem using an iterative method. The basic idea is to start with an a priori guess about the density distribution. The density is often assumed to be zero everywhere. Next, the simu-

Fig. 2.8 Result of a reconstruction using filtered backprojection. One hundred twenty projections of size 512×512

lated projection is calculated and compared with the acquired projection data. The error is backprojected (without filtering) and then accumulated from each projection leading to an improved guess. Iteratively applying this course of simulated projection, error calculation and error backprojection, the algorithm converges towards the most likely solution.

There are different implementations. The original ART operates on a ray-to-ray basis, i.e. the projection image of a single ray is calculated, then the error is determined and is finally backprojected to correct the volume. In the simultaneous iterative reconstruction technique (SIRT) the error is considered in all projections simultaneously. SART (Andersen and Kak 1984) can be seen as a combination of ART and SIRT. It uses a more accurate algorithm for the simulated projection and a heuristic to emphasize corrections near the center of a ray.

2.6.2 Expectation Maximization Technique

Expectation maximization (EM; Lange and Carson 1984) is based on a statistical description of the imaging process. It considers the noise distribution in the image and tries to find a solution that generates the observed result with maximum probability. Ordered

Fig. 2.9. Example of simultaneous iterative reconstruction technique reconstructions on a phantom, 36 projections (512×512), 30 iterations

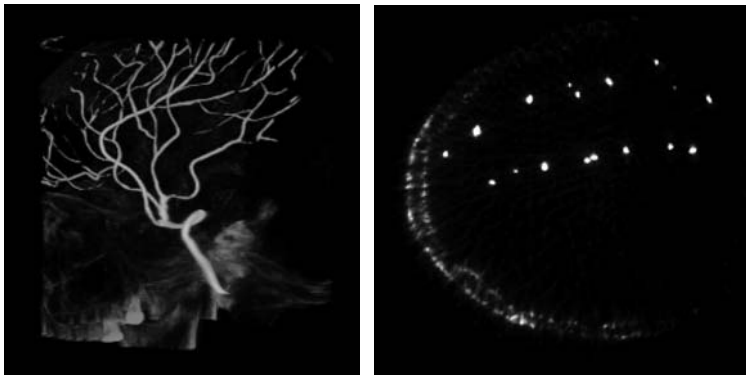

Fig. 2.10. Ordered-subsets expectation maximization result: 36 projections (512×512); three subsets (12 projections in subset); and 3 iterations

subset methods where a subset of all projections for each iteration step is chosen (Hudson and Larkin 1994; Hsiao et al. 2002) can speed up convergence by a factor of approximately 10, although this is not as fast as SIRT or SART.

2.7 Regularization Techniques

Iterative approaches, at best, yield a maximum-likelihood solution. This is a solution, given only the information about the physical process of imaging and the data, which describes the most probable density distribution of physical parameters. In many cases, however, one has additional knowledge about the object to be imaged. For example, restrictions can be imposed on the size of the object and the maximal, minimal or average X-ray density; there may also be an a priori data set, etc. Including this information in the reconstruction process can substantially increase the reconstruction quality and accuracy.

Let us refer to the reconstruction problem as described above: Given the function (matrix) that describes the physical imaging process, U, find the density distribution $\vec{\mu}$ so that the error $E(\vec{\mu})=(\vec{\mu}-U\vec{p})^2$ is minimal. This is the least-square approximation. A regularization modifies this function by adding a regularization function $R(\vec{\mu})$: $E(\vec{\mu})=(\vec{p}-U\vec{\mu})^2+\alpha R(\vec{\mu})$, where α is a coupling constant that has to be chosen manually.

Finding suited regularization functions is a difficult task (Yu and Fessler 2002). Simple examples are Tikhonov regularizations (Tikhonov et al. 1997), where $R(\vec{\mu})$ has been chosen as the scalar product $[L(\mu-\mu^*)]\cdot[L(\mu-\mu^*)]$, where L is typically either the identity matrix or the discrete approximation of the derivative operator and μ^* is the a priori distribution of the absorption coefficient. More advanced and recent techniques are impulse-noise priors (Donoho et al. 1992; Qi and Leahy 2000), Markov random-fields priors (Geman and Yang 1995; Villain et al. 2003) and total variation regularization (Rudin et al. 1992; Persson et al. 2001).

2.8 Hardware Acceleration

2.8.1 Parallelization

One of the significant disadvantages of the cone-beam reconstruction technique is the high computational demands preventing use in daily practice; therefore, parallelization has been a natural means for acceleration. The naive approach is to subdivide the volume into small subvolumes, assign each subvolume to one processor and then compute simulated projection and backprojection locally. Since the projection result is combined by the partial projection results from all subvolumes, processors have to send their intermediate results to a central node where the final projection is generated and then distributed to all other processors again. Current parallel computers are generally limited for this sort of processing by their network bandwidth. In other words, the processors process the data faster than the network can transmit the results to other processors; therefore, parallelization is not very attractive. There are, however, two new upcoming technologies that promise a solution.

2.8.2 Field Programmable Gate Arrays

Field programmable gate arrays are chips where the internal structure can be configured to any hardware logic, e.g. some sort of CPU or, which is interesting in our application, to a special-purpose processor. The main advantage is that recent chips have hundreds of multipliers and several million logic elements that can be configured as switches, adders or memory. Recently, it has been demonstrated that these systems can be more than ten times faster than a normal PC for backprojection, and this factor will grow over the next few years since the amount of computing resources grows faster than the performance of CPUs (Stsepankou et al. 2003).

2.8.3 Graphics Accelerators

Graphics cards contain special-purpose processors optimized for 3D graphics and that internally have the processing power which is much higher than that of normal PCs. Internal graphics can now be pro-

grammed by a C-like language. This opens the opportunity to implement projection (using so-called texture mapping) and backprojection on them. While projection is relatively fast (since it is similar to 3D graphics algorithms), backprojection is still the limitation where currently the performance of standard PCs is achieved (Cabral et al. 1994; Mueller 1998; Chidlow and Möller 2003). Since the internal performance of graphics chips grows much faster than for normal CPUs, it is foreseeable that in the future these accelerators will be a good candidate for implementation of the advanced reconstruction algorithms and, therefore, will allow their use in practice.

2.9 Outlook

In the past few years, with the advent of high-performance PCs, the aspect of reconstruction has become increasingly important in medicine. We have seen that from the current state of the art of cone-beam CT there exist already reconstruction algorithms that promise fewer visible artefacts and a reduction of the required dose for obtaining a given image quality. Most of these algorithms are of iterative nature, partially including regularization techniques based on a priori knowledge. Due to the current hardware developments and the ever-increasing speed of normal CPUs in PCs, these techniques will find their way into practice in the next few years and may revolutionize the way 3D volumes are generated. Normal X-ray systems may therefore be considered for configuration as CT devices, as they are much more cost-effective and more flexible in practice.

References

Andersen AH, Kak AC (1984) Simultaneous algebraic reconstruction technique (SART): a superior implementation of the ART algorithm. Ultrasound Imaging 6:81–94

Cabral B, Cam N, Foran J (1994) Accelerated volume rendering and tomographic reconstruction using texture mapping hardware. 1994 symposium on volume visualization, Tysons Corner, Virginia, ACM SIGGRAPH, pp 91–98

Chang LT, Herman GT (1980) A scientific study of filter selection for a fan-beam convolution algorithm. Siam J Appl Math 39:83–105

Chidlow K, Möller T (2003) Rapid emission tomography reconstruction. Workshop on volume graphics (VG03), pp 15–26

Cormack AM (1963) Representation of a function by its line integrals, with some radiological applications. J Appl Phys 34:2722–2727

Defrise M, Clack R (1994) A cone-beam reconstruction algorithm using shift variant filtering and cone-beam backprojection. IEEE Trans Med Imaging 13:186–195

Donoho DL, Johnstone IM, Hoch JC, Stern AS (1992) Maximum entropy and the near black object. J R Statist Ser B 54:41–81

Euler E, Wirth S, Pfeifer KJ, Mutschler W, Hebecker A (2000) 3D-imaging with an isocentric mobile C-Arm. Electromedica 68:122–126

Feldkamp LA, Davis LC, Kress JW (1984) Practical cone-beam algorithm. J Opt Soc Am A 1:612–619

Geman D, Yang C (1995) Nonlinear image recovery with half-quadratic regularization. IEEE Trans Image Processing 4:932–946

Gordon R, Bender R, Herman GT (1970) Algebraic reconstruction techniques (ART) for three-dimensional electron microscopy and X-ray photography. J Theor Biol 29:471–481

Grangeat P (1991) Mathematical framework of cone-beam 3D reconstruction via the first derivative of the Radon transform. In: Herman GT, Louis AK (eds) Mathematical methods in tomography, lecture notes in mathematics. Springer, Berlin Heidelberg New York, pp 66–97

Hounsfield GN (1973) Computerized traverse axial scanning (tomography). Part I. Description of system. Br J Radiol 46:1016–1022

Hsiao IT, Rangarajan A, Gindi G (2002) A provably convergent OS-EM like reconstruction algorithm for emission tomography. Proc SPIE 4684:10–19

Hudson HM, Larkin RS (1994) Accelerated image reconstruction using ordered subsets of projection data. IEEE Trans Med Imaging 13:601–609

Kachelriess M, Schaller S, Kalender WA (2000) Advanced single slice rebinning in cone-beam spiral CT. Med Phys 27:754–772

Kalender WA, Seissler W, Klotz E, Vock P (1990) Spiral volumetric CT with single-breathhold technique, continuous transport, and continuous scanner rotation. Radiology 176:181–183

Kudo H, Saito T (1994) Derivation and implementation of a cone-beam reconstruction algorithm for non-planar orbits. IEEE Trans Med Imaging 13:196–211

Lange K, Carson R (1984) EM reconstruction algorithms for emission and transmission tomography. J Comput Tomogr 8:306–316

Mueller K (1998) Fast and accurate three-dimensional reconstruction from cone-beam projection data using algebraic methods. PhD dissertation, Ohio State University

Persson M, Bone D, Elmqvist H (2001) Total variation norm for three-dimensional iterative reconstruction in limited view angle tomography. Phys Med Biol 46:853–866

Qi J, Leahy RM (2000) Resolution and noise properties of MAP reconstruction for fully 3-D PET. IEEE Trans Med Imaging 19:493–506

Rudin LI, Osher LI, Fatemi E (1992) Nonlinear total variation-based noise removal algorithms. Physica D 60:259–268

Schaller S, Flohr T, Steffen P (1997) New, efficient Fourier-reconstruction method for approximate image reconstruction in spiral cone-beam CT at small cone angles. SPIE Med Imag Conf Proc 3032:213–224

Shepp L, Logan BF (1974) Reconstructing interior head tissue from X-ray transmissions. IEEE Trans Nucl Sci 21:228–236

Stsepankou D, Müller U, Kornmesser K, Hesser J, Männer R (2003) FPGA-accelerated volume reconstruction from X-ray. World Conference on Medical Physics and Biomedical Engineering, Sydney, Australia

Tam KC, Samarasekera S, Sauer F (1998) Exact cone-beam CT with a spiral scan. Phys Med Biol 43:1015–1024

Tikhonov AN, Leonov AS, Yagola A (1997) Nonlinear ill-posed problems. Kluwer, Dordrecht

Toft P (1996) The radon transform: theory and implementation. PhD thesis, Department of Mathematical Modelling, Technical University of Denmark

Villain N, Goussard Y, Idier J, Allain M (2003) Three-dimensional edge-preserving image enhancement for computed tomography. IEEE Trans Med Imaging 22:1275–1287

Yan XH, Leahy RM (1992) Cone-beam tomography with circular, elliptical, and spiral orbits. Phys Med Biol 37:493–506

Yu DF, Fessler JA (2002) Edge-preserving tomographic reconstruction with nonlocal regularization. IEEE Trans Med Imaging 21:159–173

3 Processing and Segmentation of 3D Images

Georgios Sakas and Andreas Pommert

CONTENTS

3.1 Introduction

For a very long time, ranging approximately from early trepanizations of heads in Neolithic ages until little more than 100 years ago, the basic principles of medical practice did not change significantly. The application of X-rays for gathering images from the body interior marked a major milestone in the history of medicine and introduced a paradigm change in the way humans understood and practiced medicine.

The revolution introduced by medical imaging is still evolving. After X-rays, several other modalities have been developed allowing us new, different, and more complete views of the body interior: tomography (CT, MR) gives a very precise anatomically clear view and allows localization in space; nuclear medicine gives images of metabolism; ultrasound and inversion recovery imaging enable non-invasive imaging; and there are many others.

All these magnificent innovations have one thing in common: they provide images as primary information, thus allowing us to literally "see things" and to capitalize from the unmatched capabilities of our visual system. On the other hand, the increasing number of images produces also a complexity bottleneck: it becomes continuously more and more difficult to handle, correlate, understand, and archive all the different views delivered by the various imaging modalities.

Computer graphics as an enabling technology is the key and the answer to this problem. With increasing power of even moderate desktop computers, the present imaging methods are able to handle the complexity and huge data volume generated by these imaging modalities.

While in the past images were typically two-dimensional – be they X-rays, CT slices or ultrasound scans – there has been a shift towards reproducing the three-dimensionality of human organs. This trend has been supported above all by the new role of surgeons as imaging users who, unlike radiologists (who have practiced "abstract 2D thinking" for years), must find their way around complicated structures and navigate within the body (Hildebrand et al. 1996).

Modern computers are used to generate 3D reconstructions of organs using 2D data. Increasing computer power, falling prices, and general availability have already established such systems as the present standard in medicine. Legislators have also recognized this fact. In the future, medical software may be used (e.g. commercially sold) in Europe only if it displays a CE mark in compliance with legal regulations (MDD, MPG). To this end, developers and manufacturers must carry out a risk analysis in accordance with EN 60601-1-4 and must validate their software. As soon as software is used with humans, this is true also for research groups, who desire to disseminate their work for clinical use, even if they do not have commercial ambitions.

The whole process leading from images to 3D views can be organized as a pipeline. An overview of the volume visualization pipeline as presented in this chapter and in Chap. 4 is shown in Fig. 3.1. After the acquisition of one or more series of tomographic images, the data usually undergo some pre-processing such as image filtering, interpolation, and image fusion, if data from several sources are to be used. From this point, one of several paths may be followed.

G. Sakas, PhD
Fraunhofer Institute for Computer Graphics (IGD),
Fraunhoferstrasse 5, 64283 Darmstadt, Germany
A. Pommert, PhD
Institut für Medizinische Informatik (IMI),
Universitätsklinikum Hamburg-Eppendorf,
Martinistrasse 52, 20246 Hamburg, Germany

The more traditional surface-extraction methods first create an intermediate surface representation of the objects to be shown. It can then be rendered with any standard computer-graphics utilities. More recently, direct volume-visualization methods have been developed which create 3D views directly from the volume data. These methods use the full image intensity information (gray levels) to render surfaces, cuts, or transparent and semi-transparent volumes. They may or may not include an explicit segmentation step for the identification and labeling of the objects to be rendered.

Extensions to the volume visualization pipeline not shown in Fig. 3.1, but covered herein, include the visualization of transformed data and intelligent visualization.

3.2 Pre-processing

The data we consider usually comes as a spatial sequence of 2D cross-sectional images. When they are put on top of each other, a contiguous image volume is obtained. The resulting data structure is an orthogonal 3D array of volume elements or voxels each representing an intensity value, equivalent to picture elements or pixels in 2D. This data structure is called the voxel model. In addition to intensity information, each voxel may also contain labels, describing its membership to various objects, and/or data from different sources (generalized voxel model; Höhne et al. 1990).

Many algorithms for volume visualization work on isotropic volumes where the voxel spacing is equal in all three dimensions. In practice, however, only very few data sets have this property, especially for CT. In these cases, the missing information has to be approximated in an interpolation step. A very simple method is linear interpolation of the intensities between adjacent images. Higher-order functions, such as splines, usually yield better results for fine details (Marschner and Lobb 1994; Möller et al. 1997).

In windowing techniques only a part of the image depth values is displayed with the available gray values. The term "window" refers to the range of CT numbers which are displayed each time (Hemmingsson et al. 1980; Warren et al. 1982). This window can be moved along the whole range of depth values of the image, displaying each time different tissue types in the full range of the gray scale achieving this way better image contrast and/or focusing on material with specific characteristics (Fig. 3.2). The new brightness value of the pixel Gv is given by the formula:

$$Gv = \left(\frac{Gv_{\max} - Gv_{\min}}{We - Ws} \right) \cdot (Wl - Ws) + Gv_{\min}$$

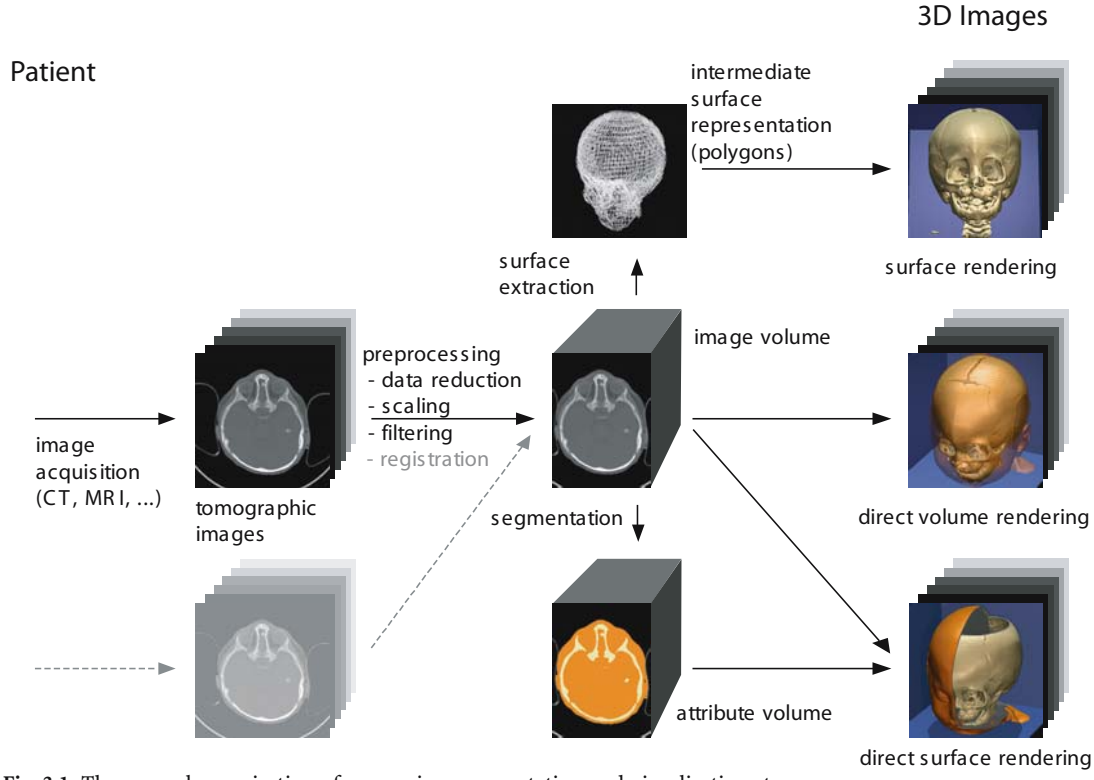

Fig. 3.1. The general organisation of processing, segmentation and visualisation steps

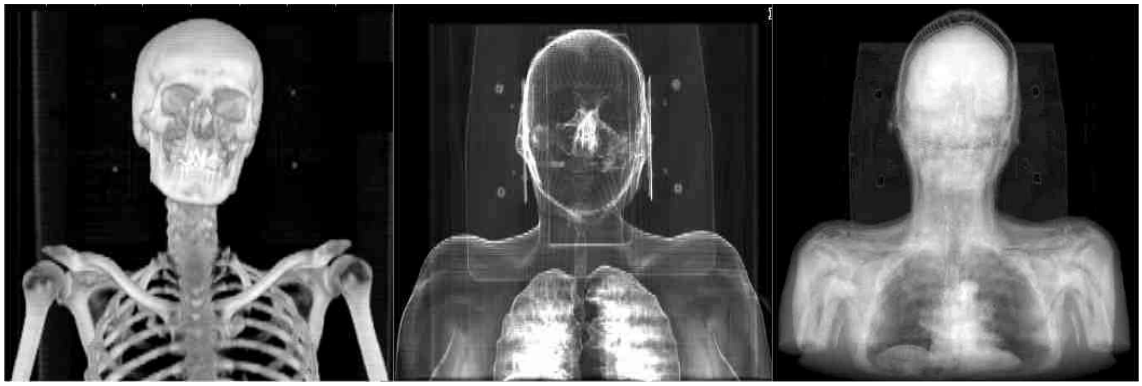

Fig. 3.2. by applying different windowing techniques different aspects of the same volume can be emphasized

where $[Gv_{max}, Gv_{min}]$, is the gray-level range, [Ws, We] defines the window width, and Wl the window center. This is the simplest case of image windowing. Often, depending on the application, the window might have more complicated forms such as double window, broken window, or non-linear windows (exponential or sinusoid or the like).

The sharpening when applied to an image aims to decrease the image blurring and enhance image edges. Among the most important sharpening methods, high-emphasis masks, unsharp masking, and high-pass filtering (Fig. 3.3) should be considered.

There are two ways to apply these filters on the image: (a) in the spatial domain using the convolution process and the appropriate masks; and (b) in the frequency domain using high-pass filters.

Generally, filters implemented in the spatial domain are faster and more intuitive to implement, whereas filters in the frequency domain require prior transformation of the original, e.g., by means of the Fourier transformation. Frequency domain implementations offer benefits for large data sets (3D volumes), whereas special domain implementations are preferred for processing single images.

Image-smoothing techniques are used in image processing to reduce noise. Usually in medical imaging the noise is distributed statistically and it exists in high frequencies; therefore, it can be stated that image-smoothing filters are low-pass filters. The drawback of applying a smoothing filter is the simultaneous reduction of useful information, mainly detail features, which also exist in high frequencies (Sonka et al. 1998).

Typical filters (Fig. 3.4) here include averaging masks as well as Gaussian and median filtering. Averaging and Gaussian filtering tend to reduce the sharpness of edges, whereas median filters preserve edge sharpness. Smoothing filters are typically implemented in the spatial domain.

In MRI, another obstacle may be low-frequency intensity inhomogeneities, which can be corrected to some extent (Arnold et al. 2001).

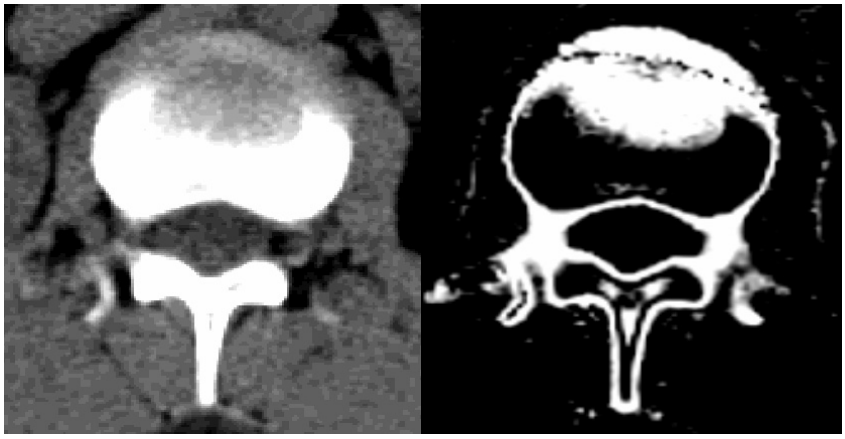

Fig. 3.3. Original CT slice (left) and contour extraction (right)

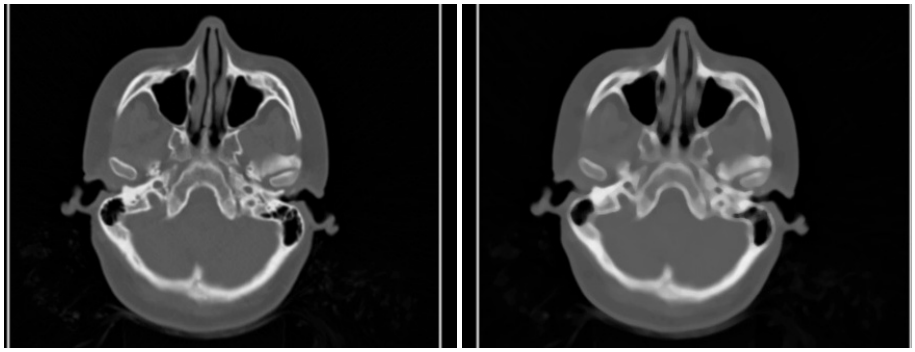

Fig. 3.4. CT image of a head (left: original image, right: after applying a median filter of size 7×7)

3.3 Segmentation

An image volume usually represents a large number of different structures obscuring each other. To display a particular one, we thus have to decide which parts of the volume we want to use or ignore. A first step is to partition the image volume into different regions, which are homogeneous with respect to some formal criteria and correspond to real (anatomical) objects. This process is called segmentation. In a subsequent interpretation step, the regions may be identified and labeled with meaningful terms such as "white matter" or "ventricle." While segmentation is easy for a human expert, it has turned out to be an extremely difficult task for the computer.

All segmentation methods can be characterized as being either binary or fuzzy, corresponding to the principles of binary and fuzzy logic, respectively (Winston 1992). In binary segmentation, the question of whether a voxel belongs to a certain region is always answered by either yes or no. This information is a prerequisite, e.g., for creating surface representations from volume data. As a drawback, uncertainty or cases where an object takes up only a fraction of a voxel (partial-volume effect) cannot be handled properly. Strict yes/no decisions are avoided in fuzzy segmentation, where a set of probabilities is assigned to every voxel, indicating the evidence for different materials. Fuzzy segmentation is closely related to the direct volume-rendering methods (see below).

Following is a selection of the most common segmentation methods used for volume visualization, ranging from classification and edge detection to recent approaches such as snakes, atlas registration, and interactive segmentation. In practice, these basic approaches are often combined. For further reading, the excellent survey on medical image analysis (Duncan and Ayache 2000) is recommended.

3.3.1 Classification

A straightforward approach to segmentation is to classify a voxel depending on its intensity, no matter where it is located. A very simple but nevertheless important example is thresholding: a certain intensity range is specified with lower and upper threshold values. A voxel belongs to the selected class if – and only if – its intensity level is within the specified range. Thresholding is the method of choice for selecting air, bone or soft tissue in CT. In direct volume visualization, it is often performed during the rendering process itself so that no explicit segmentation step is required. Image 3.5 gives such an example.

Instead of a binary decision based on a threshold, Drebin et al. use a fuzzy maximum likelihood classifier which estimates the percentages of the different materials represented in a voxel, according to Bayes' rule (Drebin et al. 1988). This method requires that the gray-level distributions of different materials be different from each other and known in advance.

A similar method is the region growing algorithm and its numerous derivates (Zucker et al. 1976). In this case the user has to select a point within a structure, which is regarded to be "characteristic" for the structure of interest. The algorithm compares the selected point with its "neighbors." If a pre-defined similarity criterion is fulfilled, the checked neighbor is accepted as new member of the data set and becomes himself a new seed point. The points selected by this method form a set, which grows to the point where no similar neighbors can be found – then the algorithm terminates.

There are numerous variations of this principal idea, which works equally in 2D and 3D space. The principal problem of this method consists in identifying neighbors with "similar", but not "good" similarity, a case common in medical imaging. In this case the growing process stops too early. In the opposite

Fig. 3.5. CT thoracic data set (left: original axial image, middle: axial image after thresholding, right: direct volume rendered 3D view after thresholding)

site, a "leakage" on the boundary of the segmented object immediately creates parasitic branches or whole structures, which obviously do not belong to the structure of interest. Additional constrains can be used for reducing this effect. A common one is to require a "smoothness" or a "continuity" of the generated region, such as continuity in curvature. Image 3.6 displays such an example: starting from a central point in the middle, the algorithm grows until it finds secure points, in this case the bone boundary in the upper and lower image half. The uncertain parts to the left and right are interpolated (middle) by requiring a concave shape connecting the upper and the lower boundary segments. A snake-approach can be user here, see also paragraph 3.3.2 below. Similarly "gaps" between vertebral bodies in 3D space can be interpolated as well.

Simple classification schemes are not suitable if the structures in question have mostly overlapping or even identical gray-level distributions, such as different soft tissues from CT or MRI. Segmentation becomes easier if multi-spectral images are available, such as T1- and T2-weighted images in MRI, emphasizing fat and water, respectively. In this case, individual threshold values can be specified for every parameter. To generalize this concept, voxels in an n-parameter data set can be considered as n-dimensional vectors in an n-dimensional feature space. This feature space is partitioned into subspaces, representing different tissue classes or organs. This is called the training phase: in supervised training, the partition is derived from feature vectors, which are known to represent particular tissues (Cline et al. 1990; Pommert et al. 2001). In unsupervised training, the partition is generated automatically (Gerig et al. 1992). In the subsequent test phase, a voxel is classified, according to the position of its feature vector in the partitioned feature space.

With especially adapted image-acquisition procedures, classification methods have successfully been applied to considerable numbers of two- or three-parametric MRI data volumes (Cline et al. 1990; Gerig et al. 1992). Quite frequently, however, isolated voxels or small regions are classified incorrectly such

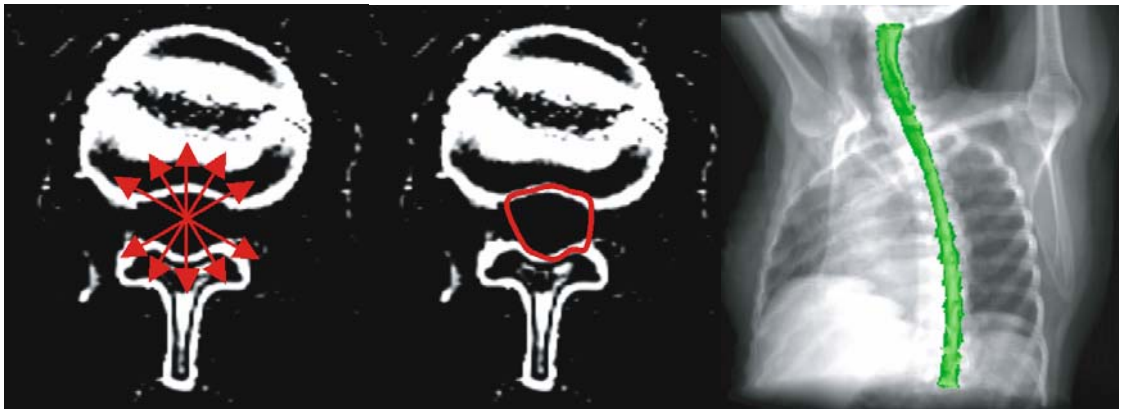

Fig. 3.6. 2D based segmentation. In case of homogeneous objects (right) and extension to 3D space is straight-forward

as subcutaneous fat in the same class as white matter. To eliminate these errors, a connected components analysis may be carried out to determine whether the voxels which have been classified as belonging to the same class are part of the same (connected) region. If not, some of the regions may be discarded.

Instead of intensity values alone, tissue textures may be considered, which are determined using local intensity distributions (Saeed et al. 1997). A survey of intensity-based classification methods is presented by Clarke et al. (1995).

3.3.2 Edge Detection

Another classic approach to segmentation is the detection of edges, using first or second derivatives of the 3D intensity function. These edges (in 3D, they are actually surfaces; it is, however, common to refer to them as edges) are assumed to represent the borders between different tissues or organs.

There has been much debate over what operator is most suitable for this purpose. The Canny operator locates the maxima of the first derivative (Canny 1986). While the edges found with this operator are very accurately placed, all operators using the first derivative share the drawback that the detected contours are usually not closed, i.e., they do not separate different regions properly. An alternative approach is to detect the zero crossings of the second derivative. With a 3D extension of the Marr-Hildreth operator, the complete human brain was segmented and visualized from MRI for the first time (Bomans et al. 1987). A free parameter of the Marr-Hildreth operator has to be adjusted to find a good balance between under- and oversegmentation.

Snakes (Kass et al. 1987) are 2D image curves that are adjusted from an initial approximation to image features by a movement of the curve caused by simulated forces (Fig. 3.7). Image features produce the so-called external force. An internal tension of the curve resists against highly angled curvatures, which makes the Snakes' movement robust against noise. After a starting position is given, the snake adapts itself to an image by relaxation to the equilibrium of the external force and internal tension. To calculate the forces an external energy has to be defined. The gradient of this energy is proportional to the external force. The segmentation by Snakes is due to its 2D definition performed in a slice-by-slice manner, i.e., the resulting curves for a slice are copied into the neighboring slice and the minimization is started again. The user may control the segmentation process, by stopping the automatic tracking, if the curves run out of the contours and define a new initial curve.

3.3.3 2.5-D Boundary Tracking

The main drawback of the above-mentioned method is its typical limitation to 2D structures; thus, the snakes (Fig. 3.8) work well on a plane image but do not capitalize from the principal coherence of structures in the 3D space. The "boundary tracking" (BT) algorithm tries to encompass this difficulty. The main assumption of BT is that the shape of an organ does not change significantly between adjacent slices; thus,

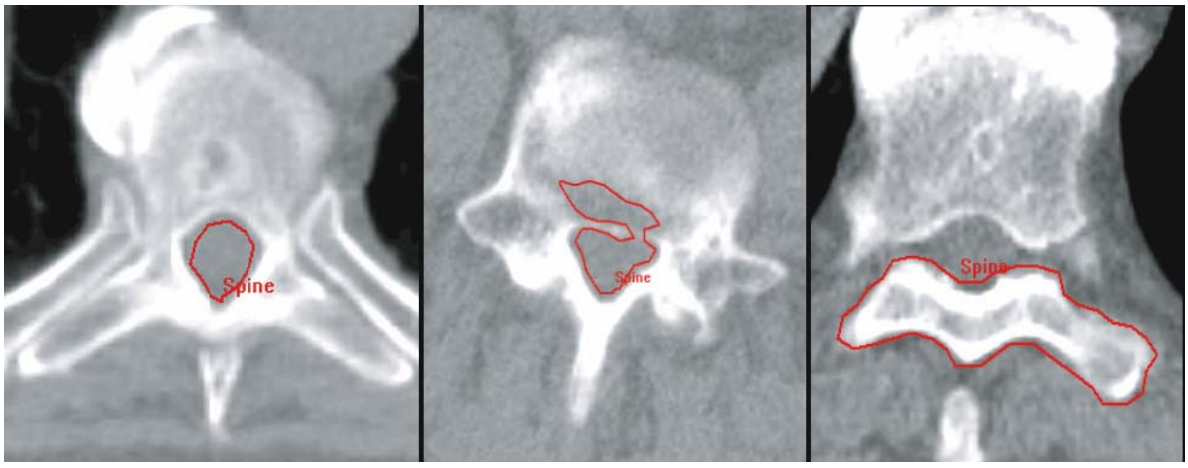

Fig. 3.7. The principle of segmentation using Snakes. The spinal canal in the left image has been correctly identified, whereas in the middle and the right examples the algorithm tracked the wrong boundary!

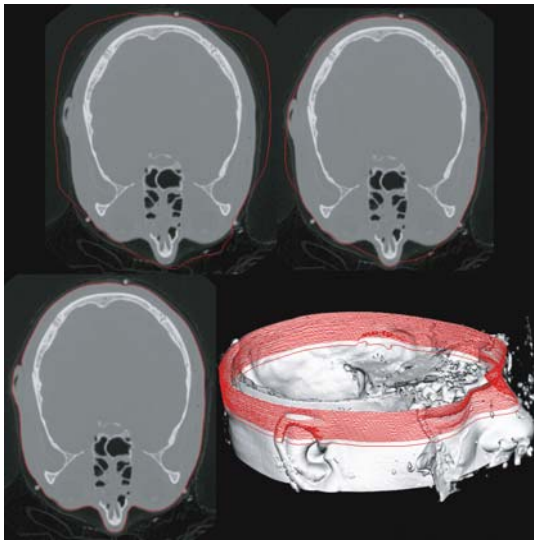

Fig. 3.8. Adaptation of a snake on one slice and propagation to the next slice

a contour found on one slice can be copied in the subsequent one as a reasonable approximation of the new shape. The snake algorithm is then re-started in order to fine-tune and adjust this initial approximation on the new slice until the whole data set has been processed (Herman 1991).

The quality of the result depends fundamentally on the similarity of two adjacent slices. Normally, this varies within a data set. This can be partly compensated by re-estimating the initial value for each new-segmented shape. However, this is not always possible; therefore, in regions with low similarity, the slices to be segmented by the interactive method must be selected tightly.

An alternative method is a combination of 2D and 3D approach. The segmentation approach works at one image level at a time in order to find a local contour, and once this has been done, the found structure "jumps" on the next slice in the volume. In the case of tomographic modalities, such as CT and MRI, the algorithm is applied on the original (axial) cross-sectional images. The algorithm requires an initial point to start the tracing of the edge of the object under investigation. The initial point travels to the vertical or horizontal direction until and edge of the investigated object is reached (region growing). Then the algorithm will start to exam the surrounding pixel of that edge and check whether they belong to the current edge or not. The algorithm uses a constant threshold selection. Once the shape is filled, the "mid-point" (center of gravity for convex shapes, center of largest included ellipse for concave ones) of the shape is copied as the starting value on the next slice and the process starts again. If on the slice under investigation a shape fulfilling the constrains can not be found, the slice is temporally ignored and the same process is applied on the next slice etc. When a valid contour is found, intermediate shapes for the ignored slices are calculated by shape interpolation and the gap is filled, in other case the algorithm terminates. This process has been used in the example of figure 3.6 for 3D-segmentation of the spinal canal on the right image.

The main drawback of the BT is that it is a binary approach and hence is very sensitive to gray-value variations. If the threshold value is not selected properly, the system will fail to detect the appropriate shape. An error that usually occurs is when the user attempts to define the starting point for the algorithm: e.g. selecting a good point is possible on image 3.6 left, but impossible in the middle slice. Due to the restrictions of the BT mentioned above, in this case it is not possible to initialize the tracing process from an arbitrary slice. Due to this limitation, the user must be trained under the trial-and-error principle until the desired contour is found.

3.3.4 Geodesic Active Contours

Generally, geodesic active contours (GAC) is based on fast marching and level sets. The GAC expects two inputs, the initial level set (zero level set) and a feature image (edge image), and works in 2D and 3D data sets. Following the forces defined by the edge image, the level set iteratively approximates the area to be segmented. The result is binarized by thresholding and the binary image is overlapped in the 2D view. The processing of the original MR images is schematically described in Fig. 3.9. Usually an anisotropic diffusion filter is used to reduce noise in MR images. A sigmoid filter for contrast enhancement shows the interesting edges. After a gradient-magnitude (edge detection) filter, a second sigmoid filter is used to inverse the image.

In addition to this automated image pre-processing, a number of seed points have to be selected in the data. Approximately 10–15 seed points located within the liver are used in this example. These seed points can be placed within one or more slices. In addition, we generate a potential distance map around each image contour. With these two inputs a fast-marching algorithm is started generating all level sets, includ-

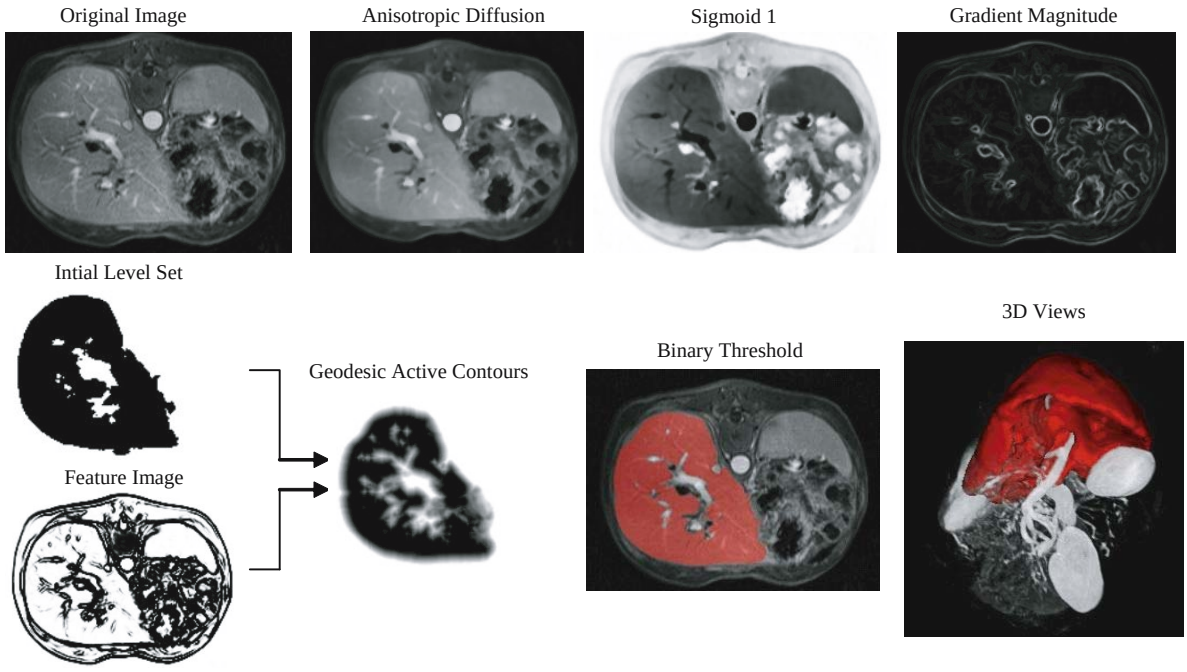

Fig. 3.9. Result of a liver segmentation based on MRI. Fast marching produces the initial level set and the GAC algorithm segments the contour of the liver.

ing the zero level set, which is used for the starting point called initial level set. The process is described in detail in Caselles (1997).

3.3.5 Extraction of Tubular Objects

For the segmentation of tubular objects, such as vessels, specialized segmentation algorithms have been developed (Kirbas et al. 2003). These techniques take into account the geometrical structure of the objects that have to be segmented. Besides conventional approaches, such as pattern-recognition techniques (e.g., region growing, mathematical morphology schemes), or model-based approaches (e.g., deformable models, generalized cylinders) there is the group of tracking-based algorithms. The latter ones start usually from a user-given initial point and detect the center line and the boundaries by finding edges among the voxels orthogonal to the tracking direction. Prior to the segmentation step, the data are pre-processed for lowering noise and enhancing edges within the image. The most sophisticated tracking-based algorithms generate a twofold output, the center line as well as the boundaries of the tubular object (Fig. 3.10), allowing for a further analysis of the segmented structure. That output may be generated in a single step (Verdonck et al. 1995) or in an iterative manner where first an approximate estimation of the center line is computed and afterwards corrected repeatedly by detecting the boundaries orthogonal to that line (Wesarg et al. 2004).

3.3.6 Atlas Registration

A more explicit representation of prior knowledge about object shape are anatomical atlases (see below). Segmentation is based on the registration of the image volume under consideration with a prelabeled volume that serves as a target atlas. Once the registration parameters are estimated, the inverse transformation is used to map the anatomical labels back on to the image volume, thus achieving the segmentation.

In general, these atlases do not represent one individual – but "normal" –anatomy and its variability in terms of a probabilistic spatial distribution, obtained from numerous cases. Methods based on atlas registration were reported suitable for the automatic segmentation of various brain structures, including lesions and objects poorly defined in the image data (Arata et al. 1995; Collins et al. 1999; Kikinis et al. 1996); however, registration may not be very ac-

Fig. 3.10. Tracking-based segmentation of coronary arteries in cardiac CT data sets (left: vessel boundary, right: colour-coded centreline corresponding to the vessel's diameter)

curate. For improved results, atlas registration may be complemented with intensity-based classification (Collins et al. 1999).

3.3.7 Interactive Segmentation

Even though there are a great variety of promising approaches for automatic segmentation, "… no one algorithm can robustly segment a variety of relevant structures in medical images over a range of datasets" (Duncan and Ayache 2000). In particular, the underlying model assumptions may not be flexible enough to handle various pathologies; therefore, there is currently a strong tendency to combine simple, but fast, operations carried out by the computer with the unsurpassed recognition capabilities of the human observer (Olabarriaga and Smeulders 2001).

A practical interactive segmentation system was developed by Höhne and Hanson (1992) and later extended to handle multiparametric data (Pommert et al. 2001; Schiemann et al. 1997). Regions are initially defined with thresholds. The user can subsequently apply connected components analysis, volume editing tools, or operators from mathematical morphology. Segmentation results are immediately visualized on orthogonal cross-sections and 3D images in such a way that they may be corrected or further refined in the next step. With this system, segmentation of gross structures is usually a matter of minutes (Fig. 3.11).

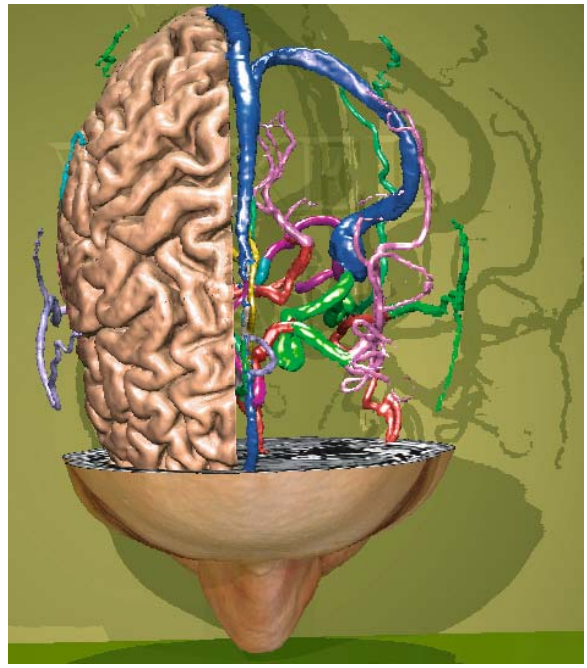

Fig. 3.11. Results of interactive segmentation of MRI (skin, brain) and Magnetic Resonance Angiography (vessels) data.

References

References for this chapter are included in the References for chapter 4.

4 3D Visualization

Georgios Sakas and Andreas Pommert

CONTENTS

4.1 Introduction

After segmentation, the choice of which rendering technique to use must be made. The more traditional surface-based methods first create an intermediate surface representation of the object to be shown. It may then be rendered with any standard computer graphics method. More recently, volume-based methods have been developed which create a 3D view directly from the volume data. These methods use the full gray-level information to render surfaces, cuts, or transparent and semi-transparent volumes. As a third way, transform-based rendering methods may be used.

G. Sakas, PhD
Fraunhofer Institute for Computer Graphics (IGD),
Fraunhoferstr 5, 64283 Darmstadt, Germany
A. Pommert, PhD
Institut für Medizinische Informatik (IMI),
Universitätsklinikum Hamburg-Eppendorf,
Martinistraße 52, 20246 Hamburg, Germany

4.2 Cut Planes

Once a surface view is available, a very simple and effective method of visualizing interior structures is cutting. When the original intensity values are mapped onto the cut plane, they can be better understood in their anatomical context (Höhne et al. 1990). A special case is selective cutting, where certain objects are left untouched (Fig. 4.1).

4.3 Surface Rendering

Surface rendering bridges the gap between volume visualization and more traditional computer graphics (Foley et al. 1995; Watt 2000). The key idea is to create intermediate surface descriptions of the relevant objects from the volume data. Only this information is then used for rendering images. If triangles are used as surface elements, this process is called triangulation.

An apparent advantage of surface extraction is the potentially very high data reduction from volume to surface representations. Resulting computing times can be further reduced if standard data structures, such as polygon meshes, are used which are supported by standard computer graphics hard- and software.

On the other hand, the extraction step eliminates most of the valuable information on the cross-sectional images. Even simple cuts are meaningless because there is no information about the interior of an object, unless the image volume is also available at rendering time. Furthermore, every change of surface definition criteria, such as adjusting a threshold, requires a recalculation of the whole data structure.

The classic method for surface extraction is the marching-cubes algorithm, developed by Lorensen and Cline (1987). It creates an iso-surface, approximating the location of a certain intensity value in the data volume. This algorithm basically considers cubes

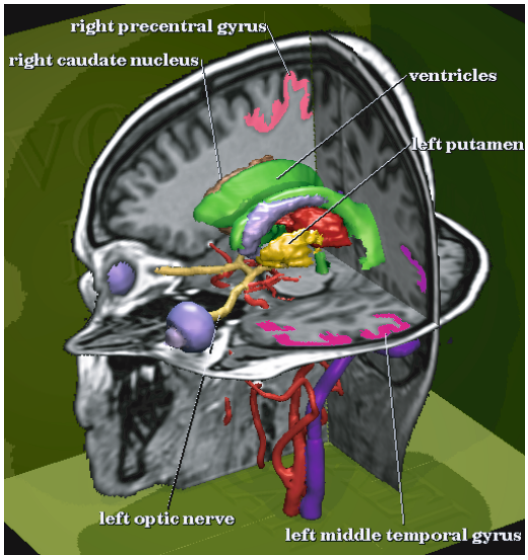

Fig. 4.1. Brain from MRI. Original intensity values are mapped onto the cut planes.

of 2×2×2 contiguous voxels. Depending on whether one or more of these voxels are inside the object (i.e., above a threshold value), a surface representation of up to four triangles is placed within the cube. The exact location of the triangles is found by linear interpolation of the intensities at the voxel vertices. The result is a highly detailed surface representation with sub-voxel resolution (Fig. 4.2).

Various modifications of the marching-cubes algorithm have been developed; these include the correction of topological inconsistencies (Natarajan 1994), and improved accuracy by better approximating the true isosurface in the volume data, using higher order curves (Hamann et al. 1997) or an adaptive refinement (Cignoni et al. 2000).

As a major practical problem, the marching-cubes algorithm typically creates hundreds of thousands of triangles when applied to clinical data. As has been shown, these numbers can be reduced considerably by a subsequent simplification of the triangle meshes (Cignoni et al. 1998; Schroeder et al. 1992; Wilmer et al. 1992).

4.4 Direct Volume Visualization Methods

In direct volume visualization, images are created directly from the volume data. Compared with surface-based methods, the major advantage is that all gray-level information which has originally been acquired is kept during the rendering process. As shown by Höhne et al. (1990) this makes it an ideal technique for interactive data exploration. Threshold values and other parameters which are not clear from the beginning can be changed interactively. Furthermore, volume-based rendering allows a combined display of different aspects such as opaque and semi-transparent surfaces, cuts, and maximum intensity projections. A current drawback of direct volume visualization is that the large amount of data which has to be handled allows only limited real-time applications on present-day computers.

4.4.1 Scanning the Volume

In direct volume visualization, we basically have the choice between two scanning strategies: pixel by pixel (image order) or voxel by voxel (volume order). These strategies correspond to the image and object order rasterization algorithms used in computer graphics (Foley et al. 1995).

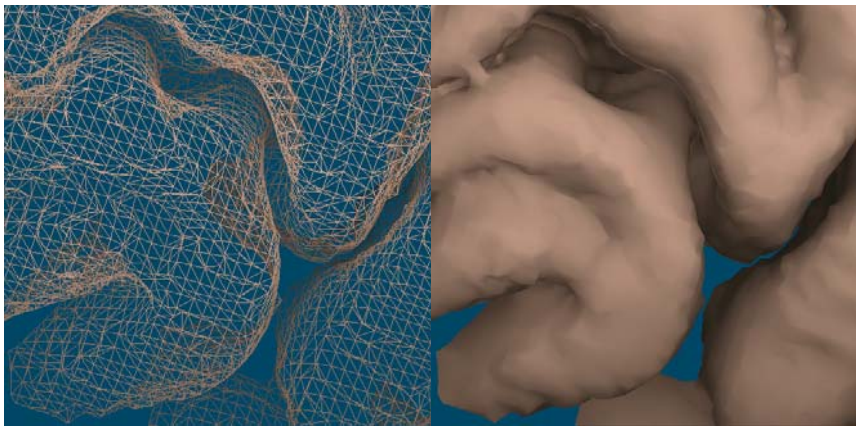

Fig. 4.2. Triangulated (*left*) and shaded (*right*) portion of the brain from MRI, created with the marching-cubes algorithm

In image order scanning, the data volume is sampled on rays along the viewing direction. This method is commonly known as ray casting.The principle is illustrated in Fig. 4.3. At the sampling points, the intensity values are interpolated from the neighboring voxels, using tri-linear interpolation or higher-order curves (Marschner and Lobb 1994; Möller et al. 1997). Along the ray, visibility of surfaces and objects is easily determined. The ray can stop when it meets an opaque surface. Yagel et al. (1992) extended this approach to a full ray-tracing system, which follows the viewing rays as they are reflected on various surfaces. Multiple light reflections between specular objects can thus be handled.

Image-order scanning can be used to render both voxel and polygon data at the same time, known as hybrid rendering (Levoy 1990). Image quality can be adjusted by choosing smaller (oversampling) or wider (undersampling) sampling intervals (Pommert 2004). Unless stated otherwise, all 3D images shown in this chapter were rendered with a ray-casting algorithm.

As a drawback, the whole input volume must be available for random access to allow arbitrary viewing directions. Furthermore, interpolation of the intensities at the sampling points requires a high computing power. A strategy to reduce computation times is based on the observation that most of the time is spent traversing empty space, far away from the objects to be shown. If the rays are limited to scanning the data, only within a pre-defined bounding volume around these objects, scanning times are greatly reduced (Šrámek and Kaufman 2000; Tiede 1999; Wan et al. 1999).

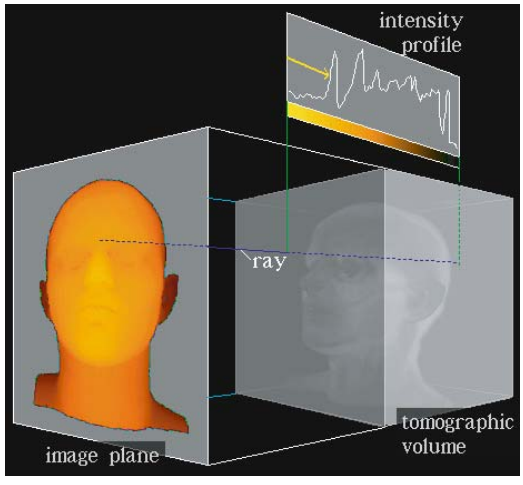

Fig. 4.3. Principle of ray casting for volume visualization. In this case, the object surface is found using an intensity threshold.

In volume-order scanning, the input volume is sampled along the lines and columns of the 3D array, projecting a chosen aspect onto the image plane in the direction of view. The volume can either be traversed in back-to-front (BTF) order from the voxel with maximal distance to the voxel with minimal distance to the image plane, or vice versa in front-to-back (FTB) order. Scanning the input data as they are stored, these techniques are reasonably fast even on computers with small main memories; however, implementation of display algorithms is usually much more straightforward using the ray-casting approach.

4.4.2 Splatting in Shear-Warp Space

The shear-warp factorization-rendering algorithm belongs to the fastest object space-rendering algorithms. The advantages of shear-warp factorization are that sheared voxels are viewed and projected only along ±X, ±Y, and ±Z axis, i.e., along the principal viewing directions in sheared object space, rather than an arbitrary viewing direction, which makes it possible to traverse and accumulate slice by slice. Neighbor voxels share the same footprint and are exactly one pixel apart.

In the original shear-warp algorithm (Lacroute and Levoy 1994) only slices are sheared rather than each voxel itself (see the dotted line in Fig. 4.4, left). In other words, slices are displaced (sheared) relatively to each other, but the voxels within each slice are remaining orthogonal cubes. We call this case "projective shear warp" in order to discriminate it from "splatting shear warp" introduced in Cai and Sakas (1998).

In splatting shear warp the mathematically correct shear of the object space is calculated. The complete data set is regarded to be a continuous space sheared by the shearing transformation; thus, each voxel is sheared as well, resulting in parallelepipeds rather than cubes. Therefore, the projection area of a voxel is now in general greater than 1.0. This difference is illustrated in Fig. 4.4 (right: in projective shear-warp pixel A only accumulates the value of voxel *i+1* (dashed line). In splatting shear warp instead, pixel A accumulates values from both voxel *i* and *i+1* (solid line). The implication of this is that in the latter case a sub-voxel splatting sampling calculation according to an individual splatting table (footprint) becomes necessary.

The general footprint table is established by digitizing and scanning the 2×2 shear footprint area under different reconstruction kernel, as seen in Fig. 4.5.

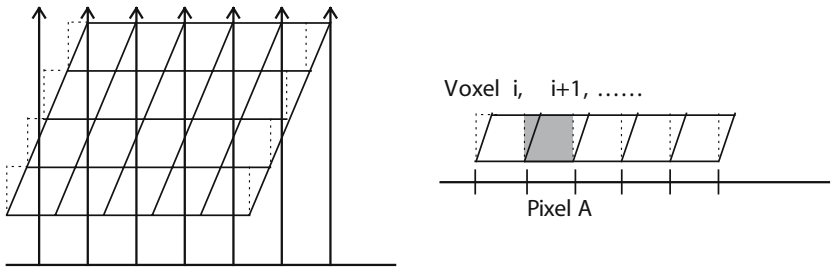

Fig. 4.4 .The difference between voxel splatting and projection in shear warp

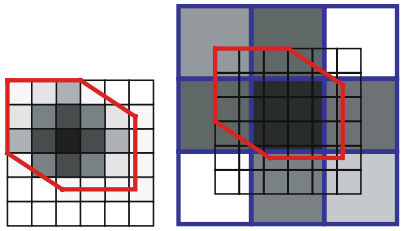

Fig. 4.5. Shear footprint and its convolution matrix

The size of the table is 2N×2N, where N×N is the digitization degree, i.e., the number of subpixels within one pixel, which is usually selected between 10 and 20 or even more, depending on the required accuracy. The weight of each subpixel is calculated by employing the integral of next equation at the mid-point of the subpixel.

$$W_i = \int_{Z_0}^{Z_1} h_v(x_0, y_0, z)dz$$

where (x_0, y_0) is the center of subpixel, $h_v(x, y, z)$ is the volume reconstruction kernel, and (Z_0, Z_1) is the integral range. In Cai and Sakas (1998) , different digitally reconstructed radiography (DRR) rendering algorithms, ray casting, projective shear warp, and splattering shear warp, are compared with each other under different sampling methods, nearest-neighbor interpolation, and tri-linear interpolation.

4.5 Visualization Primitives in Direct Volume Rendering

Once one decides the principal traversing method (FTB or BTF) and chooses a principal algorithm (ray casting or splatting), one is able to traverse the volume visiting the voxels of interest. Now a decision has to be taken about how the value (density, material, property, etc.) represented by each voxel will be transferred to visible characteristics on the image place. The following sections summarize the methods most commonly used in medical applications.

4.5.1 Maximum and Minimum Intensity Projection

For small bright objects, such as vessels from CT or MR angiography, maximum intensity projection (MIP) is a suitable display technique (Fig. 4.6). Along each ray through the data volume, the maximum gray level is determined and projected onto the imaging plane. The advantage of this method is that neither segmentation nor shading are needed, which may fail for very small vessels. But there are also some drawbacks: as light reflection is totally ignored, maximum intensity projection does not give a realistic 3D impression. Sampling

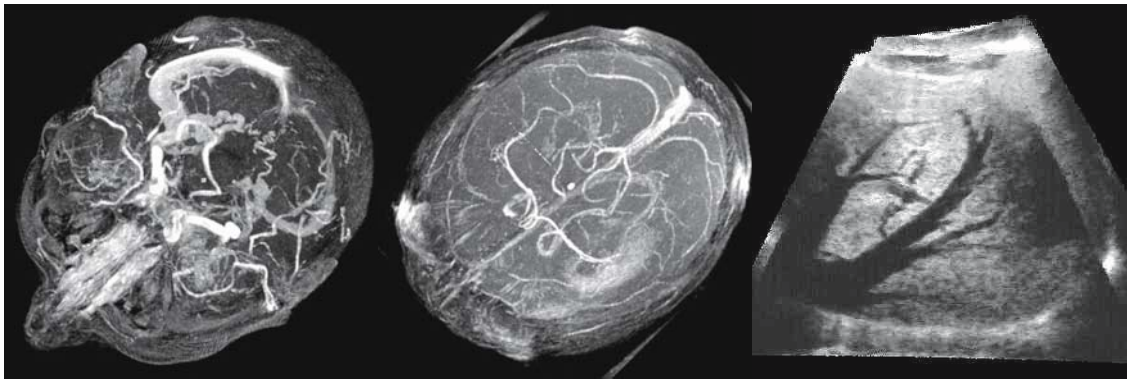

Fig. 4.6. Maximum intensity projection for brain (*left*, *middle*) and minimum intensity projection for US vessels (*right*)

of small vessels can be subject to errors, accurate and fast solutions to this problem have been proposed in (Sakas, 1995). Spatial perception can be improved by real-time rotation (Mroz et al. 2000) or by a combined presentation with other surfaces or cut planes (Höhne et al. 1990).

4.5.2 Digitally Reconstructed Radiographies

The optical model in DRR volume rendering is the so-called absorption only (Max 1995), in which particles only absorb the energy of incident light. If I_0 is the intensity of incident ray, the light intensity after penetrating distance s within the medium is

$$I(s) = I_0 \exp(-\int_0^s K_\lambda(t)dt)$$

where K_λ is the attenuation coefficient and λ is the wavelength.

In Fig. 4.7, the intensity when the ray arrives at the screen is

$$I_p = I_0 * (1-T) + I_{background} * T$$

where $T = \exp(\Gamma(P_0 P_1))$ is the transparency and

$$\Gamma(P_0 P_1) = \int_{P_0}^{P_1} K_\lambda(t)dt$$

is the optical length.

The main computation cost in DRR volume rendering is to calculate the integration of optical length, i.e.,

$$\Gamma(s) = \sum K_\lambda(s)\Delta s,\ s \in [p_0, p_1]$$

where $\Delta s = L/N, L = |P_0 P_1|$ and N is the number of sampling points (consider even distance sampling). Thus,

$$\Gamma(s) = \frac{L}{N}\sum_{i=0}^{N} K_\lambda(i) = L(\frac{1}{N}\sum_{i=0}^{N} K_{\lambda,m}\rho)$$

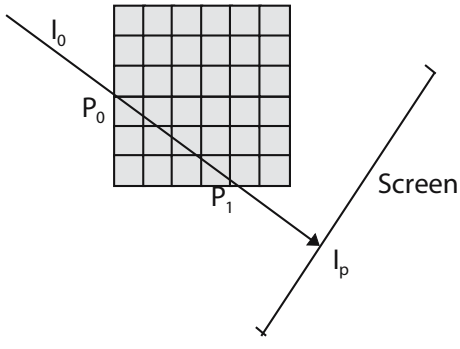

Fig. 4.7. X-ray optical model

where $K_{\lambda,m}$ is the mass attenuation coefficient and ρ is the density. See Cai and Sakas (1999) for a discussion of the transfer functions.

DRRs are extremely useful in numerus medical applications. Figure 4.8 shows examples of DRRs generated from CT data for a virtual cancer treatment simulation (Cai 1999, Cai 2000, Zamboglou 2003, Zamboglou 2004). Most of the DRR rendering algorithms are ray casting (called X-ray casting), which is image space-rendering algorithm; however, also shear-warp algorithms can be used. They have superior speed, however algorithmic advantages.

4.5.3 Direct Surface Rendering

Using one of the scanning techniques described, the visible surface of an object can be rendered directly from the volume data. This approach is called direct surface rendering (DSR). To determine the surface position, a threshold or an object membership label may be used, or both may be combined to obtain a highly accurate iso-surface (Pommert 2004; Tiede et al. 1998; Tiede 1999). Typically with CT data a threshold value is employed for extracting the location of the surface, whereas the local gradient approximates the surface normally used for shading. Note that the position of the observer may also be inside the object, thus creating a virtual endoscopy.

For realistic display of the surface, one of the illumination models developed in computer graphics may be used. These models, such as the Phong shading model, take into account both the position and type of simulated light sources, as well as the reflection properties of the surface (Foley et al. 1995; Watt 2000). A key input into these models is the local surface inclination, described by a normal vector perpendicular to the surface. Depending on the selected threshold, skin or bone or other surfaces can be visualized without having to explicitly segment them in a pre-processing step. Fig. 4.9 left and middle shows examples of direct volume rendering from CT and MRI datasets displaying the possibilities of displaying surfaces of various impression.

As shown by Höhne and Bernstein (1986), a very accurate estimate of the local surface normal vectors can be obtained from the image volume. Due to the partial-volume effect, the intensities in the 3D neighborhood of a surface voxel represent the relative proportions of different materials inside these voxels. The surface inclination is thus described by the local gray-level gradient, i.e., a 3D vector of the partial derivatives. A number of methods to calculate the gray-level gradient are

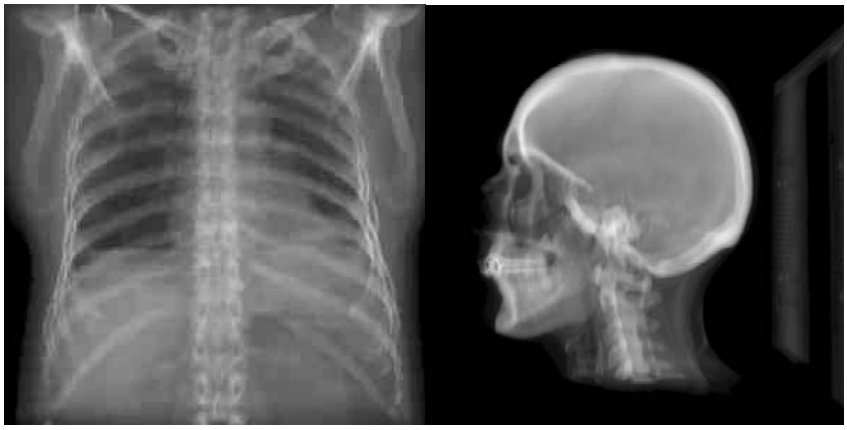

Fig. 4.8. Digitally reconstructed radiography (DRR) generated from CT data sets

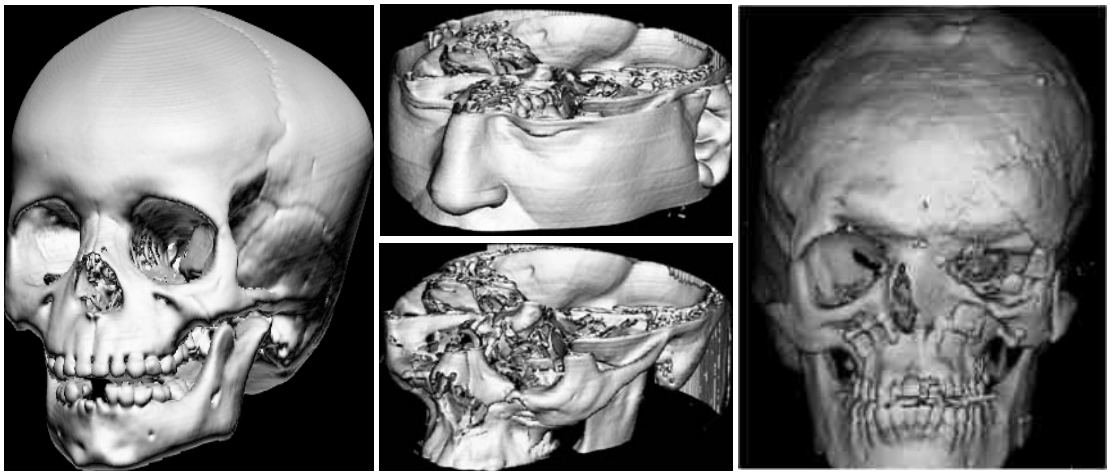

Fig. 4.9. Direct rendering shaded volume from CT and MRI data. Left and middle surface rendering, right semi-transparent rendering

presented and discussed elsewhere (Marschner and Lobb 1994; Tiede et al. 1990; Tiede 1999).

4.5.4 Direct Semi-Transparent Volume Rendering

Direct volume rendering (DVR), or volume rendering for short, is the visualization equivalent of fuzzy segmentation (see section 1.2.2). For medical applications, these methods were first described by Drebin et al. (1988) and Levoy (1988). A commonly assumed underlying model is that of a colored, semi-transparent gel with suspended reflective particles. Illumination rays are partly reflected and change color while traveling through the volume.

Each voxel is assigned a color and opacity. This opacity is the product of an object-weighting function and a gradient-weighting function. The object-weighting function is usually dependent on the intensity, but it can also be the result of a more sophisticated fuzzy segmentation algorithm. The gradient-weighting function emphasizes surfaces for 3D display. All voxels are shaded, using, for example, the gray-level gradient method. The shaded values along a viewing ray are weighted and summed up.

A simplified recursive equation which models frontal illumination with a ray-casting system is given as follows:

I	intensity of reflected light
p	index of sampling point on ray (0 . . . max. depth)
L	fraction of incoming light (0.0 . . . 1.0)
α	local opacity (0.0 . . . 1.0)
s	local shading component

$$I(p,L) = \alpha(p)Ls(p) + (1.0-\alpha(p))I(p+1,(1.0-\alpha(p))L)$$

The total reflected intensity as displayed on a pixel of the 3D image is given as *I (0, 1.0)*. Since binary de-

cisions are avoided in volume rendering, the resulting images are very smooth and show a lot of fine details, see e. g. the shape of the fine heart vessels in Fig. 4.10. Another advantage is that even coarsely defined objects can be rendered (Tiede et al. 1990). On the other hand, the more or less transparent images produced with volume rendering are often hard to understand so that their value is sometimes questionable. To some extent, spatial perception can be improved by rotating the object.

Concluding, all visualization methods listed here have benefits and drawbacks and emphasize different aspects of the examined dataset as shown in Fig. 4.12. A selection of the "correct" method has to be done by the end-user on a case-by-case basis.

4.5.5 Volume Rendering Using Transfer Functions

An improvement over conventional semi-transparent rendering is the use of transfer functions for assigning optical properties such as color and opacity to the original values of the data set as shown on Fig. 4.11. If, for instance, the true colors for the organs that are included in the rendered scene are known, a very realistic rendering result can be obtained. For that, the relationship between CT number (Hounsfield unit), gray, red, green, and blue values of the tissues, and their refractive indices have to be retrieved (Biswas and Gupta 2002). As a result of those measurements a table that assigns CT number to gray, red, green, and blue values describing the corresponding relations for different parts of the body (brain, abdomen, thorax, etc.) can be compiled. Direct volume rendering using a color transfer function that is based on such a table reflects more or less the true colors of the tissue.

An extension of the assignment of color or opacity only to gray value that represents in fact a 1D transfer function is the usage of multi-dimensional transfer functions (Kniss et al. 2002). There, in addition to a voxel's scalar value, the first and second derivative of the image data set are taken into account. This allows for a better separation of different tissues for the purpose of direct volume rendering; however, using multi-dimensional transfer functions requires interacting in a multi-dimensional space. This task can be facilitated dramatically if those transfer functions are generated semi-automatically (Kindlmann and Durkin 1998). It has been shown that using multi-dimensional transfer functions for assigning opacity in direct volume rendering results in a smoother and more "correct" visualization of the image data, since complex boundaries are better separated from each other than if only a 1D transfer function is used.

4.6 Transform-Based Rendering

While both surface extraction and direct volume visualization operate in a 3D space, 3D images may be created from other data representations as well. One

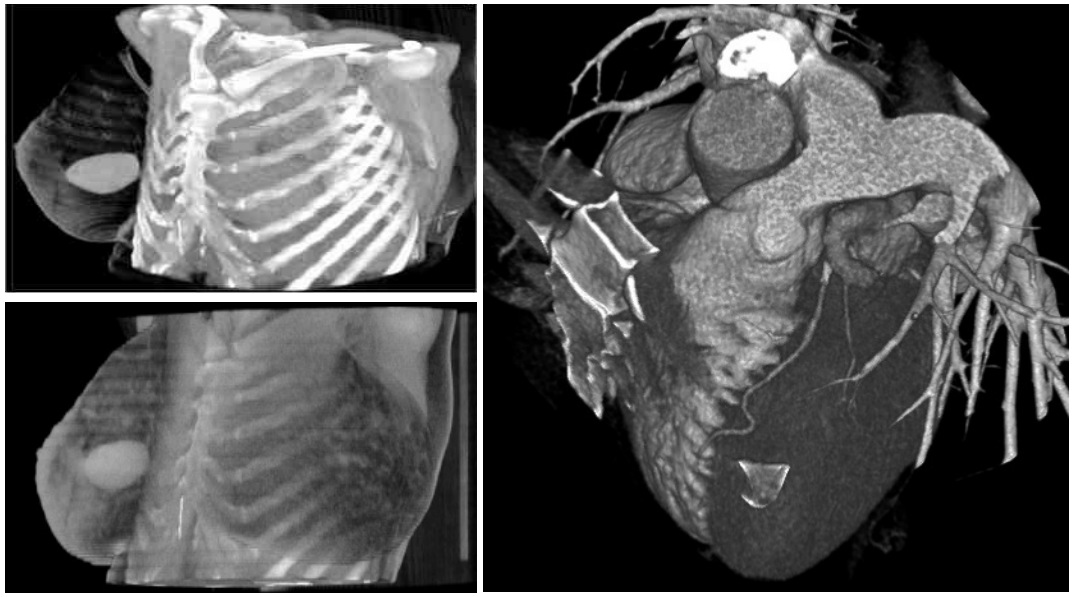

Fig. 4.10. Direct semi-transparent volume rendering technique

Fig. 4.11. Direct volume-rendered shaded cardiac CT data set using a color transfer function based on the measured true colors of the thoracic tissue

Fig. 4.12. Comparison of surface, maximum intensity projection, DRR, and semi-transparent rendering for the same data set. Each method emphasizes different aspects of the data set.

such method is frequency domain volume rendering, which creates 3D images in Fourier space, based on the projection-slice theorem (Totsuka and Levoy 1993). This method is very fast, but the resulting images are somewhat similar to X-ray images, lacking real depth information.

The Fourier projection slice theorem states that the inverse transformation of a slice extracted from the frequency domain representation of a volume results in a projection of the volume, in a direction perpendicular to the slice. Based on this theorem, the description of the FDR can be summarized in the following three steps (Fig. 4.13):

1. Transformation of the 3D volume from spatial domain to the frequency domain, using an FFT. Supposing that f(x, y, z) is the description of the volume in spatial domain, the resulting volume F(i, j, k) in frequency domain will be taken, with the application of the 3D fast Fourier transformation:

   $$F(i, j, k) = \sum_{x=0}^{N-1} \sum_{y=0}^{N-1} \sum_{z=0}^{N-1} f(x, y, z)\exp[-\mathrm{i}2\pi(ix+jy+kz)/N]$$

   where $\mathrm{i} = \sqrt{-1}$ and i, j, and k vary from 0 to N-1.

2. Extraction of a 2D slice from the 3D spectrum along a plane which includes the origin and is perpendicular to the viewing plane, resulting in an F(u, v) slice.

3. Inverse transformation of the 2D extracted spectrum to the spatial domain using a 2D IFFT:

   $$f(l, m) = \frac{1}{N} \sum_{u=0}^{N-1} \sum_{v=0}^{N-1} F(u, v)\exp[\mathrm{i}2\pi(ul + vm))/N]$$

   where $\mathrm{i} = \sqrt{-1}$ and l, m vary from 0 to N-1.

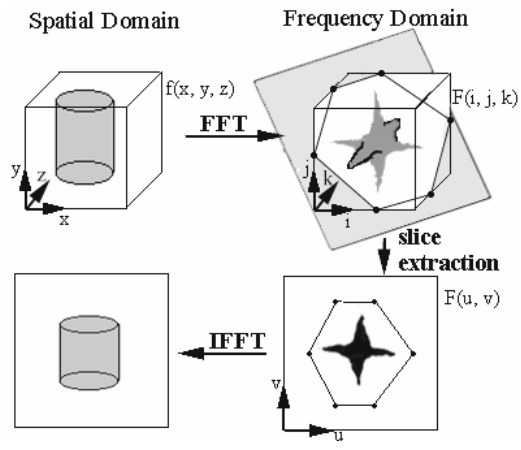

Fig. 4.13. General description of the frequency domain volume rendering method

The time-consuming 3D FFT is a data pre-processing step that is done only once and is finished before rendering; thus, the rendering time consists of the costs from the second and third steps.

A more promising approach is wavelet transforms. These methods provide a multi-scale representation of 3D objects, with the size of represented detail locally adjustable. The amount of data and rendering times may thus be reduced dramatically. Application to volume visualization is shown by He et al. (1998).

4.7 Image Fusion

For many applications, it is desirable to combine or fuse information from different imaging modalities. For example, functional imaging techniques, such as magnetoencephalography (MEG), functional MRI (fMRI), or PET, show various physiological aspects but give little or no indication for the localization of the observed phenomena. For their interpretation, a closely matched description of the patient's morphology is required, as obtained by MRI. Considering only soft tissue anatomy, bone morphology or functional information in separate 3D data sets is not sufficient anymore in clinical practice. Pre-processing and visualizing all this complex information in a way that is easy to handle for clinicians is required to exploit the benefit of the unique clinical information of each of the modalities.

In general, image volumes obtained from different sources do not match geometrically (Fig. 4.14). Variations in patient orientation and differences in resolution and contrast of the modalities make it almost impossible for a clinician to mentally fuse all the image information accurately. It is therefore required to transform one volume with respect to the other, i.e., in a common coordinate frame. This process is known as image registration.

Image registration can be formulated as a problem of minimizing a cost function that quantifies the match between the images of the two modalities. In order to determine this function, different common features of those images can be used. Maintz and Viergever (1998) and van den Elsen et al. (1993) have given detailed surveys about the classification of the registration process. Maintz et al. describe the classification of the registration procedures based on nine different criteria:

1. The dimensionality (e.g., 3D to 3D or 2D to 3D)
2. The nature of the registration basis (e.g., intrinsic or extrinsic)
3. The nature of the transformation (e.g., rigid or curved)
4. The domain of the transformation (e.g., local or global)
5. The interaction (e.g., manual of automatic)
6. The optimization procedure (e.g., iterative closest point or simulated annealing)
7. The modalities involved (e.g., CT, MR, or PET)

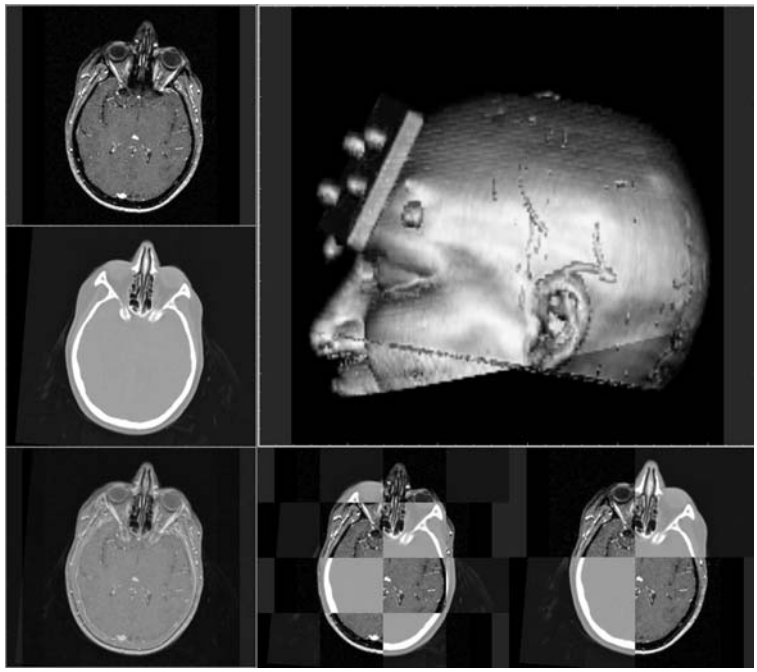

Fig. 4.14. Fusion of a CT and MR data set illustrates the differences of the patient alignment in both acquisitions.

8. The subject (e.g., inter-subject, intra-subject, or atlas)
9. The object (e.g., head or abdomen)

When considering the nature of the registration base, for example, the transformation may be defined using corresponding landmarks in both data sets. In a simple case, artificial markers attached to the patient are available which are visible on different modalities (Bromm and Scharein 1996); otherwise, pairs of preferably stable matching points, such as the AC–PC line, may be used. A more robust approach is to interactively match larger features such as surfaces (Schiemann et al. 1994). Figure 4.15 shows the result of the registration of a PET and an MRI data set.

Segmentation-based registration approaches can be divided into those using rigid models, such as, points, curves, or surfaces, and those using deformable models (e.g., snakes or nets). In all cases the registration accuracy of this method is limited to the accuracy of the segmentation step. Herewith any two modalities can be registered given the fact that the structures are visible within both. As an example, in some cases the target area in US images is not as visible as it should be to ensure a qualitatively high treatment of prostate cancer, whereas other modalities, such as CT, provide a better image. Unfortunately, CT cannot be used in a live-imaging procedure in the treatment room during intervention such as ultrasound imaging. To overcome these limitations, the images of both modalities can be registered in a unique data set, i.e., gathering preoperatively a CT volume and using it in combination with the intra-operative US-guided live procedure. To realize this, the separate volumes of CT and US can be registered with respect to each other based on the geometry of the urethra or by mutual information based on their greylevels as shown in Fig. 4.16 (Firle et al. 2003).

In a fundamentally different approach, the results of a registration step are evaluated at every point of the combined volume, based on intensity values (Studholme et al. 1996; Wells et al. 1996). Starting from a coarse match, registration is achieved by adjusting position and orientation until the mutual information ("similarity") between both data sets is maximized. These methods are fully automatic, do not rely on a possibly erroneous definition of landmarks, and seem to be more accurate than others (West et al. 1997).

Mutual information, originating in the information theory, is a voxel-based similarity measure of the statistical dependency between two data sets, which has been proposed by Collignon et al. (1995) and Viola and Wells (1997). It evaluates the amount of information that one variable contains about the other. By superimposing two data sets of the same object, but from different modalities, this method states that they are correctly aligned if the mutual information of geometrically corresponding gray values is maximal. Since no assumptions are made about the two signals, this method is not restricted to specific modalities and does not require the extraction of features in a preprocessing step. A recent survey about mutual information-based registration approaches was given by Pluim et al. (2003; Figs. 4.17, 4.18).

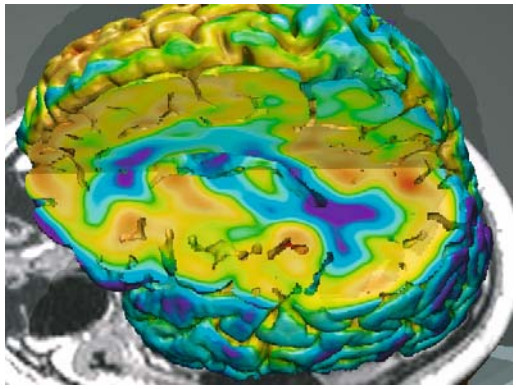

Fig. 4.15. Fusion of different imaging modalities for therapy control in a clinical study of obsessive-compulsive disorder. Magnetic resonance imaging shows that morphology is combined with a positron emission tomography (PET) scan, which shows glucose metabolism. Since the entire volume is mapped, the activity can be explored at any location of the brain.

The calculation of the transformation based on mutual information is a very time-consuming optimization process. Exploiting the coarse-to-fine resolution strategy (pyramidal approach) is one common possibility to speed up the registration process (Pluim et al. 2001). Another approach, when allowing only rigid transformations, is the usage of the "3D cross model" (Firle et al. 2004). This partial-volume based matching assumes that the center of the volume comprises the majority of the overlapping information between both images. The data from all three directions through the reference image (Maes et al. 1997) is taken without any high sub-sampling factors or lowering the number of histogram bins (Capek et al. 2001). Figures 4.17 and 4.18 depict the registration result of a whole-body CT and PET data set.

4.8 3D Anatomical Atlases

Whereas in classical medicine knowledge about the human body is represented in books and atlases,

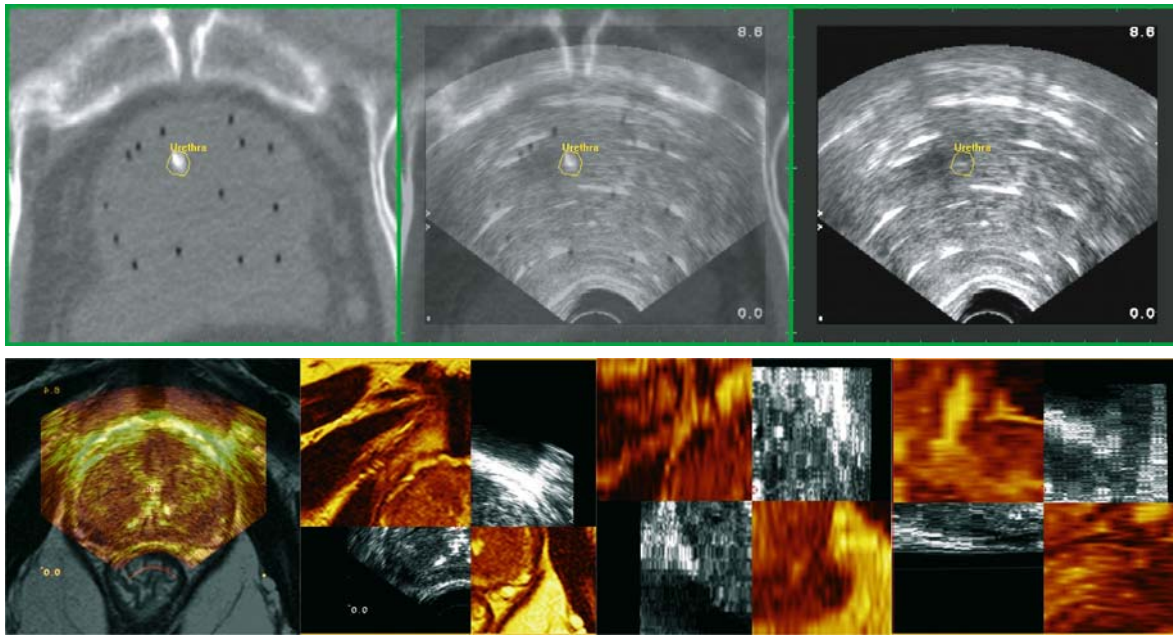

Fig. 4.16. Fusion of CT and 3D US volumes based on the urethra geometry (upper) and MRI with 3D U/S based on mutual information (lower)

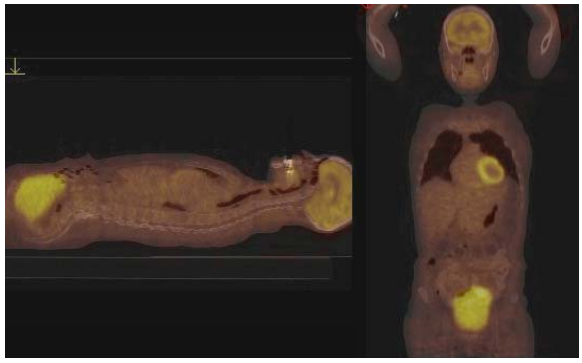

Fig. 4.17. While CT identifies the precise size, shape, and location of a mass, PET detects changes in the metabolism caused by the growth of abnormal cells in it. Fusion of the whole-body scans of both modalities

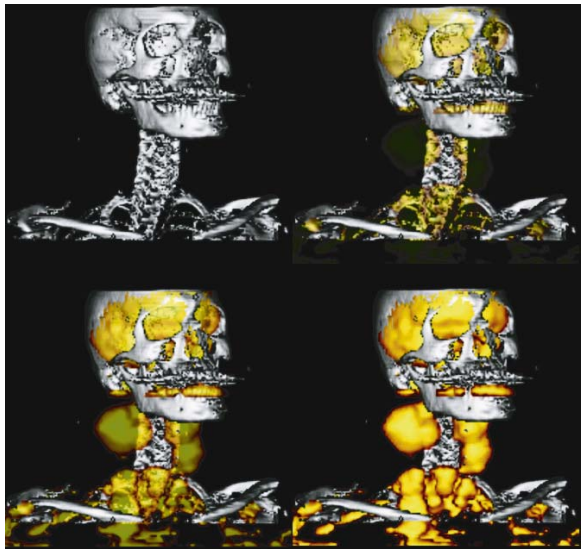

Fig. 4.18. A 3D image fusion after mutual-information-based registration of a CT and PET data set. Blending of the PET into the CT volume using image-level intermixing and different opacity settings

present-day computer science allows for new, more powerful and versatile computer-based representations of knowledge. The most straightforward example are multimedia CD-ROMs containing collections of classical pictures and text, which may be browsed arbitrarily. Although computerized, such media still follow the old paradigm of text printed on pages, accompanied by pictures.

Using methods of volume visualization, spatial knowledge about the human body may be much more efficiently represented by computerized 3D models. If such models are connected to a knowledge base of descriptive information, they can even be interrogated or disassembled by addressing names of organs (Brinkley et al. 1999; Golland et al. 1999; Höhne et al. 1996; Pommert et al. 2001).

A suitable data structure for this purpose is the intelligent volume (Höhne et al. 1995), which combines a detailed spatial model enabling realistic visualization with a symbolic description of human anatomy (Fig. 4.19). The spatial model is represented as a 3D volume as described above. The membership of voxels to an object is indicated by labels which are stored in attribute volumes congruent to the image volume. Different attribute volumes may be generated, e.g., for structure or function. Further attribute volumes may be added which contain, for example, the incidence of a tumor type or a time tag for blood propagation on a per-voxel basis.

The objects themselves bear attributes as well. These attributes may be divided into two groups: firstly, attributes indicating meaning such as names, pointers to text or pictorial explanations, or even features such as vulnerability or mechanical properties, which might be important (e.g. for surgical simulation); secondly, attributes defining their visual appearance, such as color, texture, and reflectivity. In addition, the model describes the interrelations of the objects with a semantic network. Examples for relations are part of or supplied by.

Once an intelligent volume is established, it can be explored by freely navigating in both the pictorial and descriptive worlds. A viewer can compose arbitrary views from the semantic description or query semantic information for any visible voxel of a picture. Apart from educational purposes, such atlases are also a powerful aid for the interpretation of clinical images (Kikinis et al. 1996; Nowinski and Thirunavuukarasuu 2001; Schiemann et al. 1994; Schmahmann et al. 1999).

Because of the high computational needs, 3D anatomical atlases are not yet suitable for present-day personal computers. Schubert et al. (1999) make such a model available for interactive exploration via precomputed Intelligent QuickTime virtual-reality videos, which can be viewed on any personal computer. A 3D atlas of regional, functional, and radiological anatomy of the brain based on this technique has been published (Höhne et al. 2001), along with a high-resolution atlas of the inner organs, based on the Visible Human (Höhne et al. 2003). A screenshot is shown in Fig. 4.20.

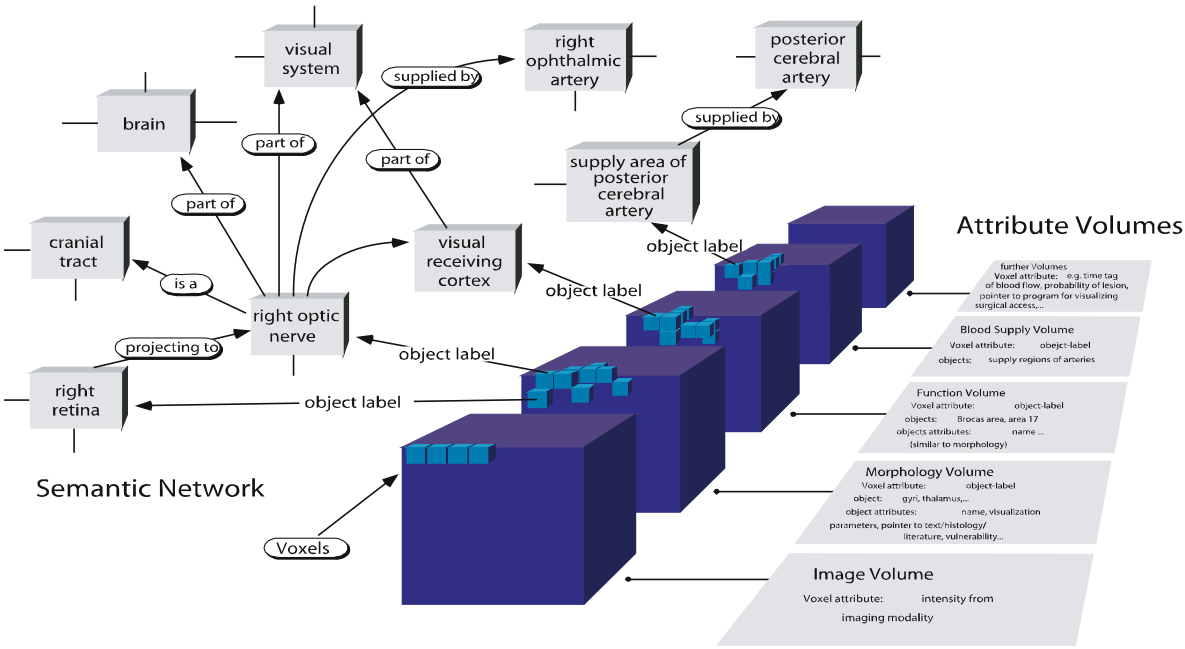

Fig. 4.19. Basic structure of the intelligent volume, integrating spatial and symbolic description of anatomy

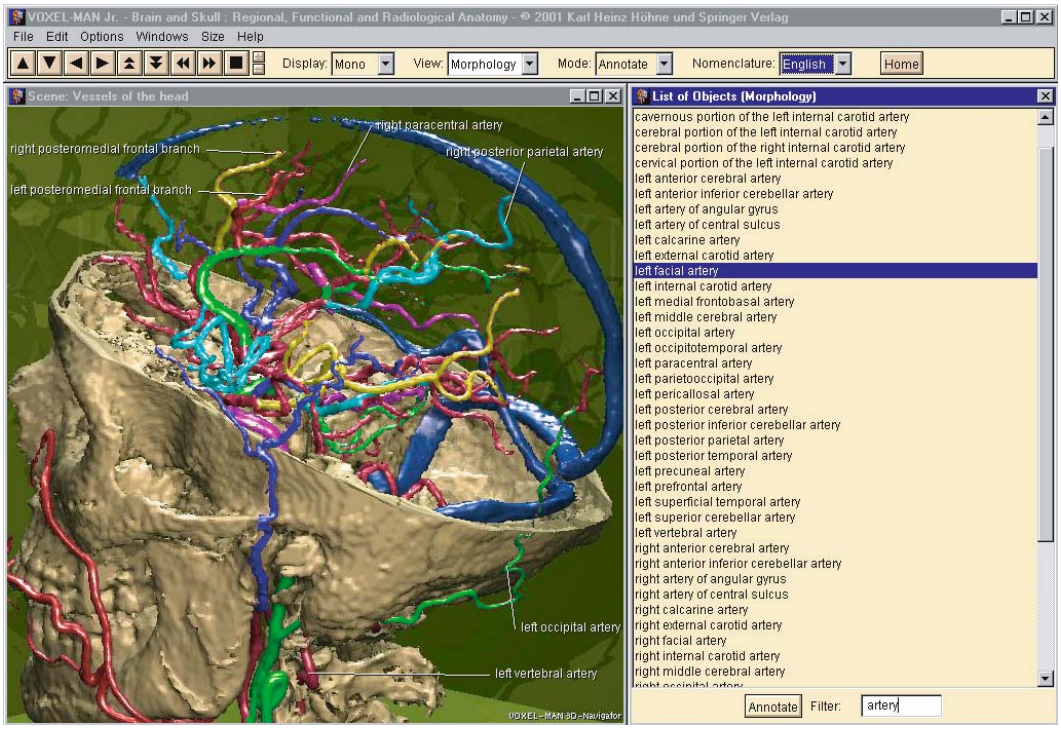

Fig. 4.20. User interface of VOXEL-MAN 3D-Navigator: brain and skull, a PC-based 3D atlas of regional, functional, and radiological anatomy. The user may navigate freely in both the pictorial (*left*) and descriptive (*right*) context.

To date, most 3D anatomical atlases are based on the data derived from one individual only. The inter-individual variability of organ shape and topology in space and time is thus not yet part of the model. Methods for measuring and modeling variability are currently being developed (Mazziotta et al. 1995; Styner and Gerig 2001; Thompson et al. 2000).

Acknowledgements
We thank C. Dold, E. Firle, K.-H. Höhne, G. Karangelis, T. Schiemann, U. Tiede, and S. Wesarg for their contributions to this work.

References

Arata LK, Dhawan AP, Broderick JP, Gaskil-Shipley MF, Levy AV, Volkow ND (1995) Three-dimensional anatomical model-based segmentation of MR brain images through principal axes registration. IEEE Trans Biomed Eng 42:1069–1078

Arnold JB, Liow J-S, Schaper KA, Stern JJ, Sled JG, Shattuck DW, Worth AJ, Cohen MS, Leahy RM, Mazziotta JC, Rottenberg DA (2001) Qualitative and quantitative evaluation of six algorithms for correcting intensity nonuniformity effects. NeuroImage 13:931–943

Biswas TK, Gupta AK (2002). Retrieval of true color of the internal organ of CT images and attempt to tissue characterization by refractive index: initial experience. Ind J Radiol Imaging 12:169–178

Bomans M, Riemer M, Tiede U, Höhne KH (1987) 3D-Segmentation von Kernspin-Tomogrammen. In: Paulus E (ed) Mustererkennung 1987. Proc of the 9th DAGM symposium. Informatik-Fachberichte, vol 149. Springer, Berlin Heidelberg New York, pp 231–235

Brinkley JF, Wong BA, Hinshaw KP, Rosse C (1999) Design of an anatomy information system. IEEE Comput Graphics Appl 19:38–48

Bromm B, Scharein E (1996) Visualisation of pain by magnetoencephalography in humans. In: Höhne KH, Kikinis R (eds) Visualization in biomedical computing. Proc VBC '96. Springer, Berlin Heidelberg New York, pp 477–481 (Lect Notes Comput Sci, vol 1131)

Cai W, Sakas G (1998) Maximum intensity projection using splatting in sheared object space. Comput Graph Forum 17:113–124

Cai W, Sakas G, (1999) Transfer functions in DRR volume rendering. In: Lemke HU et al. Computer assisted radiology and surgery (CARS). Proceedings. Amsterdam, Lausanne:Elsevier, pp. 284–289 (International Congress Series 1191).

Cai W, Karangelis G, Sakas G (1999) Volume interaction techniques in the virtual simulation of radiotherapy treatment planning. In: Keldysh Institute of Applied Mathematics: Graphicon. Proceedings. Moscow, pp. 231–239

Cai W, Walter S, Karangelis G, Sakas G (2000) Collaborative virtual simulation environment for radiotherapy treatment planning. In: Computer Graphics Forum 19, 3 pp. C-379 –C-390

Canny J (1986) A computational approach to edge detection. IEEE Trans Pattern Anal Machine Intell 8:679–698

Capek M, Mroz L, Wegenkittl R (2001) Robust and fast medical registration of 3D multi-modality data sets, Medicon 2001, IXth Mediterranean conference on medical and biological engineering and computing, Pula, Croatia, pp 515–518

Caselles V, Kimmel R, Sapiro G (1997). Geodesic active contours. International Journal on Computer Vision, 22(1):61–97, 1997

Cignoni P, Montani C, Scopigno R (1998) A comparison of mesh simplification algorithms. Comput Graph 22:37–54

Cignoni P, Ganovelli F, Montani C, Scopigno R (2000) Reconstruction of topologically correct and adaptive trilinear isosurfaces. Comput Graph 24:399–418

Clarke LP, Velthuizen RP, Camacho MA, Heine JJ, Vaidyanathan M, Hall LO, Thatcher RW, Silbiger ML (1995) MRI segmentation: methods and applications. Magn Reson Imaging 13:343–368

Cline HE, Lorensen WE, Kikinis R, Jolesz F (1990) Three-dimensional segmentation of MR images of the head using probability and connectivity. J Comput Assist Tomogr 14:1037–1045

Collignon A, Maes F, Delaere D, Vandermeulen D, Suetens P, Marchal G, Viola P, Wells W (1995) Automated multimodality medical image registration using information theory. Fourteenth International Conference on Information Processing in Medical Imaging. Kluwer, Boston, pp 263–274 (Computational Imaging and Vision, vol 3)

Collins DL, Zijdenbos AP, Barré WFC, Evans AC (1999) ANIMAL+INSECT: improved cortical structure segmentation. In: Kuba A, Samal M, Todd-Pokropek A (eds) Information processing in medical imaging. Proc IPMI 1999. Springer, Berlin Heidelberg New York, pp 210–223 (Lect Notes Comput Sci, vol 1613)

Drebin RA, Carpenter L, Hanrahan P (1988) Volume rendering. Comput Graphics 22:65–74

Duncan JS, Ayache N (2000) Medical image analysis: progress over two decades and the challenges ahead. IEEE Trans Pattern Anal Machine Intell 22:85–105

Firle E, Wesarg S, Karangelis G, Dold C (2003) Validation of 3D ultrasound–CT registration of prostate images. Medical Imaging 2003. Proc SPIE 5032, Bellingham, pp 354–362

Firle E, Wesarg S, Dold C (2004) Fast CT/PET registration based on partial volume matching. Computer assisted radiology and surgery. Proc CARS 2004. Elsevier, Amsterdam, pp 31–36

Foley JD, van Dam A, Feiner SK, Hughes JF (1995) Computer graphics: principles and practice, 2nd edn. Addison-Wesley, Reading, Massachusetts

Gerig G, Martin J, Kikinis R, Kübler O, Shenton M, Jolesz FA (1992) Unsupervised tissue type segmentation of 3D dual-echo MR head data. Image Vision Comput 10:349–360

Golland P, Kikinis R, Halle M, Umans C, Grimson WEL, Shenton ME, Richolt JA (1999) Anatomy browser: a novel approach to visualization and integration of medical information. Comput Aided Surg 4:129–143

Hamann B, Trotts I, Farin G (1997) On approximating contours of the piecewise trilinear interpolant using triangular rational-quadratic Bézier patches. IEEE Trans Visual Comput Graph 3:215–227

He T (1998) Wavelet-assisted volume ray casting. Pac Symp Biocomput 1998, pp 153–164

Hemmingsson A, Jung B (1980) Modification of grey scale in computer tomographic images. Acta Radiol Diagn (Stockh) 21:253–255

Herman GT (1991) The tracking of boundaries in multidimensional medical images. Comput Med Imaging Graph 15:257–264

Hildebrand A, Sakas G (1996) Innovative 3D-methods in medicine. Korea Society of Medical and Biomedical Engineering. Advanced Medical Image Processing Proceedings 1996, Seoul, Korea

Höhne KH, Bernstein R (1986) Shading 3D-images from CT using gray level gradients. IEEE Trans Med Imaging MI-5:45–47

Höhne KH, Hanson WA (1992) Interactive 3D-segmentation of MRI and CT volumes using morphological operations. J Comput Assist Tomogr 16:285–294

Höhne KH, Bomans M, Pommert A, Riemer M, Schiers C, Tiede U, Wiebecke G (1990) 3D-visualization of tomographic volume data using the generalized voxel-model. Visual Comput 6:28–36

Höhne KH, Pflesser B, Pommert A, Riemer M, Schiemann T, Schubert R, Tiede U (1995) A new representation of knowledge concerning human anatomy and function. Nat Med 1:506–511

Höhne KH, Pflesser B, Pommert A, Riemer M, Schiemann T, Schubert R, Tiede U (1996) A virtual body model for surgical education and rehearsal. IEEE Comput 29:25–31

Höhne KH, Petersik A, Pflesser B, Pommert A, Priesmeyer K, Riemer M, Schiemann T, Schubert R, Tiede U, Urban M, Frederking H, Lowndes M, Morris J (2001) VOXEL-MAN 3D navigator: brain and skull. Regional, functional and radiological anatomy. Springer Electronic Media, Heidelberg (2 CD-ROMs, ISBN 3-540-14910-4)

Höhne KH, Pflesser B, Pommert A, Priesmeyer K, Riemer M, Schiemann T, Schubert R, Tiede U, Frederking H, Gehrmann S, Noster S, Schumacher U (2003) VOXEL-MAN 3D navigator: inner organs. Regional, systemic and radiological anatomy. Springer Electronic Media, Heidelberg (DVD-ROM, ISBN 3-540-40069-9)

Kass M, Witkin A, Terzopoulos D (1987) Snakes: active contour models. Proc 1st ICCV, June 1987, London, pp 259–268

Kikinis R, Shenton ME, Iosifescu DV, McCarley RW, Saiviroonporn P, Hokama HH, Robatino A, Metcalf D, Wible CG, Portas CM, Donnino RM, Jolesz FA (1996) A digital brain atlas for surgical planning, model driven segmentation, and teaching. IEEE Trans Visual Comput Graphics 2:232–241

Kindlmann G, Durkin JW (1998) Semi-automatic generation of transfer functions for direct volume rendering, volume visualization. IEEE symposium on 19–20 October 1998, pp 79–86, 170

Kirbas C, Quek FKH (2003) Vessel extraction techniques and algorithms: a survey, bioinformatics and bioengineering 2003. Proc 3rd IEEE Symposium, 10–12 March 2003, pp 238–245

Kniss J, Kindlmann G, Hansen C (2002) Multidimensional transfer functions for interactive volume rendering, visualization and computer graphics. IEEE Trans 8:270–285

Lacroute P, Levoy M (1994) Fast volume rendering using a shear-warp factorization of the viewing transformation. Proc SIGGRAPH 1994, Orlando, Florida, July 1994, pp 451–458

Levoy M (1988) Display of surfaces from volume data. IEEE Comput Graph Appl 8:29–37

Levoy M (1990) A hybrid ray tracer for rendering polygon and volume data. IEEE Comput Graph Appl 10:33–40

Lorensen WE, Cline HE (1987) Marching cubes: a high resolution 3D surface construction algorithm. Comput Graph 21:163–169

Maes F, Collignon A, Vandermeulen D, Marchal G, Suetens P (1997) Multimodality image registration by maximization of mutual information. IEEE Trans Med Imaging 16:187–198

Maintz JBA, Viergever M (1998) A survey of medical image registration. Med Image Anal 2:1–36

Marschner SR, Lobb RJ (1994) An evaluation of reconstruction filters for volume rendering. In: Bergeron RD, Kaufman AE (eds) Proc IEEE visualization 1994. IEEE Computer Society Press, Los Alamitos, Calif., pp 100–107

Max N (1995) Optical models for direct volume rendering, IEEE Trans Visual & Comput Graph, 1(2):99–108

Mazziotta JC, Toga AW, Evans AC, Fox P, Lancaster J (1995) A probabilistic atlas of the human brain: theory and rationale for its development. NeuroImage 2:89–101

Möller T, Machiraju R, Mueller K, Yagel R (1997) Evaluation and

design of filters using a Taylor series expansion. IEEE Trans Visual Comput Graph 3:184–199

Mroz L, Hauser H, Gröller E (2000) Interactive high-quality maximum intensity projection. Comput Graphics Forum 19:341–350

Natarajan BK (1994) On generating topologically consistent isosurfaces from uniform samples. Visual Comput 11:52–62

Nowinski WL, Thirunavuukarasuu A (2001) Atlas-assisted localization analysis of functional images. Med Image Anal 5:207–220

Olabarriaga SD, Smeulders AWM (2001) Interaction in the segmentation of medical images: a survey. Med Image Anal 5:127–142

Pluim J, Maintz J, Viergever M (2001) Mutual information matching in multiresolution contexts. Image Vision Comput 19:45–52

Pluim J, Maintz J, Viergever M (2003) Mutual information based registration of medical images: a survey. IEEE Trans Med Imaging 22:986–1004

Pommert A (2004) Simulationsstudien zur Untersuchung der Bildqualität für die 3D-Visualisierung tomografischer Volumendaten. Books on Demand, Norderstedt 2004 (zugleich Dissertation, Fachbereich Informatik, Universität Hamburg)

Pommert A, Höhne KH, Pflesser B, Richter E, Riemer M, Schiemann T, Schubert R, Schumacher U, Tiede U (2001) Creating a high-resolution spatial/symbolic model of the inner organs based on the visible human. Med Image Anal 5:221–228

Saeed N, Hajnal JV, Oatridge A (1997) Automated brain segmentation from single slice, multislice, or whole-volume MR scans using prior knowledge. J Comput Assist Tomogr 21:192–201

Sakas G, Grimm M, Savopoulos A (1995) Optimized maximum intensity projection (MIP). In: Hanrahan P et al. 6th Eurographics workshop on rendering. Proceedings. Eurographics, pp. 81-93

Schiemann T, Höhne KH, Koch C, Pommert A, Riemer M, Schubert R, Tiede U (1994) Interpretation of tomographic images using automatic atlas lookup. In: Robb RA (ed) Visualization in biomedical computing 1994. Proc SPIE 2359, Rochester, Minnesota, pp 457–465

Schiemann T, Tiede U, Höhne KH (1997) Segmentation of the visible human for high quality volume based visualization. Med Image Anal 1:263–271

Schmahmann JD, Doyon J, McDonald D, Holmes C, Lavoie K, Hurwitz AS, Kabani N, Toga A, Evans A, Petrides M (1999) Three-dimensional MRI atlas of the human cerebellum in proportional stereotaxic space. NeuroImage 10:233–260

Schroeder WJ, Zarge JA, Lorensen WE (1992) Decimation of triangle meshes. Comput Graph 26:65–70

Schubert R, Pflesser B, Pommert A et al.(1999) Interactive volume visualization using "intelligent movies". In: Westwood JD, Hoffman HM, Robb RA, Stredney D (eds) Medicine meets virtual reality. Proc MMVR 1999. IOS Press, Amsterdam, pp 321–327 (Health Technology and Informatics, vol 62)

Sonka M, Hlavac V, Boyle R (1998) Image processing, analysis, and machine vision, 2nd edn. PWS Publishing, Boston, Mass

Šrámek M, Kaufman A (2000) Fast ray-tracing of rectilinear volume data using distance transforms. IEEE Trans Visual Comput Graph 6:236–251

Studholme C, Hill DLG, Hawkes DJ (1996) Automated 3-D registration of MR and CT images of the head. Med Image Anal 1:163–175

Styner M, Gerig G (2001) Medial models incorporating object variability for 3D shape analysis. In: Insana MF, Leahy RM (eds) Information processing in medical imaging. Proc IPMI 2001. Springer, Berlin Heidelberg New York, pp 502–516 (Lect Notes Comput Sci, vol 2082)

Thompson PM, Woods RP, Mega MS, Toga AW (2000) Mathematical/computational challenges in creating deformable and probabilistic atlases of the human brain. Hum Brain Mapping 9:81–92

Tiede U (1999) Realistische 3D-Visualisierung multiattributierter und multiparametrischer Volumendaten. PhD thesis, Fachbereich Informatik, Universität Hamburg

Tiede U, Höhne KH, Bomans M, Pommert A, Riemer M, Wiebecke G (1990) Investigation of medical 3D-rendering algorithms. IEEE Comput Graph Appl 10:41–53

Tiede U, Schiemann T, Höhne KH (1998) High quality rendering of attributed volume data. In: Ebert D, Hagen H, Rushmeier H (eds) Proc IEEE Visualization 1998. IEEE Computer Society Press, Los Alamitos, Calif., pp 255–262

Totsuka T, Levoy M (1993) Frequency domain volume rendering. Comput Graph 27:271–278

Van den Elsen P, Pol E, Viergever M (1993) Medical image matching: a review with classification. IEEE Eng Med Biol 12:26–39

Verdonck B, Bloch I, Maître H, Vandermeulen D, Suetens P, Marchal G (1995) Blood vessel segmentation and visualization in 3D MR and spiral CT angiography HU. In: Lemke (ed) Proc CAR 1995. Springer, Berlin Heidelberg New York, pp 177–182

Viola P, Wells W (1997) Alignment by maximization of mutual information. Int J Comput Vis 24:137–154

Wan M, Kaufman A, Bryson S (1999) High performance presence-accelerated ray casting. Proc IEEE Visualization 1999, San Francisco, Calif., pp 379–386

Warren RC, Pandya YV (1982) Effect of window width and viewing distance in CT display. Br J Radiol 55:72–74

Watt A (2000) 3D computer graphics, 3rd edn. Addison-Wesley, Reading, Massachusetts

Wells WM III, Viola P, Atsumi H, Nakajima S, Kikinis R (1996) Multi-modal volume registration by maximization of mutual information. Med Image Anal 1:35–51

Wesarg S, Firle EA (2004) Segmentation of vessels: the corkscrew algorithm. Proc of SPIE medical imaging symposium 2004, San Diego (USA), vol 5370, pp 1609–1620

West J, Fitzpatrick JM, Wang MY, Dawant BM, et al. (1997) Comparison and evaluation of retrospective intermodality brain image registration techniques. J Comput Assist Tomogr 21:554–566

Wilmer F, Tiede U, Höhne KH (1992) Reduktion der Oberflächenbeschreibung triangulierter Oberflächen durch Anpassung an die Objektform. In: Fuchs S, Hoffmann R (eds) Mustererkennung 1992. Proc 14th DAGM symposium. Springer, Berlin Heidelberg New York, pp 430–436

Winston PH (1992) Artificial intelligence, 3rd edn. Addison-Wesley, Reading, Massachusetts

Yagel R, Cohen D, Kaufman A (1992) Discrete ray tracing. IEEE Comput Graph Appl 12:19–28

Zamboglou N, Karangelis G, Nomikos I, Zimeras S, Helfmann T, Uricchio R, Martin T, Röddiger S, Kolotas C, Baltas D, Sakas G (2003) EXOMIO virtual simulation: oropharynx, prostate and breast cancers. In: Mould, RF (Ed) Progress in CT-3D simulation. Bochum: Medical Innovative Technology, 2003, pp 1–18

Zamboglou N, Karangelis G, Nomikos I, Zimeras S, Kolotas C, Baltas D, Sakas G (2004) Virtual CT-3D simulation using Exomio: With special reference to prostate cancer. In: Nowotwory Journal of Oncology 54, 6 pp 547–554

Zucker S (1976) Region growing: childhood and adolesence. Comput Graph Image Proc 5:382–399

5 Image Registration and Data Fusion for Radiotherapy Treatment Planning

Marc L. Kessler and Michael Roberson

CONTENTS

5.1 Introduction

Treatment planning for conformal radiotherapy requires accurate delineation of tumor volumes and surrounding healthy tissue. This is especially true in inverse planning where trade-offs in the dose-volume relationships of different tissues are usually the driving forces in the search for an optimal plan. In these situations, slight differences in the shape and overlap regions between a target volume and critical structures can result in different optimized plans. While X-ray computed tomography (CT) remains the primary imaging modality for structure delineation, beam placement and generation of digitally reconstructed radiographs, data from other modalities, such as magnetic resonance imaging and spectroscopy (MRI/MRSI) and positron/single photon emission tomography (PET/SPECT), are becoming increasingly prevalent for tumor and normal tissue delineation (Fig. 5.1).

M. L. Kessler, PhD, Professor
M. Roberson, BS
Department of Radiation Oncology
The University of Michigan Medical School
1500 East Medical Center Drive
Ann Arbor, MI 48109-0010
USA

There are many reasons to include image data from other modalities into the treatment-planning process. In many sites, MRI provides superior soft tissue contrast relative to CT and can be used to enhance or suppress different tissues such as fat and conditions such as edema. Magnetic resonance imaging also permits imaging along arbitrary planes which can improve visualization and segmentation of different anatomic structures. More recently, MRI has been used to acquire localized information about relative metabolite concentrations, fluid mobility, and tissue microstructure. With a variety of tracer compounds available, PET and SPECT can provide unique information about different cellular and physiologic processes to help assess normal and diseased tissues.

In addition to static treatment planning, volumetric image data is playing a larger role in treatment delivery and adaptive radiotherapy. Modern treatment machines can now be equipped with imaging devices that allow acquisition of volumetric CT data at the time of treatment. These "treatment-delivery CT" studies can be used to adapt a treatment plan based on the patient's anatomy at the time of treatment and allow more accurate tracking of delivered dose. Furthermore, data from magnetic resonance and nuclear medicine acquired during the course of therapy may also help assess the efficacy of therapy and indicate prescription changes (Chenevert et al. 2000; Mardor et al. 2003; Barthel et al. 2003; Brun et al. 2002; Allal et al. 2004).

To fully realize the benefits of the information available from different imaging studies, the data they provide must be mapped to a single coordinate system, typically that of the treatment planning CT. This process is called image registration. Once they are all linked to a common coordinate system, data can be transferred between studies and integrated to help construct a more complete and accurate representation of the patient. This process is called data fusion. This chapter describes the mechanics of image registration and data fusion processes.

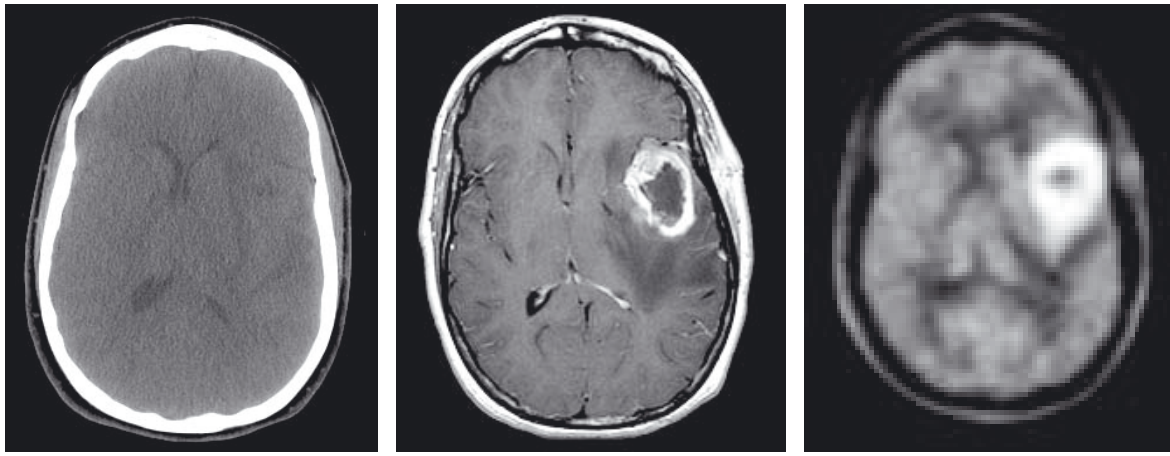

Fig. 5.1. Examples of different multimodality imaging data available for treatment planning

5.2 Image Registration

Image registration is the process of determining the geometric transformation that maps the coordinates between identical points in different imaging studies. With this mapping, information can be transferred between the studies or fused in various ways (Fig. 5.2).

For the discussion that follows, we describe the mechanics of automated image registration using two data sets which are labeled Study *A* and Study *B*. Study *A* is the base or reference data set and is held fixed and Study *B* the homologous data set that is manipulated to be brought into geometric alignment with Study *A*. Study *B'* is the transformed data from Study *B*.

Numerous techniques exist for image registration. The choice of technique depends on the imaging modalities involved, the anatomic site, and the level of control over the imaging conditions. A detailed review is given by Maintz and Viergever (1998). The general approach in each of the methods is to devise a registration metric that measures the degree of mismatch (or similarity) between one or more features in two data sets and to use standard numerical optimization methods to determine the parameters of a

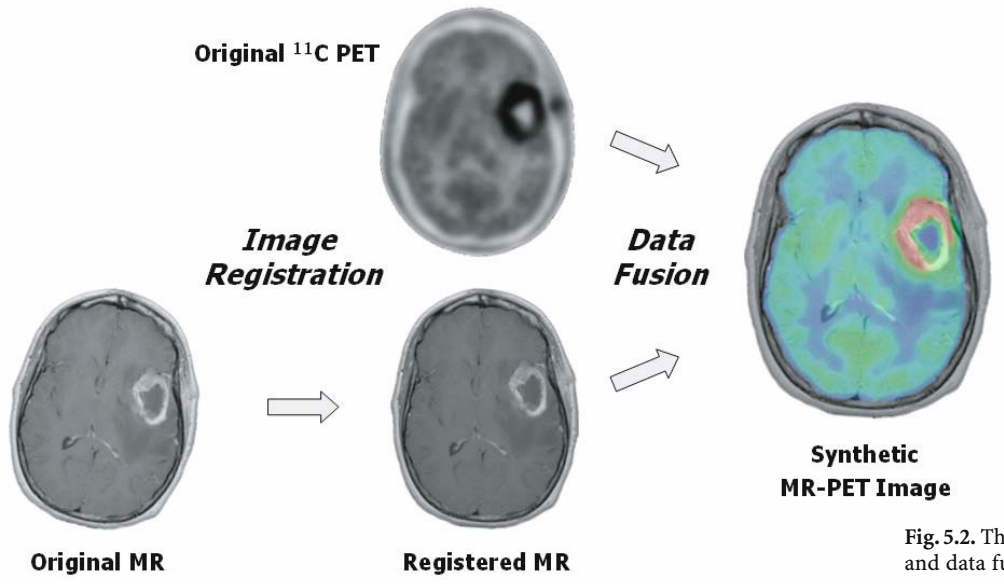

Fig. 5.2. The image registration and data fusion processes

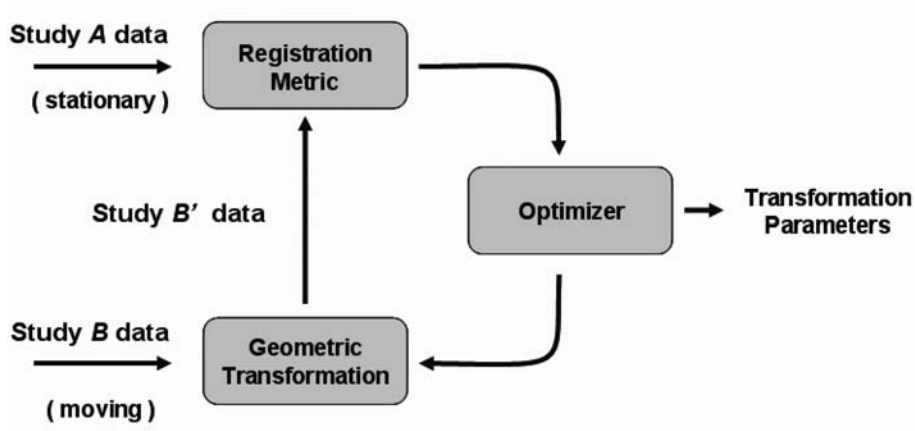

Fig. 5.3. The image registration process

geometric transformation that minimize (maximize) the metric. Differences between various techniques include the metric used, the features used to measure the mismatch, the particular form of the geometric transformation used, and the optimization method used for computing the required parameters.

The image registration process illustrated in Fig. 5.3 can be either automated or manual. Automated image registration is analogous to inverse treatment planning, with the registration metric replacing the "plan cost function" and the parameters of the transformation replacing the plan defining parameters such as beamlet intensities or weights. In both cases the parameters are iterated using an optimizer until an "optimal" set of parameters is found. Manual image registration is more like forward treatment planning. The "optimizer" is a human with a suite of interactive tools that let the user perform various image transformations and visualize the results in real time. While manual registration tools typically only support rotation and translation, they can also be used to initialize more complex automated registrations.

5.2.1 Geometric Transformations

The fundamental task of image registration is to find the geometric transformation, T, which maps the coordinates of a point in Study A to the coordinates of the corresponding point in Study B. In general, this transformation can be written as

$$\mathbf{x}_B = T\,(\mathbf{x}_A, \{\beta\}),$$

where $\mathbf{x}_A$ is the coordinate of the point in Study A, $\mathbf{x}_B$ is the coordinate of the same anatomic point in Study B, and $\{\beta\}$ is the set of parameters of the transformation. The output of the image registration process is the parameters $\{\beta\}$ for a particular pair of imaging studies (Fig. 5.3). The number of parameters required to determine the transformation depends on the form of *T, which in turn depends on the clinical site, clinical application, and the modalities involved.*

In the ideal case, where the patient is positioned in an identical orientation in the different imaging studies and the scale and center of the coordinate systems coincide, T is simply an identity transformation **I** and $\mathbf{x}_B = \mathbf{x}_A$ for all points in the two imaging studies. This situation most closely exists for combined imaging modality devices such as PET–CT machines, especially if physiologic motion is controlled or absent. Unfortunately, it is far more common for the orientation of the patient to change between imaging studies, making more sophisticated transformations necessary.

For situations where the anatomy of interest can be assumed to move as a rigid body, the set of parameters consists of three rotation angles (θ_x, θ_y, θ_z) and three translations (t_x,t_y,t_z). The rigid body transformation is then written as

$$\mathbf{x}_B = \mathrm{T}_{rigid}\,(\mathbf{x}_A, \{\beta\}) = \mathbf{A}\,\mathbf{x}_A + \mathbf{b},$$

where **A** is a 3×3 rotation matrix and **b** is a 3×1 translation vector. This transformation is simply the familiar one dimensional function "y = m·x+b", except in three dimensions.

In matrix notation this can be written as

$$\begin{bmatrix} x_B \\ y_B \\ z_B \end{bmatrix} = \begin{bmatrix} & \mathsf{A} & \end{bmatrix} \begin{bmatrix} x_A \\ y_A \\ z_A \end{bmatrix} + \begin{bmatrix} \mathsf{b} \end{bmatrix}.$$

If the scales of the two data sets are not identical, it is necessary to also include scale factors (s_x, s_y, s_z) into the matrix **A**. This is usually a device calibration issue rather than an image registration problem, but if these factors exist and are not compensated for by a preprocessing step, they must be determined during the registration process.

The rigid and scaling transformations are special cases of the more general *affine* transformation. A *full* affine transformation includes parameters for rotation, translation, scale, shear, and plane reflection. One attribute of affine transformations is that all points lying on a line initially still lie on a line after transformation and "parallel lines stay parallel."

Another notation used to specify rigid or affine transformations is to combine the 3×3 matrix **A** and the 3×1 translation vector **b** into a single 4×4 matrix, i.e.,

$$\begin{bmatrix} x_B \\ y_B \\ z_B \\ 1 \end{bmatrix} = \left[\begin{array}{ccc:c} & \mathsf{A} & & \mathsf{b} \\ \hdashline 0 & 0 & 0 & 1 \end{array}\right] + \begin{bmatrix} x_A \\ y_A \\ z_A \\ 1 \end{bmatrix}.$$

The DICOM imaging standard uses this representation for affine transformations to specify the spatial relationship between two imaging studies (National Electrical Manufacturers Association 2004).

The assumption of global rigid movement of anatomy is often violated, especially for sites other than the head and large image volumes that extend to the body surface. Differences in patient setup (arms up versus arms down), organ filling, and uncontrolled physiologic motion confound the use of a single affine transform to register two imaging studies. In some cases where *local* rigid motion can be assumed, it may be possible to use a rigid or affine transformation to register sub-volumes of two imaging studies. For example, the prostate itself may be considered rigid, but it can move relative to the pelvis depending on the filling of the rectum and bladder. By considering only a limited field-of-view that includes just the region of the prostate, it is often possible to use an affine transformation to accurately register the prostate anatomy in two studies. One or more sub-volumes can be defined by simple geometric cropping or derived from anatomic surfaces (Fig. 5.4).

Even with a limited field-of-view approach, there are many sites in which affine registration techniques are not powerful enough to achieve acceptable alignment of anatomy. In these sites, an organ's size and shape may change as a result of normal organ behavior or the motion of surrounding anatomy. For example, the lungs change in both size and shape during the breathing cycle, and the shape of the liver can be affected by the filling of the stomach. When registering data sets that exhibit this kind of motion, a deformable model must be used to represent the transformation between studies.

One class of deformation model is called a spline, which is a curve that interpolates points in space based on a set of control points. A set of parameters associated with each control point defines the exact shape of this interpolation. The number and location of control points determine the extent of deformation that a spline can express. Two types of splines commonly used in biologic and medical imaging applications are thin-plate splines and B-splines (Bookstein 1989; Unser 1999).

Thin-plate spline transformations model the deformations of an infinite thin plate. The parameters associated with this transformation consist of a displacement at each control point. Interpolation

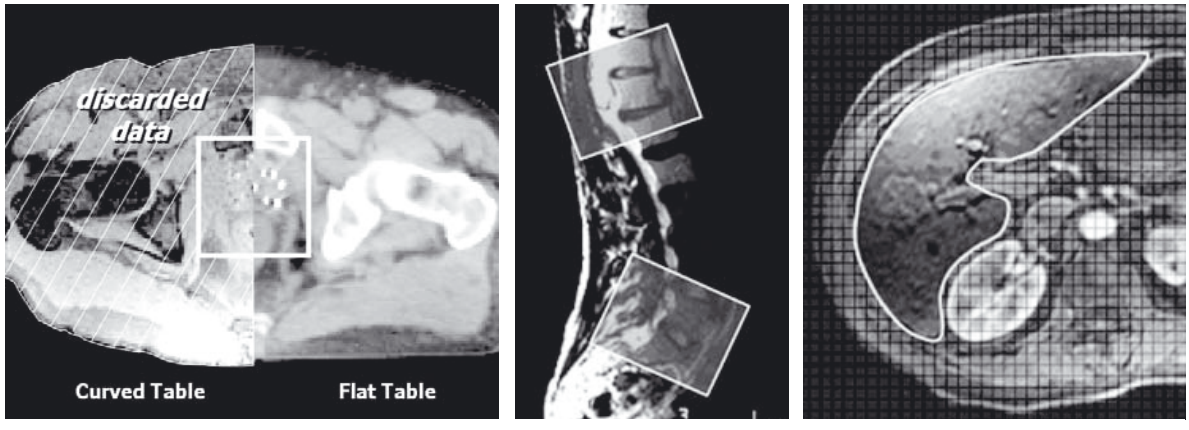

Fig. 5.4. Different types of cropping for limited field-of-view registration

between control points is done by minimizing the "bending energy" of this thin plate while leaving the control point displacements intact. This concept is not limited to flat "plates" and can be extended to three dimensions. The deformation at an arbitrary point depends on its distance from each control point, so a change in any control point affects the deformation of all points in the image volume (except the other control points). Thin-plate splines are therefore considered a global deformation model. Because of this property, they perform well with relatively few control points but do suffer from increased computation time when many (>50–100) control points are used.

B-spline transformations use control points called knots, arranged in a grid. A piecewise polynomial function is used to interpolate the transformation between these knots. Any degree polynomial can be used, but in medical image registration cubic B-splines are typical. A B-spline transformation is expressed as a weighted sum

$$\boldsymbol{x}_B = \boldsymbol{x}_A + \sum w_i \, B(\boldsymbol{x}_A - k_i),$$

where each k_i is the location of knot i, each w_i is a weight parameter associated with knot i, and B(x) is a basis function. Figure 5.5 illustrates this weighted sum in a one-dimensional cubic B-spline example. Note that the basis function has a limited extent, so each knot only affects a limited region of the overall deformation. In this way, B-splines are considered a local deformable model. This property of locality allows B-spline models to use very fine grids of thousands of knots with only a modest increase in computation time. Each knot adds more control over the transformation (more degrees of freedom), so using many knots greatly enhances the ability of B-splines to model complex deformations. Unfortunately, increasing the number of parameters to optimize during the registration process can increase the difficulty of finding the optimal solution.

Other deformable models that are possible include freeform deformations (used with physical or optical flow models) and finite element methods (Thirion 1998; Bharatha et al. 2001).

5.2.2 Registration Metrics

The goal of the image registration process is to determine the parameters of geometric transformation that optimally align two imaging studies. To achieve this goal, a registration metric is devised which quantifies the degree to which the pair of imaging studies are aligned (or mis-aligned). Using standard optimization techniques the transformation parameters are manipulated until this metric is maximized (or minimized) (Fig. 5.6). Most registration metrics in use presently can be classified as either geometry based or intensity based. Geometry-based metrics make use of features extracted from the image data such as anatomic or artificial landmarks and organ boundaries, whereas intensity-based metrics use the image data directly.

Geometry-Based Metrics

The most common geometry-based registration metrics involve the use of point matching or surface matching. For point matching, the coordinates of pairs of corresponding points from Study *A* and Study *B*

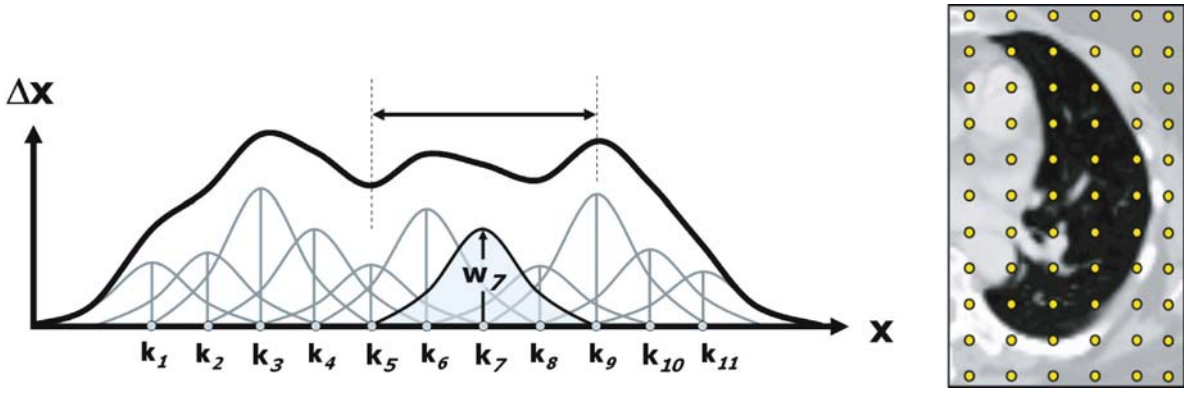

Fig. 5.5. B-spline deformation model. *Left:* 1D example of the cubic B-spline deformation model. The displacement Δx as a function of x is determined by the weighted sum of basis functions. The *double arrow* shows the region of the overall deformation affected by the weight factor w_7. The 3D deformations are constructed using 1D deformations for each dimension. *Right:* B-spline knot locations relative to image data for lung registration using deformation

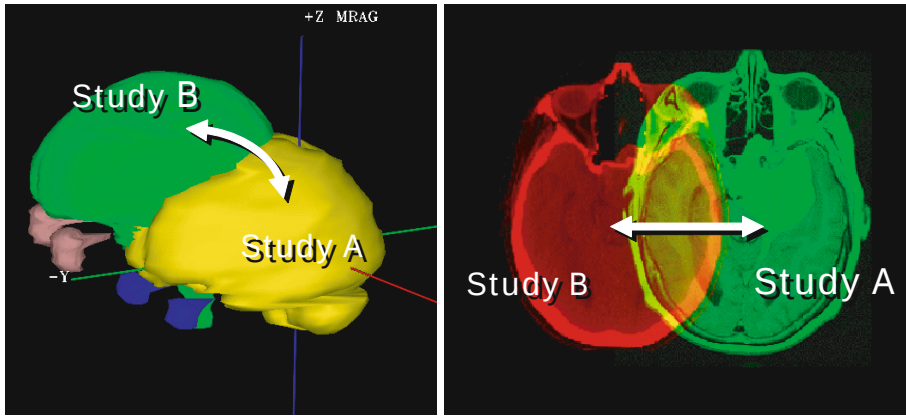

Fig. 5.6. Examples of image registration using geometric data (*left*) and image data (*right*). Geometry-based registration aligns points or surfaces while intensity-based registration aligns image intensity values.

are used to define the registration metric. These points can be anatomic landmarks or implanted or externally placed fiducial markers. The registration metric is defined as the sum of the squared distances between corresponding points:

$$R = \sum (p_A - p_{B'})^2 / N,$$

p_A is the coordinate of the a point in Study A, $p_{B'}$ is the coordinate of the transformed point from Study B and N is the number of pairs of points.

To compute the rotations and translations for a rigid transformation, a minimum of three pairs of points are required. For affine transformations, a minimum of four pairs of non-coplanar points are required. Using more pairs of points reduces the bias that errors in the delineation of any one pair of points has on the estimated transformation parameters; however, accurately identifying more than the minimum number of corresponding points can be difficult as different modalities often produce different tissue contrasts (a major reason why multiple modalities are used in the first place) and placing or implanting larger numbers of markers is not always possible or desirable.

Alternatively, surface matching does not require a one-to-one correspondence of specific points but instead tries to maximize the overlap between corresponding surfaces extracted from two imaging studies, such as the brain or skull surface or pelvic bones. These structures can be easily extracted using automated techniques and minor hand editing. The surfaces from Study A are represented as a binary volume or as an explicit polygon surface and the surfaces from Study B are represented as a set of points sampled from the surface (Fig. 5.7). The metric, which represents the degree of mismatch between the two datasets, can be computed as the sum or average of the squared distances of closest approach from the points from Study B to the surfaces from Study A. It is written as

$$R = \sum \text{dist}(p_{B'}, S_A)^2 / N,$$

where $\text{dist}(p_{B'}, S_A)$ computes the (minimum) distance between point $p_{B'}$ and the surfaces S_A.

As with defining pairs of points, it may be inherently difficult or time-consuming to accurately delineate corresponding surfaces in both imaging studies. Furthermore, since the extracted geometric features are surrogates for the entire image volume, any anatomic or machine-based distortions in the image data away from these features are not taken into account during the registration process.

Intensity-Based Metrics

To overcome some of the limitations of using explicit geometric features to register image data, another class of registration metric has been developed which uses the numerical gray-scale information directly to measure how well two studies are registered. These metrics are also referred to as similarity measures since they determine how similar the distributions of corresponding voxel values from Study A and a transformed version of Study B are. Several mathematical formulations are used to measure this similarity. The more common similarity measures in clinical use include: sum of squared differences; cross correlation; and mutual information.

The sum of squared differences (SSD) metric is computed as the average squared intensity difference between Study A and Study B', i.e.,

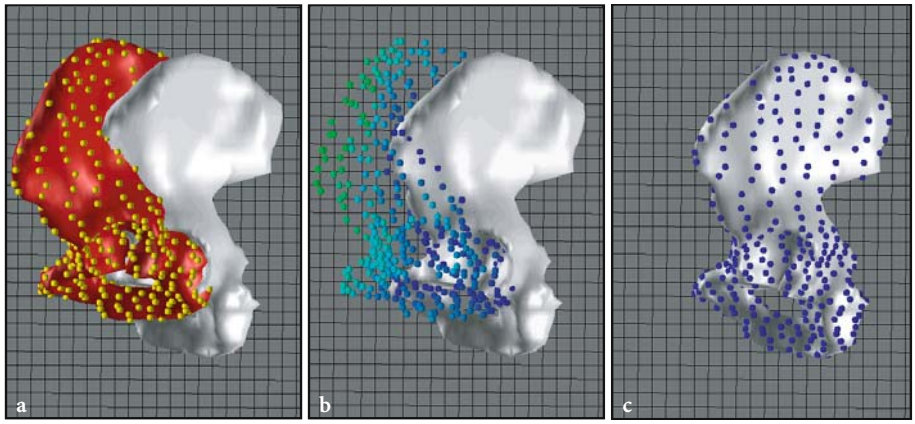

Fig. 5.7. a Extracted surface from Study *A* and extracted surface and surface points from Study *B*. **b** Points colorized based on computed distance of closest approach. **c** Study *B* points registered to Study *A* surface

$$SSD = \sum(I_A - I_{B'})^2 / N.$$

This metric is simple to compute and is effective for registering two imaging studies which have essentially identical intensities for corresponding anatomy, such as serial or 4D CT data.

When this condition is not met but there is still a linear relationship between the intensities of Study *A* and Study *B*, the cross correlation (CC) metric may be used. Rather than minimizing the intensity difference, cross correlation registration maximizes the intensity product:

$$CC = \sum(I_A * I_{B'}) / N.$$

A normalized version of the cross correlation metric exists and is called the correlation coefficient metric (Kim and Fessler 2004).

For data from different modalities where the pixel intensities of corresponding anatomy are typically (and inherently) different, registration metrics based on simple differences or products of intensities are not effective. In these cases, sophisticated metrics based on intensity statistics are more appropriate. When using these metrics, there is no dependence on the absolute intensity values. One such metric that has proved very effective for registering image data from different modalities is called mutual information (MI). As the name implies, this metric is based on the information content of the two imaging studies and is computed directly from the intensity distributions of the studies. Since this metric is widely used in clinical image registration systems, it is described in detail here (see also Wells et al. 1996).

According to information theory, the information content *H* of a "signal" is measured by the expectation (of the log) of the probability distribution function (PDF) of the signal values (Roman 1997). For image data, the signal values are the gray-scale intensities and the PDF is the normalized histogram of these intensities. The information content in the image data is

$$H(I_A) = - E [\log_2 p(I_A)] = -\sum p(I_A) \log_2 p(I_A),$$

where $p(I_A)$ is the probability distribution function of the intensities I_A of Study *A* (Fig. 5.8).

The joint or combined information content of two imaging studies has the same form and represents the information content of the two studies fused together. This is computed as

$$H(I_A, I_{B'}) = -\sum\sum p(I_A, I_{B'}) \log_2 p(I_A, I_{B'})$$

where $p(I_A, I_{B'})$ is the 2D joint probability distribution function of the intensities I_A of Study *A* and $I_{B'}$ of Study *B'* (Fig. 5.9). This PDF is constructed from the pairs of gray-scale values at each common point in Study *A* and Study *B'*.

The joint or total information content for the two imaging studies is always less than or equal to the sum of the individual information contents:

$$H(I_A,I_{B'}) \leq H(I_A) + H(I_{B'}).$$

If there is no redundant information in the pair of imaging studies (e.g., they are completely independent), the joint information of the pair is simply the sum of the information in Study *A* and Study *B'*:

$$H(I_A,I_{B'}) = H(I_A) + H(I_{B'}).$$

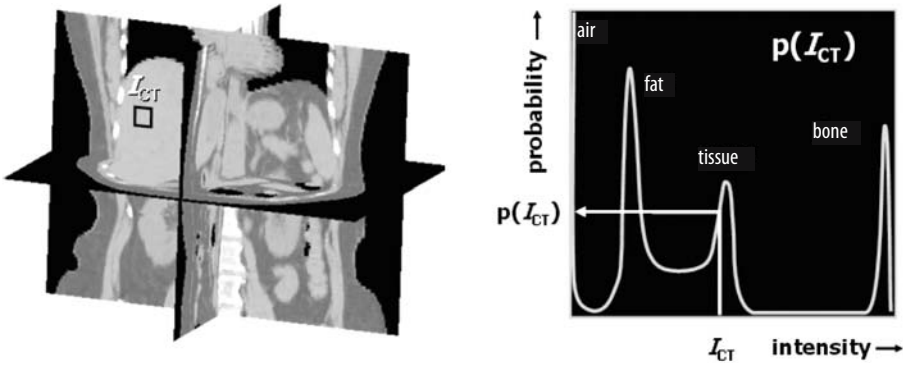

Fig. 5.8. *Left*: 3D image volume; *Right:* probability density function of the image intensities

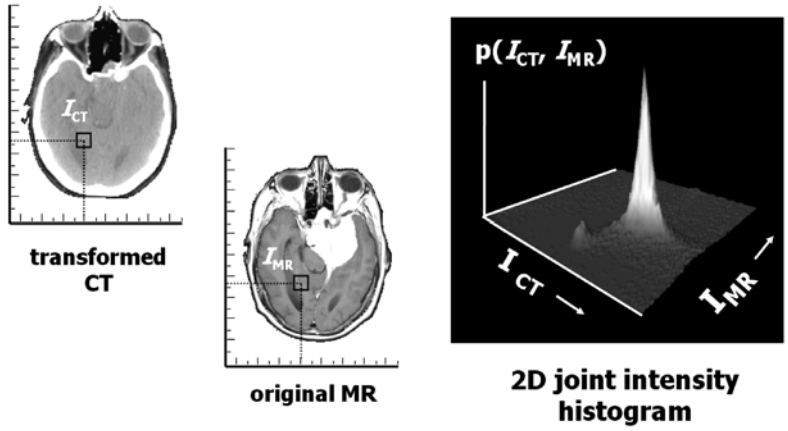

Fig. 5.9. Two-dimensional joint-intensity histogram constructed from an MR scan (Study *A*) and a transformed (reformatted) CT (Study *B'*)

If there is some redundant information, then the joint information content will be less than the sum of the information in the two studies:

$$H(I_A,I_{B'}) < H(I_A) + H(I_{B'}).$$

The amount of shared or mutual information is just the difference between the sum of the individual information contents and the joint information content,

$$MI(I_A,I_{B'}) = H(I_A) + H(I_{B'}) - H(I_A,I_{B'}).$$

Solving for MI from the above equations,

$$MI(I_A,I_{B'}) = \sum \sum p(I_A,I_{B'}) \log_2 [p(I_A,I_{B'}) / p(I_{A'}) p(I_{B'})].$$

The mutual information between two imaging studies can be thought of as the information in Study *B'* that is also present in Study *A*. Accordingly, one way to describe mutual information is as the amount of information in Study *B'* that can be determined (or predicted) from Study *A*. To completely predict Study *B'* from Study *A*, each intensity value in Study *A* must correspond to exactly one intensity value in Study *B'*. When this is the case the joint intensity histogram has the same distribution as the histogram of Study *A*, and $H(I_A,I_{B'})$ equals $H(I_A)$. The MI is therefore equal to $H(I_{B'})$, and Study *B'* at this point can be thought of as a "recolored" version of Study *A*.

A major advantage of mutual information is that it is robust to missing or incomplete information. For example, a tumor might show up clearly on an MR study but be indistinct on a corresponding CT study. Over the tumor volume the mutual information is low, but no prohibitive penalties are incurred. In the surrounding healthy tissue the mutual information can be high, and this becomes the dominant factor in the registration.

5.3 Data Fusion

The motivation for registering imaging studies is to be able to map information derived from one study to another or to directly combine or fuse the imaging data from the studies to create displays that contain relevant features from each modality. For example, a tumor volume may be more clearly visualized using a specific MR image sequence or coronal image plane rather than the axial treatment-planning CT. If the geometric transformation between the MR study and the treatment-planning CT study is known, the clinician is able to outline the tumor using images from the MR study and map these outlines to the images of the CT study. This process is called structure mapping.

Figure 5.10 illustrates the structure mapping process. The contours for a target volume are defined using the images from an MR imaging study which has been registered to the treatment-planning CT. Next, a surface representation of the target volume is constructed by tessellating or "tiling" the 2D outlines. Using the computed transformation, the vertices of the surface are mapped from the coordinate system of the MR study to the coordinate system of the CT study. Finally, the transformed surface is inserted along the image planes of the CT study. The result is a set of outlines of the MR-defined structure that can be displayed over the CT images. These derived outlines can be used in the same manner as other outlines drawn directly on the CT images.

Another approach to combining information from different imaging studies is to directly map the image intensity data from one study to another so that at each voxel there are two (or more) intensity values rather than one. Various relevant displays are possible using this multi-study data. For example, functional information from a PET imaging study can be merged or fused with the anatomic information from an MR imaging study and displayed as a colorwash overlay. This type of image synthesis is referred to as image fusion.

The goal of this approach is to create a version of Study *B* (Study *B*') with images that match the size, location, and orientation of those in Study *A*. The voxel values for Study *B*' are determined by transforming the coordinates of each voxel in Study *B* using the appropriate transformation and interpolating between the surrounding voxels. The result is a set of images from the two studies with the same *effective* scan geometry (Fig. 5.11). These corresponding images can then be combined or fused in various ways to help elucidate the relationship between the data from the two studies (Fig. 5.12).

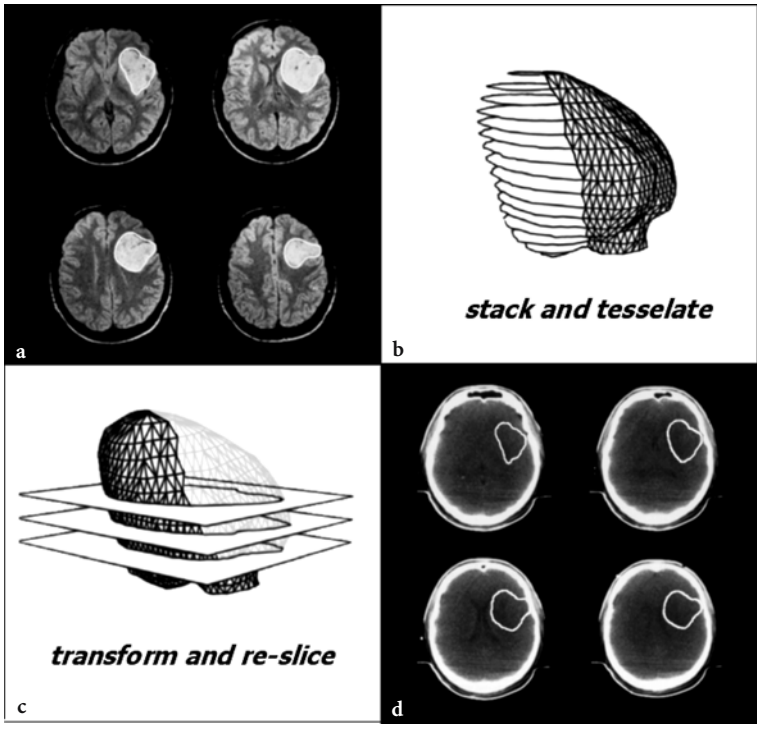

Fig. 5.10. Structure mapping. **a**) Tumor volume outlined on MR. **b**) Outlines stacked and tessellated to create a surface representation. **c**) The MR-based surface is mapped to the CT coordinate system and re-sliced along the image planes of the CT study. **d**) The derived contours are displayed over the CT images.

A variety of techniques exist to present fused data, including the use of overlays, pseudo-coloring, and modified gray scales. For example, the hard bone features of a CT imaging study can be combined with the soft tissue features of an MR imaging study by adding the bone extracted from the CT to the MR data set. Another method is to display anatomic planes in a side-by-side fashion (Fig. 5.12). Such a presentation allows structures to be defined using both images simultaneously.

In addition to mapping and fusing image intensities, 3D dose distributions computed in the coordinate system of one imaging study can be mapped to another. For example, doses computed using the treatment planning CT can be reformatted and displayed over an MR study acquired after the start of therapy. With this data, regions of radiologic abnormality post-treatment can be readily compared with the planned doses for the regions. With the introduction of volumetric imaging on the treatment units,

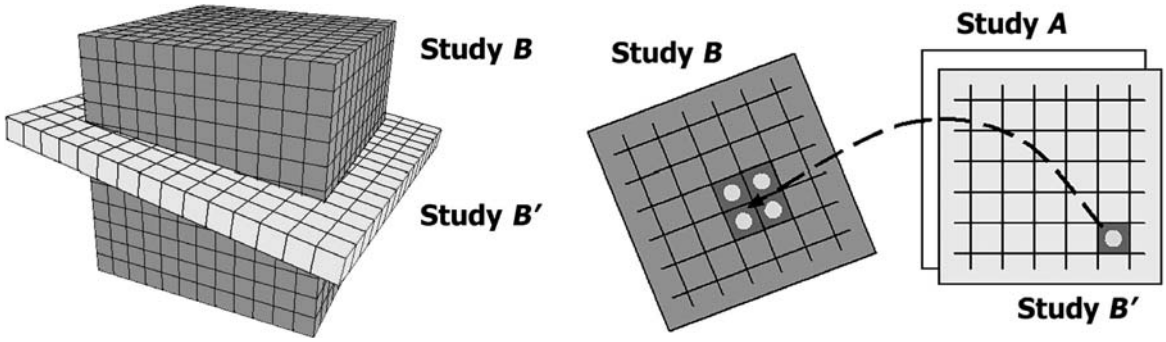

Fig. 5.11. Study *B* is reformatted to match the image planes of Study *A* to produce Study *B'*. Because the center of a pixel in one study will not usually map to the exact center of another, interpolation of surrounding pixel values is required.

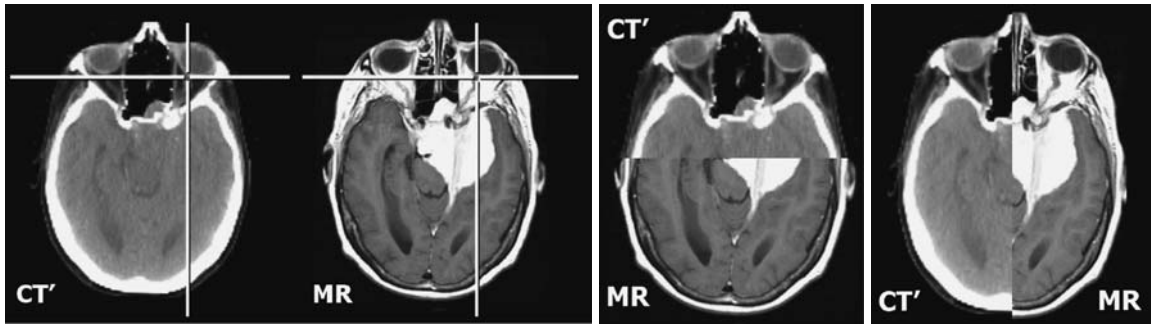

Fig. 5.12. Different approaches to display data which has been registered and reformatted

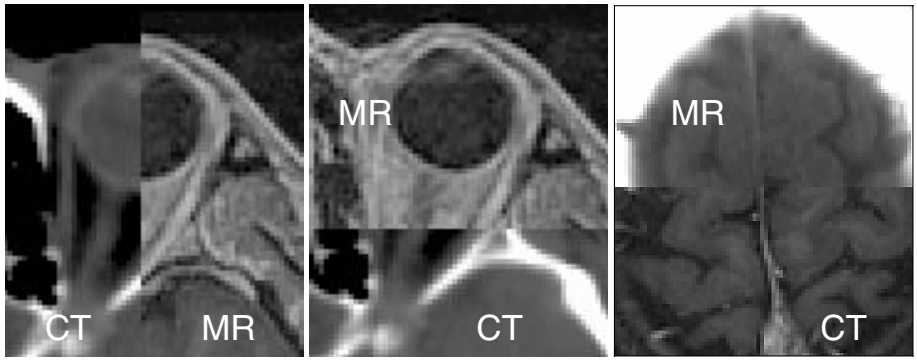

Fig. 5.13. Image–image visual validation using split-screen displays of native MR and reformatted CT study

treatment-delivery CT studies can now be acquired to more accurately determine the actual doses delivered. By acquiring these studies over the course of therapy and registering them to a common reference frame, doses for the representative treatments can be reformatted and accumulated to provide a more likely estimate of the delivered dose. This type of data can be used as input into the adaptive radiotherapy decision process.

5.4 Validation

It is important to validate the results of a registration before making clinical decisions using fused images or mapped structures. To do this, most image registration systems provide numerical and visual verification tools. A common numerical evaluation technique is to define a set of landmarks for corresponding anatomic points on Study *A* and Study *B* and compute the distance between the actual location of the points defined in Study *A* and the resulting transformed locations of the points from Study *B'*. This calculation is similar to the "point matching" metric, but as discussed previously it may be difficult to accurately and sufficiently define the appropriate corresponding points, especially when registering multimodality data. Also, if deformations are involved, the evaluation is not valid for regions away from the defined points.

Regardless of the output of any numerical technique used, which may only be a single number, it is important for the clinician to appreciate how well in three dimensions the information they define in one study is mapped to another. There are many visualization techniques possible to help qualitatively evaluate the results of a registration; most of these are based on the data-fusion techniques already described. For example, paging through the images of a split-screen display and moving the horizontal or vertical divider across regions where edges of structures from both studies are visible can help uncover even small areas of mis-registration. Another interesting visual technique involves switching back and forth between corresponding images from the different studies at about once per second and focusing on particular regions of the anatomy to observe how well they are aligned.

In addition to comparing how well the images from Study *A* and Study *B'* correspond at the periphery of anatomic tissues and organs, outlines from one study can be displayed over the images of the other. Figure 5.14 shows a brain surface which was automatically segmented from the treatment-planning CT study and mapped to the MR study. The agreement between the CT-based outlines at the different levels and planes of the MR study demonstrate the accuracy of the registration.

In practice, the accuracy of the registration process depends on a number of factors. For multimodality registration of PET/CT/MR data in the brain, registration accuracy on the order of a voxel size of the imaging studies can be achieved. Outside the head many factors confound single-voxel level accuracy, such as machine-induced geometric and intensity distortions as well as dramatic changes in anatomy and tissue loss or gain. Nevertheless, accuracy at the level of a few voxels is certainly possible in many situations.

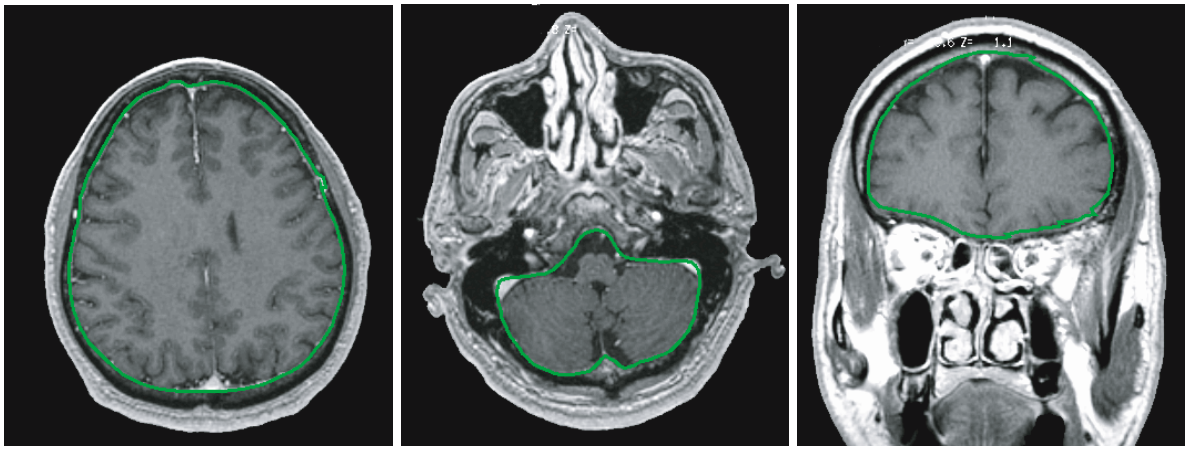

Fig. 5.14. Image-geometry visual validation structure overlay of CT-defined brain outlines (*green*) over MR images

5.5 Conclusion

Accurate delineation of tumor volumes and critical structures is a vital component of treatment planning. The use of a single imaging study to perform the delineation is not always adequate and multiple studies may need to be combined. In order to use data from multiple studies, the spatial alignment of the studies must be determined. Image registration, the process of finding a coordinate transformation between two studies, can recover rigid, affine, and deformed transformations. Automatic registration requires a similarity measure or registration metric. The metric may be specialized for particular types of registration (e.g., single modality) or may be generally applicable. Manual registration can use a metric as well, or it can be based on interactive visual inspection. Deformations are generally not manually registered. Once the coordinate transformation between the imaging studies has been found, various structure mapping and data fusion techniques can be used to integrate the data. Before the resulting data is used in the clinic, a validation process should take place. This might include numerical measurements such as comparisions of landmark positions, but should always include a visual inspection across the entire data set.

The techniques described in this chapter are tools to help use the information from different imaging studies in a common geometric framework. These techniques apply to both time-series single modality and multimodality imaging studies. Most modern radiotherapy treatment planning systems support the use of functional as well as multimodality anatomic imaging using one or more of the techniques presented. These tools, however, cannot replace clinical judgment. Different imaging modalities image the same tissues differently, and although tools may help us better understand and differentiate between tumor and non-tumor, they cannot yet make the ultimate decision of what to treat and what not to treat. These decisions still lie with the clinician, although they now have more sophisticated tools to help make these choices.

References

Allal AS, Slosman DO, Kebdani T, Allaoua M, Lehmann W, Dulguerov P (2004) Prediction of outcome in head-and-neck cancer patients using the standardized uptake value of 2-[18F]fluoro-2-deoxy-D-glucose. Int J Radiat Oncol Biol Phys 59:1295–1300

Barthel H, Cleij MC, Collingridge DR, Hutchinson OC, Osman S, He Q, Luthra SK, Brady F, Price PM, Aboagye EO (2003) 3'-deoxy-3'-[18F]fluorothymidine as a new marker for monitoring tumor response to antiproliferative therapy in vivo with positron emission tomography. Cancer Res 63:3791–3798

Bharatha A, Hirose M, Hata N, Warfield SK, Ferrant M, Zou KH, Suarez-Santana E, Ruiz-Alzola J, D'Amico A, Cormack RA, Kikinis R, Jolesz FA, Tempany CM (2001) Evaluation of three-dimensional finite element-based deformable registration of pre- and intraoperative prostate imaging. Med Phys 28:2551–2260

Bookstein FL (1989) Principal warps: thin-plate splines and the decomposition of deformations. IEEE Trans Pattern Anal Mach Intell Vol 11. 6:567–585

Brun E, Kjellen E, Tennvall J, Ohlsson T, Sandell A, Perfekt R, Perfekt R, Wennerberg J, Strand SE (2002) FDG PET studies during treatment: prediction of therapy outcome in head and neck squamous cell carcinoma. Head Neck 24:127–135

Chenevert TL, Stegman LD, Taylor JM, Robertson PL, Greenberg HS, Rehemtulla A, Ross BD (2000) Diffusion magnetic resonance imaging: an early surrogate marker of therapeutic efficacy in brain tumors. J Natl Cancer Inst 92:2029–2036

Kim J, Fessler JA (2004) Intensity-based image registration using robust correlation coefficients. IEEE Trans Med Imaging 23:1430–1444

Maintz JB, Viergever MA (1998) A survey of medical image registration. Med Image Anal 2:1–36

Mardor Y, Pfeffer R, Spiegelmann R, Roth Y, Maier SE, Nissim O, Berger R, Glicksman A, Baram J, Orenstein A, Cohen JS, Tichler T (2003) Early detection of response to radiation therapy in patients with brain malignancies using conventional and high b-value diffusion-weighted magnetic resonance imaging. J Clin Oncol 21:1094–1100

National Electrical Manufacturers Association (2004) DICOM, part 3, PS3.3 – service class specifications. Rosslyn, Virgina

Roman S (1997) Introduction to coding and information theory. Undergraduate texts in mathematics. Springer, Berlin Heidelberg New York

Thirion JP (1998) Image matching as a diffusion process: an analogy with Maxwell's demons. Med Image Anal 2:243–260

Unser M (1999) Splines: a perfect fit for signal and image processing. IEEE Sign Process Mag Vol 16. 6:22–38

Wells WM 3rd, Viola P, Atsumi H, Nakajima S, Kikinis R (1996) Multi-modal volume registration by maximization of mutual information. Med Image Anal Vol 1. 1:35–51

6 Data Formats, Networking, Archiving and Telemedicine

Karsten Eilertsen and Dag Rune Olsen

CONTENTS

6.1 Introduction

Over the past two decades, a tremendous growth in digital image acquisition systems, display workstations, archiving systems and hospital/radiology information systems has taken place. The need for networked picture archiving and communications systems (PACS) is evident.

The conception of such a system dates back to the early 1970s (Lemke 1991); however, for many years the lack of basic technology to provide required network infrastructure (e.g. network bandwidth, data communication standards, workflow management) as well as initial capital outlays in the multimillion dollar range impeded a widespread introduction of PACS into clinical practice. During the 1990s all aspects of the technology matured and the development of "filmless" digital networked enterprises with a PACS (Dreyer et al. 2002) solution as the key component took off: primarily within the field of radiology, but the technology soon gained foothold in other medical disciplines as well. As such, digital image networking is not merely a technological issue, but can contribute to improved health care as imaging modalities become readily available across traditional departmental barriers. This development has had, and will have in many years to come, a dramatic impact on the working practice of medical imaging.

In this chapter we address various aspects of digital image networking with a special focus on radiotherapy.

6.2 Data Formats

There are many different data types in use in the hospital environment ranging from comprehensive cine sequences, 3D image sets, voice recordings, to textual reports, prescriptions and procedures. They all play important roles in the field of electronic health where the electronic patient record is one of the cornerstones. Restricting the scope to that of imaging, four types of information are generally present in such data sets: image data (which may be unmodified or compressed); patient identification and demographics; and technical information about the imaging equipment in use as well as the exam, series and slice/image. The formats used for storing these images may depend on the needs of equipment-specific reviewing applications, e.g. to facilitate rapid reload of the images into dedicated viewing consoles. There are three basic families of formats in use: the fixed format (the layout is identical in each file); the block format (the header contains pointers to information); and the tag- or record-based format (each item contains its own

K. Eilertsen, PhD
Department of Medical Physics, The Norwegian Radium Hospital, Montebello, 0310 Oslo, Norway
D. R. Olsen, PhD
Institute of Cancer Research, The Norwegian Radium Hospital, Montebello, 0310 Oslo, Norway

length). Extracting image data from such files is usually easy, even if a proprietary formatting is used, but to decipher every detail may require detailed insight into the format specification. Examples of standard file formats in widespread use are Tagged Image File Format (TIFF), Graphic Interchange Format (GIF), JPEG file interchange format (JIFF), MPEG (movies), WAV and MIDI (voices). Recently, the Portable Network Graphic (PNG) has gained popularity, especially for Internet web applications. The stream of DICOM messages stored in a file may also be considered an image format and has become a common way of keeping medical images. The reading of such files may require detailed knowledge about the streaming syntax and the underlying communication protocols that were used (see below).

Extensive use of different image formats restricts the ability of cross-platform data sharing in a networked environment, as dedicated file readers and viewers are needed. Important image characteristics, such as resolution, gray and/or color scale interpretation, contrast and brightness, may deteriorate or even be lost due to inherent limitations of the format in use. The creation of sufficiently comprehensive image formats and the subsequent network transport from the modality to (any) application in a standardized fashion is therefore a major endeavor. In the next sections we explore one solution to this challenge.

6.3 Networking: Basic Concepts

The International Organization for Standardization has defined the Open System Interconnection (OSI) reference model to be used as an architectural framework for network communication. The OSI model describes how data in one application is transported trough a network medium to another application. The model concept consists of seven different layers, each layer specifying a particular network function (Table 6.1). The functions of the different layers are fairly self-contained, and the actual implementation of these functions (often called protocols) makes possible the communication or transport of data between the layers.

The design of a PACS network within a particular hospital environment would constitute a typical Local Area Network (LAN) where an Ethernet topology (or Fast Ethernet, Gigabit Ethernet) with TCP/IP is utilized to facilitate networked communication. Furthermore, several hospitals within the same health care organization can be connected into Wide-Area Networks (WAN).

Table 6.1. The seven OSI model layers and an OSI model realization with Ethernet and TCP/IP

Layer	OSI model	Ethernet with TCP/IP
7	Application	Telnet, ftp, SMTP
6	Presentation	Data formats (e.g. JPEG, MPEG, ASCII)
5	Session	Session Control Protocol (SCP), DECNet
4	Transport	Transmission Control Protocol (TCP)
3	Network	Internet Protocol (IP)
2	Data link	Ethernet Network Interface Card (NIC)
1	Physical	Twisted pair CAT 5 cabling, FiberChannel

Having defined the basic framework for network operation, the challenge is to exploit this topology to facilitate smooth connectivity between the multivendor modalities.

6.3.1 Network Connectivity: The DICOM Standard

An apparently seamless exchange of data between different computer applications (or modalities; Fig. 6.1) in the hospital network has traditionally been restricted to vendor-specific equipment that applies proprietary standards. In a modern multimodality hospital environment with a multitude of digital systems from many different manufacturers, proprietary solutions offer little flexibility. They are costly and cumbersome to operate as custom interfaces must be developed and maintained, possibly error prone and safety critical since data consistency can be jeopardized as data must be reformatted to suit a given equipment specification. An additional maintenance level may be required to assure data quality when, for instance, equipment is upgraded or replaced. The use of such solutions may therefore represent a serious obstacle to the progress and introduction of state-of-the art network technology.

During the 1980s the need for simplification and standardization became apparent in order to ensure and maintain vital connectivity and interoperability of all pieces of equipment. The medical equipment industry, represented by the National Electrical Manufacturers Association (NEMA) and the medical community, represented by the American College of Radiology (ACR), joined forces to develop the *Digital Imaging and Communications in Medicine* standard (DICOM). The intention was to create an

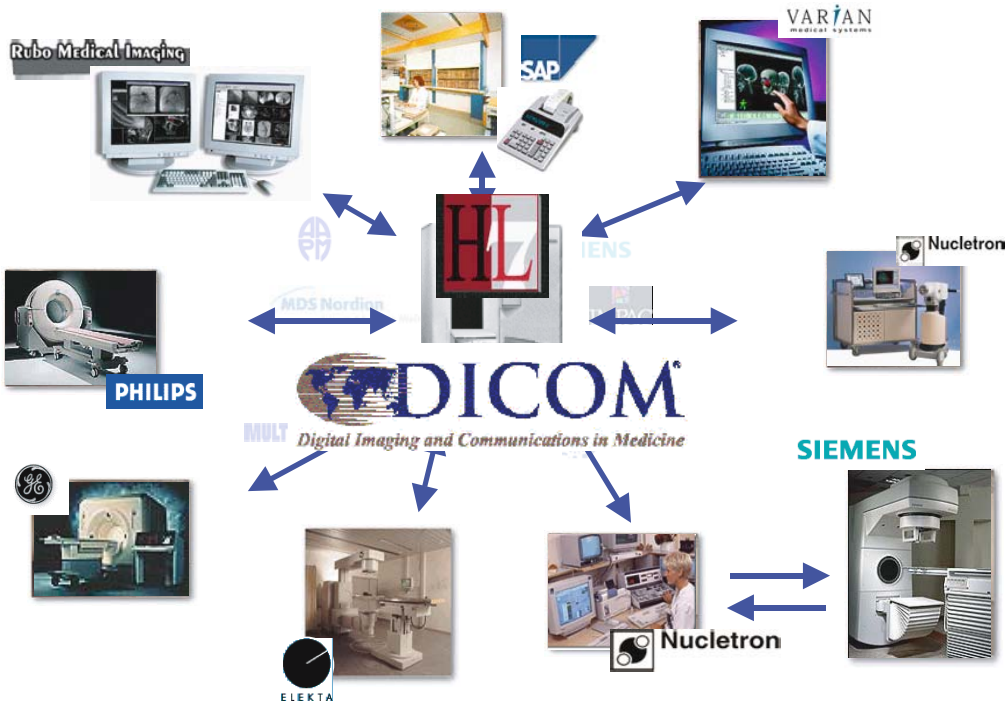

Fig. 6.1. A typical oncology LAN

industry standard to which all vendors of medical equipment could conform. This would establish a win–win situation for all involved parties: if DICOM support is built into a medical imaging device, it can be directly connected to another DICOM-compatible device, eliminating the need for a custom interface – DICOM defines the interface. Even though the first versions of the standard, ACR-NEMA 1.0 (1985) and ACR-NEMA 2.0 (1989), never became very popular among vendors, the later DICOM v3.0 (DICOM) is by present-day standards ubiquitous. One important reason for this development is that the concepts of the OSI model (e.g. the use of standard network protocols and topology) were utilized when drafting the basic network functionality of DICOM. On one hand, this makes possible the use commercial off-the-shelf hardware and software, and on the other, this ensures that DICOM remains an open standard that encourages both users and vendors to get involved in its development.

DICOM was first developed to address connectivity and inter-operability problems in radiology, but presently there are parts of the DICOM standard which define service classes for many other modalities. During the RSNA conference in 1994, a meeting was held at which a clear need was expressed for standardization of the way radiotherapy data (such as external beam and brachytherapy treatment plans, doses and images) are transferred from one piece of equipment to another. The importance of such a standard was clear. As a result of the RSNA meeting, an ad-hoc Working Group, later to become Working Group 7 (Radiotherapy Objects) was formed under the auspices of NEMA. Participating members of this group include many manufacturers of radiotherapy equipment, some academics and also members involved with the IEC. The DICOM v3.0 standard is large and consists of 16 different parts, each part addressing a particular functional side of DICOM. The standard defines fundamental network interactions such as:

- **Network Image Transfer:** Provides the capability for two devices to communicate by sending objects, querying remote devices and retrieving these objects. Network transfer is currently the most common connectivity feature supported by DICOM products.
- **Open Media Interchange:** Provides the capability to manually exchange objects and related information (such as reports or filming information). DICOM standardizes a common file format, a medical directory and a physical media. Examples include the exchange of images for a publication and mailing a patient imaging study for remote consultation.
- **Integration within the Health Care Environment:** Hospital workflow and integration with other hospital information systems have been addressed

with the addition services such as Modality Worklist, Modality Performed Procedure Step, and Structured Reporting. This allows for scheduling of an acquisition and notification of completion.

To facilitate the desired network functionality, DICOM defines a number of network services (Service Classes). These services are described in brief below (Table 6.2).

Table 6.2 DICOM service classes and their functional description

DICOM service class	Task
Storage	Object transfer/archiving
Media storage	Object storage on media
Query/retrieve	Object search and retrieval
Print management	Print service
Patient, study, results management	Create, modify
Worklist management	Worklist/RIS connection
Verification	Test of DICOM connection

6.3.2 The DICOM Radiotherapy Model

In 1997 four radiotherapy-specific DICOM objects and their data model were ratified. In 1999 three additional objects were added to the DICOM standard, along with CD-R support for the storage of all radiotherapy objects (Fig. 6.2). The seven DICOM RT objects are as follows:

- **RT Structure Set,** containing information related to patient anatomy, for example structures, markers and isocenters. These entities are typically identified on devices such as CT scanners, physical or virtual simulation workstations or treatment planning systems.
- **RT Plan,** containing geometric and dosimetric data specifying a course of external beam and/or brachytherapy treatment, e.g. beam angles, collimator openings, beam modifiers, and brachytherapy channel and source specifications. The RT Plan entity may be created by a simulation workstation and subsequently enriched by a treatment-planning system before being transferred to a record-and-verify system or treatment device. An instance of the RT Plan object usually references an RT Structure Set instance to define a coordinate system and set of patient structures.
- **RT Image,** specifying radiotherapy images that have been obtained on a conical imaging geometry, such as those found on conventional simulators and (electronic) portal imaging devices. It can also be used for calculated images using the same geometry, such as digitally reconstructed radiographs (DRRs).
- **RT Dose,** containing dose data generated by a treatment-planning system in one or more of several formats: three-dimensional dose data; isodose curves; DVHs; or dose points.
- **RT Beams Treatment Record, RT Brachy Treatment Record** and **RT Treatment Summary Record,** containing data obtained from actual radiotherapy treatments. These objects are the historical record of treatment and are linked with the other "planning" objects to form a complete picture of the treatment.

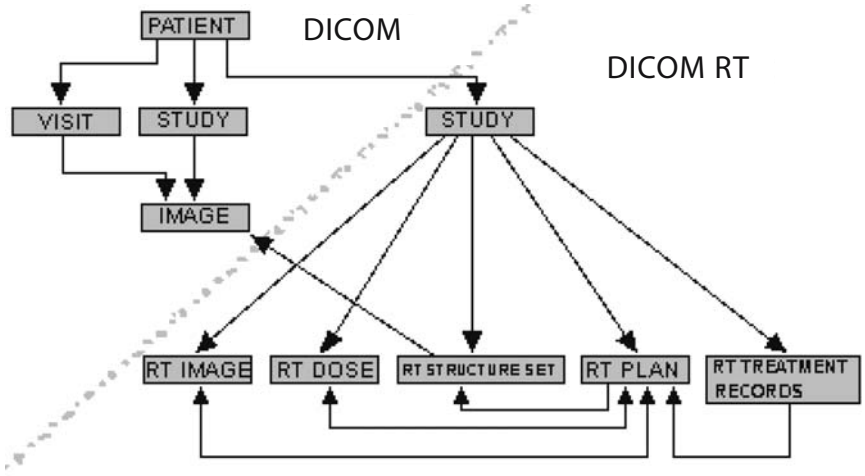

Fig. 6.2. The DICOM RT data model

Working Group 7 is constantly involved in the maintenance of the existing radiotherapy objects and is examining potential uses of newer DICOM extensions in the radiotherapy context. Presently, the DICOM RT information objects provide a means of standardized transfer of most of the information that circulates in the radiotherapy department; however, there are at present few manufacturers of radiotherapy equipment that fully support the DICOM RT standard. In particular, the full exploitation of the DICOM RT data model has only limited support.

6.3.3 A Radiotherapy Example

The equipment scenario shown in Fig. 6.3 is used to illustrate how DICOM objects are produced and furthermore utilized during patient treatment. A sequence of possible steps is listed below along with their associated specified DICOM objects:

1. The patient is scanned on a CT scanner, producing a DICOM CT image study. Other DICOM imaging modalities, such as MR, could also be involved.
2. A virtual simulation application queries the scanner using DICOM, retrieves the images and performs a virtual simulation. An RT Structure Set object is produced, containing identified structures such as the tumor and critical organs. An associated RT Plan is also created, containing beam-geometry information. Digitally reconstructed radiographs (DRRs) may also be created as RT Image objects.
3. A treatment-planning system then reads the CT images, RT Structure Set and RT Plan. It adds beam modifiers, modifies the beam geometries where necessary, and also calculates dosimetric data for the plan. A new RT Plan object is created, and RT Image DRRs may also be produced.
4. A record-and-verify system then obtains the completed RT Plan object and uses the data contained within it to initialize a treatment. Alternatively, the treatment machine itself could make use of the object directly. An EPID can create RT image verification images and compare acquired images with DRRs created by the above steps.
5. Periodically during the course of treatment, the treatment machine or record and verify system creates Treatment Record objects, generally one for each treatment session.
6. At the end of the treatment, the entire DICOM set of DICOM objects is pushed to a dedicated DICOM Archive.

The above sequence illustrates just one scenario. In reality there is a wide variety of different utilizations possible, and the DICOM RT objects have been designed with this flexibility in mind.

6.3.4 The DICOM Conformance Statement

The standard specifies that the manufacturer of any device claiming DICOM conformance shall provide a *DICOM Conformance Statement* that describes the

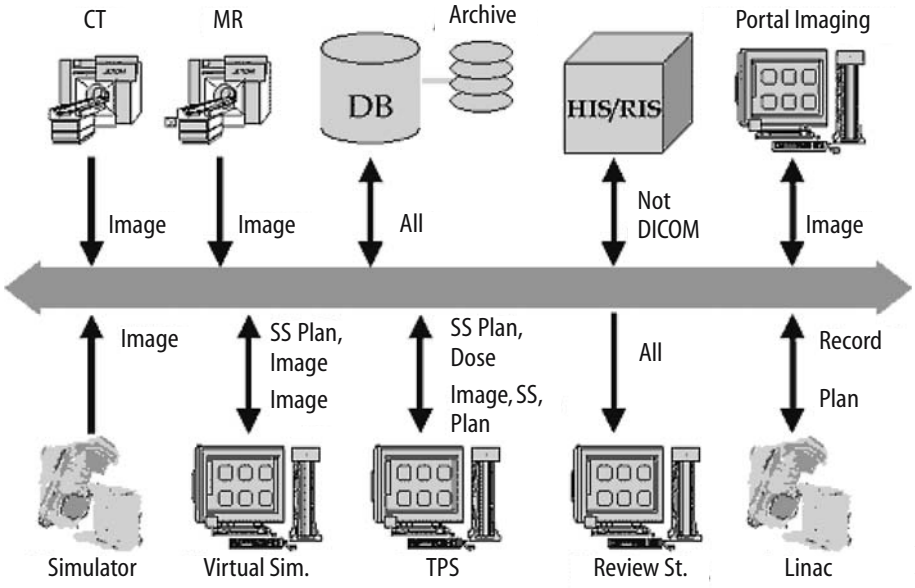

Fig. 6.3. Scenario displays the different DICOM modalities that may be involved in patient treatment

DICOM capabilities of the device (cf. part 2 of the DICOM standard). Many manufacturers make their conformance statements available on the Internet. Potential connectivity between two pieces of equipment can therefore be evaluated in advance by reading Conformance statements which provide a foundation to determine connectivity and assess the potential inter-operability of two products, and in some cases identify potential problems without ever having physically connected them.

It is not sufficent for a vendor to simply claim conformance to DICOM. The statement "This product is DICOM" has even less meaning in the radiotherapy domain, in which inter-operability is a very complex issue. For RT applications, it is usually not possible to determine inter-operability a priory – this must be established through extensive testing. Still, radiotherapy professionals should insist upon a conformance statement for any device that claims to be DICOM conformant. Even so, DICOM conformance is voluntary and there is no authority that approves or may enforce conformance; however, by conforming to DICOM, one can develop safe, reliable computer applications with a high degree of built-in connectivity.

6.3.5 DICOM Problems

Even a standard such as DICOM does not completely eliminate connectivity issues, and the inherent flexibility of the standard is a common source of confusion and frustration. The DICOM standard, and the RT parts in particular, contains numerous so-called type-2 and type-3 attributes. Type-2 attributes must be present in a DICOM message for the message to be valid, but the attribute value may be sent empty if unknown, i.e. it is left with the application vendor to fill in the value. Type-3 attributes are optional, i.e. they may or may not be present in a message. Some of these attributes can be crucial for the functionality of other applications. One example would be the tabletop positions (type 3) in the RT plan. These attributes are very useful to ensure a correct setup of the patient during external-beam radiotherapy. The attributes should be provided by the planning system for use by the record and verify system when setting up the patient at treatment. Presently, there are very few planning systems that provide these values. Another common problem is the different ways vendors organize 3D image sets (CT, MR, etc.) into series. Some applications, such as treatment-planning systems and virtual simulators, rely on all images of a given type (e.g. all axial images) to exist in the same series in order to create a 3D reconstructed volumetric data representation. Especially older CT/MR scanners tend to split such data sets into several series or even put localizer and axial images in the same series.

6.3.6 How Are the Manufacturers Doing Today?

DICOM is now a mature standard. After a lot of hard work understanding, developing and testing product inter-operability in the radiotherapy context, a large number of manufacturers now have products available that support one or more of the radiotherapy DICOM objects. Vendors who have such products available, or have demonstrated them as works in progress, include Elekta, General Electric Medical Systems, IMPAC, Merge Technologies, Multidata, NOMOS, Nucletron, Picker International, ROCS, Siemens Medical Systems, SSGI, CMS and Varian Medical Systems.

6.4 Archiving

Historically the term "archive" refers to an institution or facility that undertakes the task of preserving records for longer periods of time, sometimes indefinitely. The core tasks of such an archive are typically to provide means for access control, ensure long-term media stability and readability, and to preserve record authenticity, in addition to disaster safe storage. The records in such archives have traditionally been data on analogue media such as paper and photographic film that can be visually inspected. This description also applies to medical archives that typically contain patient records and X-ray films.

The growth of information that exists in digital format within the medical environment poses a tremendous challenge to the traditional way of archiving. The main concern is probably the media on which the data is being stored. Media storage technology is evolving rapidly and there is an inherent risk that such media is outdated in a matter of few years (10–20 years) mainly because the hardware and software components required to access the storage media are no longer manufactured and supported.

A fundamental prerequisite for digital archives is therefore that they easily can accommodate new storage technology as well as to easily scale with growing demands in capacity. In other words, the archive should have built-in technology that, for instance, facilitates automatic data migration from one media/storage technology to another. The cost of archiving digital information should thus include not only the running costs of technical maintenance and support, but also the cost of keeping up with the continuous changes in technology.

The role of the archives is also changing. Contrary to the historical "archive", an important feature of a digital archive, is potential ease and speed of access. In a PACS implementation the archive serves as a common location for receiving all images as well as the source for distribution of images. To achieve this, the notions of on-line cache or storage (meaning fast access, low capacity), and long-term or secondary storage (meaning slow access but huge capacity), are often used. The present trend is that that these two concepts tend to merge as the storage media become cheaper.

Another important aspect in the digital archive is reliability and robustness. A common measure of reliability is a system's "uptime", and it is generally accepted that this should be greater than 99% per year, i.e. less than 3.6 days/year downtime. Still, the archive is in essence the hub in the PACS network and, if unavailable, production is jeopardized. It is therefore important to invest in hardware and software with built-in redundancy that can mitigate the effect of technology failures. In addition, special procedures and plans should be developed to handle catastrophic events such as fires, earthquakes, etc., for instance, by establishing remote vaults for off-site data storage.

6.4.1 Media Storage Technology

Storage media has for years enjoyed continuous progress in increased capacity and reduction in prices. This applies to all of the most popular storage media. It makes no sense to quote absolute figures as these will soon become dated; however, a crude estimate on a relative scale would roughly be (2004) 1000, 10, 5 and 1, for solid-state memory, magnetic disk, magnetic tape storage (DLT) and optical storage (DVD), respectively, considering the media price only.

The choice of storage technology is usually a trade-off between storage price/capacity and access time. The faster access times required, the more expensive the storage. For archiving purposes there has been a tradition to use magnetic disk for the on-line storage and optical/magnetic tape for secondary storage; however, advances in both storage and LAN technology along with lower prices has demonstrated a trend towards extensive use of large-scale magnetic-disk arrays for both on-line as well as long-term storage. The concepts of Network Attached Storage (NAS) and Storage Area Networks (SAN) have furthermore promoted this trend.

6.4.2 Data Formats for Archiving

When using DICOM the problem of different or proprietary data formats is reduced to having access to a DICOM object/message viewer. If one cannot use the application that generated the object initially to review the object, there exist several applications – either as freeware or for a small fee – that can be downloaded from the internet to accomplish this task. Some of these viewer applications include built-in DICOM storage providers that can be used to receive the DICOM message. In the field of radiotherapy proper viewers are still scarce probably due to the inherent complexity of the RT DICOM objects and the amount on non-image data.

The demands on the data format used for storage in an archive are different. The amount of data to be stored is potentially enormous and many archives apply compression to allow for more data to be stored. From a user's point of view the archive can be considered a black box that talks DICOM. As long as the archive gives back what once was stored, the user is satisfied and the internal storage format of the archive is as such irrelevant; however, if compression is used, the quality of the returned image may be reduced with respect to the original and this may not be acceptable. The DICOM committee has deemed lossless JPEG and lossy JPEG acceptable techniques for compressing medical images, and several archive vendors have implemented strategies for the use of these techniques. A common option is to make the compression technique in use dependent on the age of the object, i.e. newer objects are only made subject to lossless JPEG (two to three times reduction of most images), whereas older objects are compressed using lossy JPEG (10- to 100-fold reduction in image size). This implies that the archive continuously migrates data from lossless to lossy JPEG. Another strategy is to use different compression techniques for different image types. A noisy 512×512 radiotherapy portal

image may suffer considerable loss in quality if lossy JPEG at a ratio of 10:1 is used, whereas a 4000×8000 MB chest X-ray may be compressed satisfactorily at a ratio of 60:1. Only careful testing can reveal what is the appropriate compression level.

Evidently, it is important that the user defines this strategy in accordance with health care regulations.

6.5 Workflow Management: From Connectivity to Integration

The computer network of the hospital should provide the technical infrastructure required for rapid transmission and exchange of data between the different modalities used for diagnosis, planning and treatment. The use of DICOM will eventually provide excellent connectivity between the interacting parties. But DICOM has as of yet limited support for workflow management and data integration. Custom-made solutions may be required, and DICOM was not intended to solve this task.

In order to understand what DICOM can and cannot provide, it is important to distinguish between DICOM *connectivity* and *application interoperability*. This is especially true in the domain of radiotherapy where the working process is very dynamic. DICOM connectivity refers to the DICOM message exchange standard responsible for establishing connections and exchanging properly structured messages so that an information object sent from one node will be completely received by the receiving node. In other words, the successful transfer of information: the successful "plug and exchange" between two pieces of equipment.

Beyond connectivity lies application interoperability: the ability to process and manipulate information objects. DICOM radiotherapy objects play a crucial role in enabling such interoperability, but sometimes "plug and play" at this level requires more than the standardized definition and coding of information provided by DICOM. Specification and testing of the clinical application capabilities and data flow needs to be performed by the health care facility to ensure effective integration of the various DICOM applications. For example, transfer of IMRT (intensity-modulated) data from an IMRT-capable treatment-planning system requires a record-and-verify or treatment system capable of managing such dynamic treatments. DICOM requires implementers to explicitly specify these application-specific information needs in a DICOM Conformance Statement that will provide the basis for achieving such application interoperability.

The service classes "Modality Worklist Management (MWL)", "Modality Performed Procedure Step (MPPS)" and "Storage Commitment (SC)" were all defined to facilitate the communication between information systems (RIS/HIS), PACS and the modalities. In principle, these services are designed to work independently but may also be set up to work together. The MWL enables scheduling information to be conveyed at the modalities and supplies the DICOM objects with HIS/RIS data such as patient demographics; the latter is very useful in avoiding typing errors at the modalities. The MPPS is used to update a schedule when a scheduled procedure step commences, as well as notifying the PACS when a scheduled procedure has been completed. In addition, details describing the performed procedure can be included such as a list of images acquired, accession numbers, radiation dose, etc. The SC facilitates automated or simplified deletion of the images on the modalities as the PACS confirms their safe storage.

It is customary to implement what is called a "broker" to deal with the intricate communication between the HIS/RIS, PACS and the modalities, i.e. to fully exploit the possibilities provided by MWL, MPPS and SC. The broker is often a proprietary third-party software that has been designed to provide a dedicated solution to a user-specified workflow.

6.6 Telemedicine Applications in Radiation Therapy

The advances in modern radiotherapy throughout the past decade have, to a large extent, relied on technological development, in general, and in imaging and computer technology in particular. The role of CT images in treatment planning of radiation therapy is evident, and imaging modalities, such as MR and PET, represent functional or physiological, and biological or even molecular, information that will become essential in modern radiotherapy treatment planning. Moreover, imaging tools have been developed and implemented in treatment verification and for adaptive treatment strategies. Digital representation of the image information, development of image information standards, such as DICOM, establishment of networks and protocols and improved connectivity between modalities, are all cru-

cial elements for the utilization of image information within a clinical radiotherapy environment; however, the development of information standards, protocols and network connectivity do not merely allow digital information flow within a single department, it also advocates communication between and among different institutions, and the formation of inter-institutional networks has thus become feasible.

Telemedicine has been widely adopted and provides increased access to medical expertise in a variety of medical applications. The most common areas for telemedicine have traditionally been radiology, pathology and dermatology – all examples of medical specialties where medical images play a key role. Other areas of medical practice, where digital medical information is available, e.g. emergency medicine and cardiology, have also adopted the concept of telemedicine. Telemedicine is most commonly defined as long-distance communication between medical centers. Telemedicine is, however, evolving conceptually, and The Mayo Clinic has introduced the term "telehealthcare" to include all aspects of communication between medical centers for patient care and limits the term "telemedicine" to communication between centers for purposes of individual patient care.

Although both radiology and radiation therapy are medical disciplines that utilize medical images to a large extent, telemedicine has until recently rarely been adopted in radiotherapy as compared with radiology; thus, the experience is limited and only a few reports worldwide document clinical applications (Hashimoto et al. 2001a, b; Smith et al. 1998; Eich et al. 2004); however, it is expected that applications of telemedicine in radiation therapy will become equally important in improving the quality and standardization of radiotherapy procedures. Telemedicine may especially play a key role in distributed radiotherapy services, in rural areas and possibly in developing countries, but also in the provision of high-end radiation therapy, such as proton treatment, and in treatment of rare cancers; thus, telemedicine will be an appropriate tool in maintaining high-quality, decentralized radiotherapy services, and in preventing professional isolation (Reith et al. 2003). Moreover, telemedicine may facilitate collaboration between highly specialized centers of excellence with respect to rare conditions. The role of telemedicine in radiation therapy is to provide a tool for apparent seamless dialogue between clinical experts in the following:

- Treatment planning and simulation of individual patients
- Treatment verification of individual patients
- Follow-up and clinical trial management

Treatment planning and simulation of individual patients is perhaps the most evident role of telemedicine in radiation therapy. There are at least two steps in this process where remote consultation may be of clinical importance: (a) delineation of the target volume based on 3D medical imaging, e.g. CT, MR and PET; and (b) the discussion of beam setup and evaluation of the plan options. Delineation of the target volume is perhaps the most critical part of the treatment planning and with respect to clinical outcome, moreover, an inter- as well as intra-observer variability in target-volume delineation has been well documented. Lastly, imaging modality, settings and parameters are known to influence target-volume delineation. In rare cancers or at smaller, satellite radiotherapy clinics the required expertise may not be available for the optimal use of medical imaging in radiation therapy planning. Telemedicine in such situations may be the appropriate tool for consulting remote expertise. The ideal scenario is a real-time, on-line telemedicine service, where the target volume can be jointly delineated by the two physicians. Either a complete set of data must to be available at both centers or on-line transferred, e.g. as video signal, for simultaneous display. In addition, the drawing device must be operable from both centers. A few systems have been developed dedicated to remote treatment planning and virtual simulation (Ntasis et al. 2003; Huh et al. 2000; Stitt et al. 1998; Eich et al. 2004). A less attractive, but still useful, alternative is transfer of data from one center to the other for target delineation by an expert team. This mode of operation is less technology demanding, and requires merely that exported data sets from the one institution be successfully imported by the other; however, the dialogue between the professionals is not facilitated by this procedure. Identical modes of operations are relevant with respect to beam setup and dose computation. Final plan evaluation, or selection of the preferred plan, often take place within a larger group of professionals including not only the oncologist but also the medical physicist, the dosimetrist/RTT and sometimes the radiologist and surgeon, in addition to the oncologist. If more centers are involved, telemedicine may be used to include all the professionals at the different institutions in a clinical discussion of the final treatment plan (Fig. 6.4).

Virtual simulation has become more common and frequently used in a number of radiotherapy clinics, and to a certain degree has replaced conventional simulation; however, conventional simulation is still

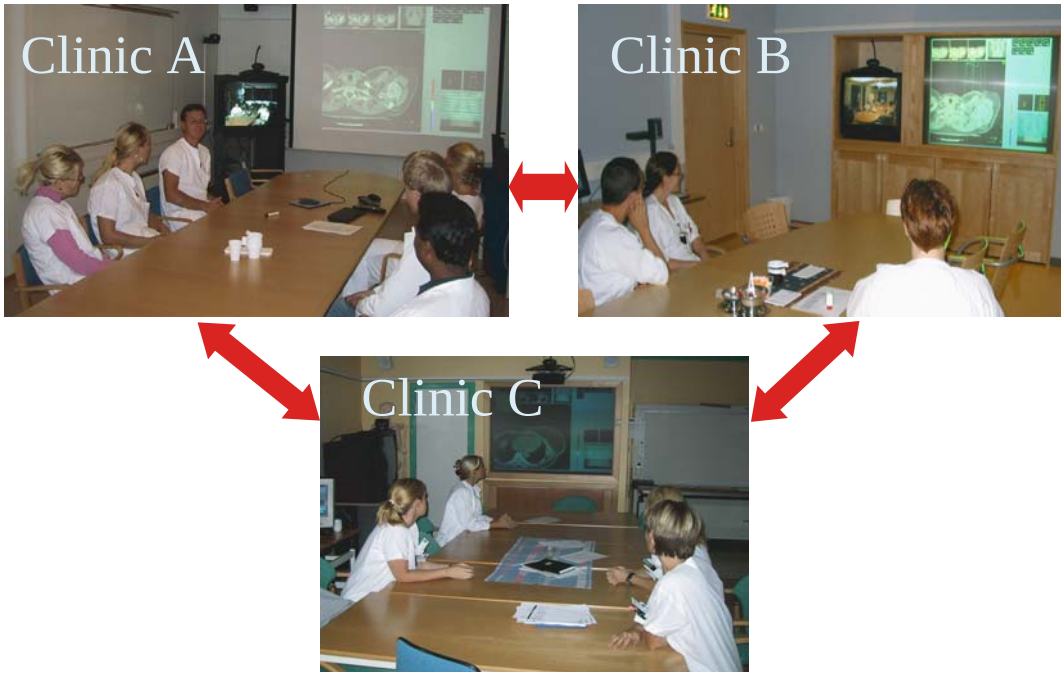

Fig. 6.4. Video-conferencing between three different radiotherapy institutions, demonstrating weekly clinical conference where a treatment plans are discussed, and electronic portal images, DRR and simulator images are reviewed

widely employed for simpler treatments where full 3D treatment planning and dose computation may be superfluous. At Hokkaido University School of Medicine, the THERAPIST system, has been applied for a number of years with success for remote simulation of emergency radiotherapy of spinal cord compression (Hashimoto et al. 2001a).

Treatment verification of individual patient involves most often acquisition of electronic portal images (EPI) and comparison with either digital simulator images of DRR. This task may very well be conducted by individuals on dedicated workstations, but compliance between intended and actual treatment is also often discussed during clinical conferences, again involving a larger group of the staff, and may represent an important arena for quality management of individual patient treatment within the framework of decentralized radiotherapy services, involving more regional or satellite units. Teleconferencing facilitates such an activity and satisfies the education aspects of quality management (Fig. 6.5). Hashimoto and co-workers have shown that remote consulting involving both DRRs and EPIs is both feasible and of value to clinical practice (Hashimoto et al. 2001b).

Follow-up and clinical trial management by telemedicine applications is a further development of the telemedicine concept in clinical radiation oncology. Telemedicine will allow multicenter participation in clinical trials that require strict adherence to protocols of complex treatment planning and verification. An example of this is the initiation of the German teleradiotherapeutic network for lymphoma trial (Eich et al. 2004) and the US dose escalation trial for early-stage prostate cancer (Purdy et al. 1996). All treatment plans, including dose-volume statistics, and treatment verifications data, both for dummy runs and actual patient treatment, are submitted to study coordination centers, such as RTOG, for protocol compliance verification. Also, efficient and consistent data collection pave the way for elaborate analysis on larger patient population materials than are commonly available; however, participation and data collection from a multitude of centers are most demanding with respect to data formats and network connectivity.

Classification of Telemedicine Functionality in Radiation Therapy

Level-1 (Table 6.3) telemedicine in radiotherapy has been defined as teleconferencing and the display of radiotherapy related information, which facilitates discussions of target volumes and organs-at-risk de-

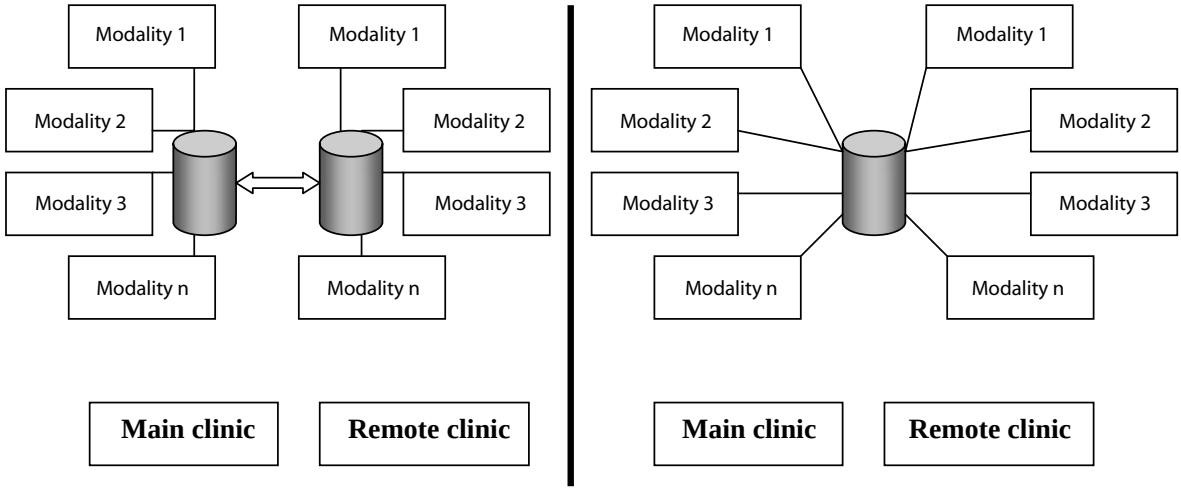

Fig. 6.5. Two different networking and data-storage strategies applicable to level-2 telemedicine functionality, allowing inter-institutional exchange of data

lineation, treatment techniques and beam arrangement, dose distributions and image-based treatment verification (Olsen et al. 2000). Remote conventional simulation of single portals is another example of level-1 functionality. Remote, on-line operations are not supported. Level-1 functionality may be based on ISDN communication and video-signal technology, and is thus a low-cost service. The disadvantages are mostly related to its functional limitations.

Level-2 (Table 6.3) telemedicine features data transfer between institutions, and limited remote image handling. Remote treatment planning, non-real time, is an example of a level-2 operation that requires transfer of data between the participating institutions. Different networking and data storage strategies may be implemented. At some institutions all data are stored in a central DICOM database that communicates with all the modalities, including those at the remote clinic. Others have chosen to establish DICOM databases at each clinic, which are replicated at certain intervals. Irrespectively of networking and storage strategy data transfer, compliant with level-2 operations, higher-speed communication than that provided by ISDN is often required at this level of operation. Finally, it is pointed out that level-2 applications may raise medico-legal issues with respect to responsibility for treatment planning of the patient.

Table 6.3. Functions featured by a telemedicine system in radiation oncology. (Adapted from Olsen et al. 2000)

	Tele conference	Image display	Data exchange	Real-time operations
Level 1	+	+	–	–
Level 2	+	+	+	–
Level 3	+	+	+	+

Level-3 (Table 6.3) telemedicine featuring remote, real-time operations and joint delineation of target volumes is an example of a level-3 functionality. The direct interaction and discussion that is feasible at this level may be of particular importance when a radiologist's review is required for target-volume delineation, or when a discussion is desirable for educational purposes. Level-3 application faces the same disadvantages as level-2 services with respect to costs and medico-legal issues.

References

Dreyer KJ, Metha A, Thrall JH (2002) PACS: a guide to the digital revolution. Springer, Berlin Heidelberg New York

DICOM (1998) Digital imaging and communications in medicine, version 3.0. NEMA, Rosslyn, Virginia 2000, URL: http://medical.nema.org

Eich HT, Muller RP, Schneeweiss A, Hansemann K, Semrau R, Willich N, Rube C, Sehlen S, Hinkelbein M, Diehl V (2004) Initiation of a teleradiotherapeutic network for patients in German lymphoma studies. Int J Radiat Oncol Biol Phys 58:805–808

Hashimoto S, Shirato H, Kaneko K, Ooshio W, Nishioka T, Miyasaka K (2001a) Clinical efficacy of telemedicine in emergency radiotherapy for malignant spinal cord compression. J Digit Imaging 14:124–130

Hashimoto S, Shirato H, Nishioka T, Kagei K, Shimizu S, Fujita K, Ogasawara H, Watanabe Y, Miyasaka K (2001b) Remote verification in radiotherapy using digitally reconstructed radiography (DRR) and portal images: a pilot study. Int J Radiat Oncol Biol Phys 50:579–585

Huh SJ, Shirato H, Hashimoto S, Shimizu S, Kim DY, Ahn YC, Choi D, Miyasaka K, Mizuno J (2000) An integrated service digital network (ISDN)-based international telecommunication between Samsung Medical Center and Hokkaido University using telecommunication helped radiotherapy planning and information system (THERAPIS). Radiother Oncol 56:121–123

Lemke HU (1991) The Berlin Communication System (BERKOM). In: Huang HK (ed) Picture Archiving and Communication Systems (PACS). Medicine, series F. Springer, Berlin Heidelberg New York (Computer and Systems Science, vol 74)

Ntasis E, Maniatis TA, Nikita KS (2003) Secure environment for real-time tele-collaboration on virtual simulation of radiation treatment planning. Technol Health Care 11:41–52

Olsen DR, Bruland S, Davis BJ (2000) Telemedicine in radiotherapy treatment planning: requirements and applications. Radiother Oncol 54:255–259

Purdy JA, Harms WB, Michalski J, Cox JD (1996) Multi-institutional clinical trials: 3-D conformal radiotherapy quality assurance. Guidelines in an NCI/RTOG study evaluating dose escalation in prostate cancer radiotherapy. Front Radiat Ther Oncol 29:255–263

Reith A, Olsen DR, Bruland O, Bernder A, Risberg B (2003) Information technology in action: the example of Norway. Stud Health Technol Inform 96:186–189

Smith CL, Chu WK, Enke C (1998) A review of digital image networking technologies for radiation oncology treatment planning. Med Dosim 23:271–277

Stitt JA (1998) A system of tele-oncology at the University of Wisconsin Hospital and Clinics and regional oncology affiliate institutions. World Med J 97:38–42

3D Imaging for Radiotherapy

7 Clinical X-Ray Computed Tomography

Marc Kachelriess

CONTENTS

7.1 Introduction

Since its introduction in 1972 by Godfrey N. Hounsfield, the importance of CT for the medical community has increased dramatically. Major technical improvements have taken place in the meantime (Fig. 7.1). Now whole-body scans with isotropic submillimeter resolution are acquired routinely during a single breath-hold.

The first step toward true 3D data acquisition was the introduction of spiral CT in 1989 by W.A. Kalender. This scan mode is based on a continuous rotation of the gantry while simultaneously translating the patient along the axis of rotation. The resulting scan trajectory is a spiral and, by symmetry, means truly 3D data acquisition. The z-interpolation step allows selection of the longitudinal position (z-position) of the reconstructed images arbitrarily and retrospectively. The continuous axial sampling is required for high-quality 3D displays and has led to a renaissance of CT (Kalender 2001). Multislice spiral CT (MSCT), which allows simultaneous scanning of *M* slices, further improved the scanner's volume coverage, z-resolution, and scan speed. For example, typical chest exams are carried out with collimations of 1×5 mm in 36 s with single-slice, 4×1 mm in 30 s with 4-slice, and 16×0.75 mm in 10 s with 16-slice scanners, and in the near future 64×0.6-mm scan modes will be used (Fig. 7.2).

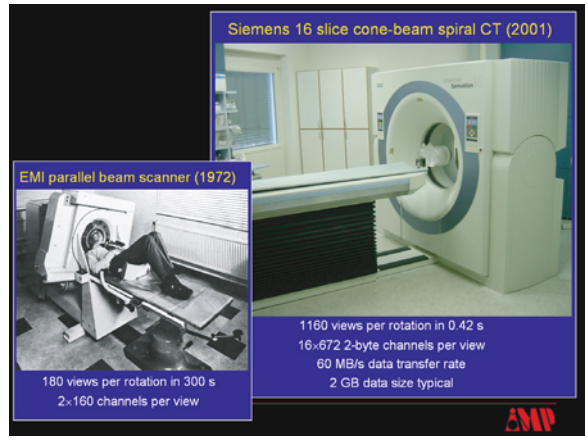

Fig. 7.1. Subsecond true 3D cone-beam scanner with submillimeter resolution

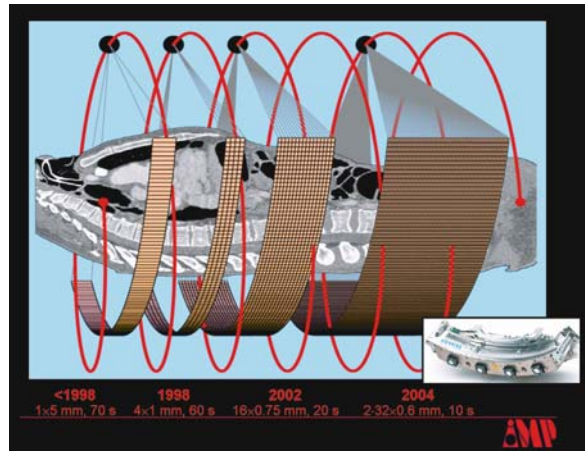

Fig. 7.2. Generations of fan-beam CT scanners: from single-slice to multislice to true cone-beam CT with up to 64 slices

M. Kachelriess, PhD
Institute of Medical Physics, Henkestrasse 91, 91052 Erlangen, Germany